Proton Transfers at the Air-Water Interface

Thesis by

Himanshu Mishra

In Partial Fulfillment of the Requirements for the Degree

of

Doctor of Philosophy

CALIFORNIA INSTITUTE OF TECHNOLOGY

Pasadena, California

2013

(Defended April 15, 2013)

Dedicated to

- *Effortless random fluctuations that led to this dedication,*
- *Tireless vectorial efforts of my parents—Shiv Kumar Mishra and Pushpa Mishra—to instill erudition in me,*
- *Sarvnipun Singh Chawla (1982 – 2010): my dearest friend and a beautiful mind, and*
- *Radhakrishnan Venkatraman (1929 – 2011): a free soul, a catalyst, and an inspiration.*

ACKNOWLEDGEMENTS

A complete acknowledgement of people and incidents that led to, and shaped, my stay at Caltech is impossible; but I will give it a shot. I would like to start by thanking my thesis co-advisers, Professor Mike Hoffmann and Professor Bill Goddard, for providing me with boundless intellectual freedom, constant access, personalized mentoring, and continuous funding during my stay at Caltech. The versatility of Professor Hoffmann's research program and his sensitivity towards students, especially during phases of stress, is remarkable. The unmatchable work ethic of Professor Bill Goddard and his child-like curiosity for science will never cease to inspire me. Words limit my gratitude towards Dr. A. J. Colussi (AJ) for his unflinching support, frank demeanor, friendship, and compassion all these years. I have invaluably gained from AJ's exemplary life style, treasure trove of knowledge, flair in literature search and ability to "squeeze" the meaning out of data, and compose 'Borgesque' manuscripts. A special note of thanks to Dr. Shinichi Enami, who not only trained me on the electrospray setup, but was also kind enough to share his projects on isoprene oligomerization and nitric acid dissociation 'on-water' with me. The contribution of Dr. Robert Nielsen (Smith) in theoretical simulations is gratefully acknowledged. I must also take this opportunity to thank Professor Harry Gray who brought me under the complementary co-advisement of Professor Goddard and Professor Hoffmann, via Professor Mamadou Diallo. This doctoral thesis was impeded by formidable 'kinetic' barriers, and was realized through multiple 'tunneling' events orchestrated by those mentioned above.

During the course of my Caltech experience, I had the fortune of forging friendships with various gifted individuals during academic 'rotations', housing assignments, courses, outdoor activities with the Caltech Y, parties I crashed, or just random on-campus meetings. I continue to cherish these friendships, and thank my friends for their support all along. These terrific guys and gals include: Steven Frankel, Nick Heinz, Sarah Douet, Matt Smith, Sujit Nair, Calyani Ganesan, Abhishek Saha, Slobodan Mitrovic, Jen Kan Yu, Chirranjeevi Balaji Gopal (BG), Pratyush Tiwary (Prat), Aron Varga, Steve Demers, Jason Crowley, Habib Ahmed, Natalya Kostondova, Jonathan Harel, Fan Liu, Alex Tkalych, Vaclav Cvicek, Clara Cho, Jonathan Sternberg, Bao Ha, Alejandro Ortega, Romelia Salomon (now Ortega), Brett Teeple, JD Bagert, Avni Gandhi, Prakhar Mehrotra, Jordan Raney, Logan Stewart, Srivatsan Hulikal, Abha Misra, Murali Gashtekar, Janna Nawroth, Bharat Prasad, Tod A. Charles-Pascal, SurendraNadh Somala, Jina Choi, Wonhee Lee, Andrés Jaramillo-Botero, Hemanth Siriki, Deb Ray, Zeeshan Ahmed, Rob Usiskin, Marco Allodi, Ravi Teja

Sukhavasi, Adam Kowalski, Jack Aldrich, Swami Krishnan, Roddam Narasimha, Fazle Hussain, Lena Forster, Joseph Varghese, Deepak Kumar, Young Shik Shin, Rong Fan, Chao Ma, Heather Agnew, Rosemary Rohde, Chao Chao, Sotiris Masmanidis, Salim Hanay, Grant Jensen, Ariane Briegel, Lydia Finlayson, Clare Hayes, and Rannevig Amundsen. Special thanks are due to Peter Kaufman, and Linda Pauling Kamb, whom I met serendipitously at Caltech, for sharing their life experiences and buying me food on numerous occasions.

My sincere thanks to the Office of the Dean of Graduate Studies, especially Ms. Natalie Gilmore, for guidance and financial support. Thanks to the staff at the Office of the Registrar—Tess Legaspi and Gloria Brewster—for their guidance, and for maintaining a perpetual stack of candies! The outdoor activities group of the Caltech Y played a tremendous role during my stay at Caltech. In addition, I enjoyed friendships with Athena Castro, and Greg Fletcher, and hope to support their endeavors in the future. Tireless work and cheerfulness of the staff at the Libraries, the International Student Program, Human Resources, the Health Center, the Center for Student Services, and the Athletics Center are gratefully acknowledged.

Thanks are also due towards the Hoffmann and Goddard Group members: Dae Jun Kwon, Clement Cid, Yan Qu, Rifkha Kameel, Asghar Aryanfar, Dr. Mamadou Diallo, Dr. Boris Merinov, Dr. Tao Cheng, Dr. Qi An, Hai Xiao, Wei Guang Liu, Caitlin Scott, Dr. Ravi Abrol, Ted Yu, Dr. Mu-Jeng Cheng, Saurabh Bajaj, Sam Johnson, and Shirley Wu.

The scientific staff at the Aqua Nano Tech LLC., Monrovia, CA: Dr. C. J. Yu (CJ), Dennis Chen, and Dr. Han-Ting Chen are acknowledged for their guidance and help in borate-specific materials research. This work constituted an important phase during my tenure as a graduate researcher at Caltech and is presented in Appendix II.

Many thanks are due towards Dr. Nathan Dalleska for solving my instrumentation-related problems at the Environmental Analysis Center at Caltech.

Some of the terrific teachers at Caltech I greatly admired I wish to acknowledge: Niles Pierce, Bill Johnson, Zhen-Gang Wang, Tom Miller, Rudy Marcus, Keith Schwab, and Frances Arnold. The equally, if not more, important contribution of the teaching assistants—Niemma Pehlvan, Jonathan Sternberg, David Abrecht, Nick Stadie, and Pratyush Tiwary—is also acknowledged.

Incessant support from the Langston Family, Dr. Ghanshyam Acharya, Dr. Baratunde Cola, Professor Tim Sands, and Professor Tim Fisher from the good ol' days at Purdue University is acknowledged. I remain grateful to Dr. Gangan Prathap, Dr. Somenath Mukherjee, and Dr Gaya Prasad and family.

Last, but very important, is my inexpressible gratitude towards my parents, sister, and my extended family, especially my Nanaji. I am profoundly thankful to Masha Belyi, and the *Zindagi-ek-paheli* Group—Vibhor Bhatt, Sangram Singh, Manish Kumar, and Karan Sarao— and Rahul Kandhal for their love.

ABSTRACT

Proton transfer reactions at the interface of water with hydrophobic media, such as air or lipids, are ubiquitous on our planet. These reactions orchestrate a host of vital phenomena in the environment including, for example, acidification of clouds, enzymatic catalysis, chemistries of aerosol and atmospheric gases, and bioenergetic transduction. Despite their importance, however, quantitative details underlying these interactions have remained unclear. Deeper insight into these interfacial reactions is also required in addressing challenges in green chemistry, improved water quality, self-assembly of materials, the next generation of micro-nanofluidics, adhesives, coatings, catalysts, and electrodes. This thesis describes experimental and theoretical investigation of proton transfer reactions at the air-water interface as a function of hydration gradients, electrochemical potential, and electrostatics. Since emerging insights hold at the lipid-water interface as well, this work is also expected to aid understanding of complex biological phenomena associated with proton migration across membranes.

Based on our current understanding, it is known that the physicochemical properties of the gas-phase water are drastically different from those of bulk water. For example, the gas-phase hydronium ion, $H_3O^+(g)$, can protonate most (non-alkane) organic species, whereas $H_3O^+(aq)$ can neutralize only relatively strong bases. Thus, to be able to understand and engineer water-hydrophobe interfaces, it is imperative to investigate this fluctuating region of molecular thickness wherein the 'function' of chemical species transitions from one phase to another via steep gradients in hydration, dielectric constant, and density. Aqueous interfaces are difficult to approach by current experimental techniques because designing experiments to specifically sample interfacial layers (< 1 nm thick) is an arduous task. While recent advances in surface-specific spectroscopies have provided valuable information regarding the structure of aqueous interfaces, but structure alone is inadequate to decipher the function. By similar analogy, theoretical predictions based on classical molecular dynamics have remained limited in their scope.

Recently, we have adapted an analytical electrospray ionization mass spectrometer (ESIMS) for probing reactions at the gas-liquid interface in real time. This technique is direct, surface-specific, and provides unambiguous mass-to-charge ratios of interfacial species. With this innovation, we have been able to investigate the following:

1. How do anions mediate proton transfers at the air-water interface?

2. What is the basis for the negative surface potential at the air-water interface?

3. What is the mechanism for catalysis 'on-water'?

In addition to our experiments with the ESIMS, we applied quantum mechanics and molecular dynamics to simulate our experiments toward gaining insight at the molecular scale. Our results unambiguously demonstrated the role of electrostatic-reorganization of interfacial water during proton transfer events. With our experimental and theoretical results on the 'superacidity' of the surface of mildly acidic water, we also explored implications on atmospheric chemistry and green chemistry. Our most recent results explained the basis for the negative charge of the air-water interface and showed that the water-hydrophobe interface could serve as a site for enhanced autodissociation of water compared to the condensed phase.

In a nutshell, this thesis presents an in-depth account of complementary experiments and theory employed to answer the questions listed above. It is primarily based on the following articles:

1. *H. Mishra, S. Enami, L. A. Stewart, R. J. Nielsen, M. R. Hoffmann, W. A. Goddard III, A. J. Colussi, Proceedings of the National Academy of Sciences (2012), 109(46), 18679 – 18683*

2. *H. Mishra, S. Enami, R. J. Nielsen, W. A. Goddard III, M.R. Hoffmann, A. J. Colussi, Proceedings of the National Academy of Sciences (2012), 109(26), 10228 – 10232*

3. *H. Mishra, R. J. Nielsen, S. Enami, M. R. Hoffmann, A. J. Colussi, W. A. Goddard III, International Journal of Quantum Chemistry (2013), 113(4), 413 – 417*

4. *S. Enami, H. Mishra, M. R. Hoffmann, A. J. Colussi, Journal of Physical Chemistry A (2012), 116 (24), 6027 – 6032*

On the recommendation of the thesis committee, Appendix I and II have been added based on the following articles: *S. Enami, H. Mishra, M. R. Hoffmann, A. J. Colussi, Journal of Chemical Physics (2012) 136(15), 154707, 1-7, and H. Mishra, C. J. Yu, D. P. Chen, W. A. Goddard, N. F. Dalleska, M. R. Hoffmann, M. S. Diallo, Environmental Science & Technology, (2012) 46(16), 8998-9004*.

TABLE OF CONTENTS

LIST OF FIGURES

Number *Page*

C h a p t e r 1

INTERFACES OF WATER WITH HYDROPHOBIC MEDIA

Water, along with fire, air, and earth, has incessantly inspired the human imagination, and held an exalted, somewhat mystical, stature across all ancient civilizations. Albert-Szent Györgyi, a pioneering biochemist and a Nobelist, echoed with *Paracelsus,* a philosopher from the sixteenth century, when he touted water as the "matrix of life": a sinew that participates, chaperones, solvates, catalyzes, and orchestrates vital chemical and physical interactions within the cellular milieu.[1, 2] Indeed, it has been increasingly realized over the last century that water plays vital roles in various phenomena in the environment leading to the origin, sustenance, and cycling of the organic matter, the atmosphere, the biosphere, the geosphere, and their delicate couplings.[3-15] Indeed, chemical reactions employing water in the condensed phase are well understood and the level of experimental techniques and theoretical framework in physical chemistry is quite satisfactory. Similarly, chemical reactions of water molecules and clusters in the gas-phase could be quantitatively analyzed, thanks to advances in the mass spectrometry, kinetic theory of gases, and the transition-state theory. However, at the confluence of bulk and gas phases, i.e., at the surface of water, the continuum theories cease to hold and physical quantities such as dielectric constant, acidity/basicity, and electrochemical potential could not be linearly extrapolated from bulk measurements. Interestingly, however, the most important phenomena involving water in biology and atmospheric chemistry take place at interfaces of water with hydrophobic media, such as air and lipids (detailed below). As a natural outcome, experimentalists and theoreticians are vigorously investigating the water-hydrophobe interfaces, though not always in unison, thereby pushing the chemical physics of aqueous interface at the forefront of natural and applied sciences. Experimentalists are pushing the frontier to resolve the molecular details of evanescent, fluctuating aqueous interfaces, while theorists are developing forcefields, coarse-grained methods, and ansatz towards self-consistently capturing the collective dynamics to capture the interfacial chemistry and physics.

This chapter introduces the essence and the efficacy of aqueous interfaces in biology, atmospheric chemistry, and green chemistry, along with challenges impeding a quantitative understanding. Towards the end, an outline of the thesis is presented.

1.1 Interfacial Water in Biology

Remarkably, all forms of known organic life are characterized by compartmentalization of structure and function within the cell wherein proteins drive cellular activities.[16] Expectedly so, the most interesting phenomena, such as molecular sensing, signaling, and chemical exchange, take place at the boundaries of compartments. Vital biological processes driven by membrane proteins at the lipid-water interface include synthesis of the adenosine triphosphate in mitochondria (energy transduction), light activated proton pumping in bacteriorhodopsin, proton channeling, neural signaling, olfaction, immunity and inflammation, and tumorigenesis.[17-24] While sustained research has unraveled structure-function relationships of biological 'actors', not much attention has been given to the roles of interfacial water enveloping them.[3-6] As a result, it is commonplace to find a pristine image of a multicomponent, self-assembled biomolecule in a textbook without a surrounding aqueous environment. In fact, it has been demonstrated that proteins isolated in their dry form exhibit drastically higher electrical impedance than their hydrated counterparts, as representing loss of their biological function.[1, 11] Hydration shells closest to biomolecules (known as the "biological water") have been demonstrated to undergo dramatic departure from typical bulk water structure, and possibly function.[25, 26] But, details of the chemical behavior of interfacial water, confined within a microscopic hydrophobic pocket, or at bulk interfaces with hydrophobic media, are not entirely clear at this point.[3, 6] Indeed, a quantitative understanding of interfacial phenomena should help us address one of the central enigmas in science, i.e., how do non-covalent interactions such as hydrogen-bonding, in addition to the electrostatics, hydrophobicity, van der Waals interactions (including London dispersion, Debye, and Keesom forces), act in concert to set the stage for proteins to construct a multifunctional and conscious entity.

Another baffling problem in biology pertains to the synthesis of ribonucleic acid (RNA) via condensation of amino acids through sequential peptide bond formation. Since these reactions involve elimination of a water molecule for every peptide bond formed, they are unfavorable in an aqueous solution. In fact, a large subunit of the ribosome is known to catalyze this reaction and involves (1) favorable orientation of peptide precursors, acid-base catalysis, and transition-state stabilization, and (2) the alteration in the pK_a of the functional groups of the precursors at the water-hydrophobe interface.[14, 17, 18, 27-30] Since the ocean contains precursors for amino acids, along with a host of transition metal ions, and acidic/basic residues exhibit pK_a switching at water-

hydrophobe interfaces[30], it has been speculated that interactions at the air-water interface played a vital role in prebiotic RNA synthesis.

1.2 Interfacial Water in Atmospheric Chemistry

An in depth investigation of chemical and physical phenomena at water-hydrophobe interfaces is crucial to understand heterogeneous processes on environmental surfaces, such as, for example, cloud drops, dew, fog, haze, aerosol, soil, and leaves. [12, 31-36] Unlike in bulk water, sharp changes in density, dielectric constant, and hydration level across the interfacial region of nanometer thickness could afford unique thermodynamic and kinetic constraints.[37-39] Thus, the air-water interface plays vital role in fundamental atmospheric processes, including (1) acidification of clouds and oceans,[40] (2) anion-catalyzed proton transfer reactions,[41] (3) formation and cycling of the secondary atmospheric aerosol, such as from biogenic isoprene,[42] (4) ocean-atmosphere exchange,[36] and (4) interactions of NO_x with marine aerosol towards formation of HONO[43]. Indeed, there is some experimental and theoretical evidence supporting the contribution of heterogeneous reactions and catalysis to be significant, even competitive to the well-established homogeneous reaction-pathways, in the life-cycles of various natural and anthropogenic emissions.[31-35, 42-57] Unfortunately, however, heterogeneous reactions are largely considered at an *ad hoc* basis in current climate models. For a detailed case study regarding isoprene, please take a look at reference [42]. Thus, quantitative estimation of heterogeneous reactions in the environment would render realism and accuracy to current climate models.

1.3 Role of Interfacial Water in Green Chemistry

Traditionally, organics are used as default solvents for organic synthesis because of the assumption "*corpora non agunt nisi solute*" (substances do no interact unless dissolved). But, curious synthetic chemists discovered dramatic rate accelerations when certain chemical reactions, including aldol condensation, Mannich reaction, Claisen rearrangement, Michael addition, benzoin condensation and Grignard-type additions, were carried out in an aqueous medium.[58-61] In addition to the rate acceleration, water also offers excellent thermophysical and chemical properties, such as high

boiling point, high dielectric constant, high specific heat, and non-toxicity under ambient and moderate conditions. More recently, it has been reported that rates of chemical reactions could be further enhanced if similar organic reactions were carried out in aqueous emulsions.[62-65] However, a challenge impeding advances in green chemistry 'on-water' has been a clear understanding of the role of water. Several proposals based on hydrophobicity[61], hydrogen-bonding enabled transition-state stabilization[66-68], and acid-base catalysis[69] have been forwarded over the years, but a clear picture has not emerged.

1.4 Challenges Associated with Investigation of Aqueous Interfaces

Air-water and lipid-water interfaces were first studied by colloidal chemists while assessing ζ-potentials of air-bubbles and oil-drops in water.[70-75] They noticed that (1) both air bubbles and oil drops in water drifted toward a positively charged plate in an electric field, (2) formation of an oil-water emulsion reduced the pH of water, and (3) the isoelectric point of air-water and lipid-water interfaces was in the pH range 2–3. These experiments speculated that OH^- ion concentration at the water-hydrophobe interface to be responsible for their negative potential and charge, but a molecular picture remained unclear. During past two decades various leading spectroscopists, including Shen[76-82], Saykally[83-90], Rossky[91, 92], Bakker[93], Zewail[94-96], and Skinner [97] have made great strides in experimentally probing the water-hydrophobe interface. It has been demonstrated that a characteristic vibration spectra of the interfacial water merges into that of bulk water within a depth, $\delta < 1$ nm, though a detailed understanding of "structure making and breaking" effects of ions is not entirely clear.[98, 99] Thus, despite their remarkable efficacy to probe the structure of the interfacial water, surface-specific spectroscopies, including the sum-frequency generation (SFG) and the sum-frequency vibrational spectroscopy, have not been able to pin-point the function of chemical species at the water-hydrophobe interface.[100, 101] As summarized by Shen and co-workers, these measurements suffer from: (1) interpretational ambiguities depending on underlying assumptions, (2) inability to capture the functional aspects of interfacial phenomena, (3) sensitivity limitations that require the use of concentrated (> 1 M) solutions, and (4) contamination issues.[76]

Theoretical predictions have played an important role in interpreting and predicting surface phenomena but current tools are limited by (1) uncertainties in the description of non-bonded

interactions, especially hydrogen-bonding interactions in water, and (2) the computational costs of dealing with realistic models.[102-106] For example, it has been realized recently that previous molecular dynamics calculations, employing polarizable versus non-polarizable forcefields, leading to inconsistent results regarding anion-fractionation at the air-water interface had inherent shortcomings.[107-111]

We have recently adapted an electrospray ionization mass spectrometer (ESIMS) for probing chemical and physical phenomena at the gas-liquid interface in real time. This innovation has enabled us to investigate **(1)** anion-mediated proton transfers at the air-water interface, **(2)** the basis for the negative surface charge of the air-water interface, and **(3)** protonation and oligomerization of isoprene gas on the surface of mildly acidic water. In addition, theoretical predictions based on quantum mechanics (density functional theory) and molecular dynamics provided insights into our experimental results. Thus, this dissertation presents a complementary approach harnessing synergy between experiment and theory towards unraveling molecular details underlying interfacial phenomena pertaining to proton transfer reactions. [112]

1.5 Outline of the Thesis

Chapter 2 describes in detail our experimental platform. We have modified an electrospray ionization mass spectrometer into a surface-specific platform for probing phenomena at liquid surfaces. In addition to physical processes, such as anion fractionation and Hofmeister effects, this technique is also capable to capturing reaction intermediates and products in real time. The experimental set up and the soft-ion-ejection process will be described in detail, along with results, to convince the reader of its high sensitivity, and surface specificity.

Chapter 3 presents our report on the anion-catalyzed proton transfer reactions at the air-water interface. We investigated the role of electrostatic pre-organization in mediating proton transfers at water-hydrophobe interfaces. Gas-phase nitric acid was employed as the proton donor, and the common salt as the source for interfacial ions. Theoretical calculations based on quantum mechanics helped us identify the reaction mechanism.

Chapter 4 clarifies a long-standing debate regarding the origin of the negative surface potential and charge of the air-water interface. By colliding gas-phase (Brønsted) acidic molecules with the surface of water, we found unambiguous confirmation of interfacial hydroxide ions to be the source of the negative charge. Against common expectation, we observed OH^- ions at the surface of water as acidic as pH = 2.5. Our complementary theoretical simulations employing density functional theory reinforced our results.

Chapter 5 presents our results on protonation and oligomerization of isoprene, a stable, hydrophobic biogenic gas (> 10^{15} g/yr), whose chemistry is tremendously important, yet unclear, in the context of atmospheric science. Our experiments, along with quantum mechanical simulations underscore the vital role of hydration in controlling thermodynamics and kinetics of heterogeneous reactions of isoprene at environmental surfaces. These findings also provide an alternative mechanism for catalysis 'on-water'.

Chapter 6 concludes the thesis by summarizing key insights and introducing the ongoing effort into additional projects that resulted from this work.

Chapter 2

EXPLORING THE GAS-LIQUID INTERFACE VIA ELECTROSPRAY IONIZATION MASS SPECTROMETRY

Abstract

Electrospray ionization mass spectrometers (ESIMSs) have been widely employed in biochemistry and chemical engineering as a reliable method for generating soft-ions in the gas-phase and detecting them. General consensus regarding ESIM spectra is that they reveal information from the solution-phase, rather than the gas-phase. We revisit this notion and demonstrate that by changing the physical configuration and operating parameters of an ESIMS, it is possible to selectively sample the interfacial region. Consequently, ESIMS affords an unambiguous surface-specific technique for liquids ideally poised to detect and analyze chemical and physical phenomena, such as proton transfers, ion fractionation, and specific-ion effects. In this chapter we present this innovation along with three experimental investigations of the gas-liquid interface: (i) anion fractionation, (ii) proton availability and proton transfers during gas-liquid collision events, and (iii) protonation of organic acids at the air-water interface. Wherever relevant, our results are compared against other established surface-specific platforms, such as sum-frequency generation and sum-frequency vibration spectroscopy, and found to be in excellent agreement. Thus, with this innovation, we have realized a reliable and unambiguous mass-spectrometry-based surface-specific platform to pursue chemical physics of liquid surfaces.

2.1 Introduction

An electrospray ionization mass spectrometer (ESIMS) is established as a versatile analytical instrument for detection of condense-phase species and their interactions in natural and applied sciences.[113-116] Availability of continually refreshed uncontaminated solution jets at ambient conditions, along with unique soft-ion ejection and unambiguous mass spectral detection of intact complex species, render ESIMS an invaluable tool capable of operating at concentrations as low as micromolar range.[117] Flexibility to configure an ESIMS—comprising an inlet capillary, a nebulizer, and a mass spectrometer—along with freedom to assign potential to the capillary, conjure a multidimensional parameter space for ESIMS functions. Consequently, a large body of literature on variational developments and possible applications has accumulated over decades. [118-120] In this chapter, we raise the question: ***Has the entire parameter space for ESIMS function been explored?*** In 1984 Yamashita and Fenn perspicaciously noted about ESIMS, "*another intriguing possibility is to use the technique on probing microscopic structure and properties of solutions*".[120] The question we set to address, in particular, in this article is: **Is there a set of operation parameters that can afford sampling of only the interfacial region of solution, rather than its bulk?**

The operation and performance of an EISMS could be parametrically adapted by the following: (i) relative directions of the nebulizer flow and the mass- spectrometer inlet vector, (ii) electric potential assigned to the capillary and the fragmentor plate, (iii) solute-solvent characteristics, including concentration, surface tension, additives, along with temperature and the rate of injection. Over the course of last few years, Colussi and co-workers have optimized a set of conditions that render an ESIMS suitable to probe phenomena at the gas-liquid interface. They found that with an electrically grounded capillary augmented with a concentric high-speed nebulizer, imparting momentum to the sheared jet layers in a direction perpendicular to the mass-spectrometer inlet, it is possible to selectively sample the interfacial layers while the bulk of the jet goes unsampled (see the Experimental section and Figure 2.1). In this chapter we present our experimental method in detail to be followed by experiments probing chemical and physical phenomena at the gas-liquid interface and comparison with *bona fide* surface-specific techniques. We will present our results on (1) relative anion fractionation at air-water interface[121, 122] in an equimolar polyelectrolyte solution and (2) proton transfer reactions at the air-water interface, including protonation of gas-phase

bases[123] and weak carboxylic acids[124], which provide convincing evidence of the surface specificity of our technique.

2.2 Experimental Method: ESIMS as a Surface-Specific Platform

An electrospray ionization mass spectrometer (HP-1100 MSD) with an atmospheric pressure ionization interface of orthogonal geometry was used in this study. The orthogonal geometry ensured that only a small fraction of analyte reached the quadrupole mass-spectrometer, while the rest continued its forward trajectory without contributing to the ion-current (Figure 2.1). Since mass spectrometers only detect charged species, the ESIMS technique necessarily requires separation of pre-existing anions from cations from the charge-neutral anlayte as a first step.

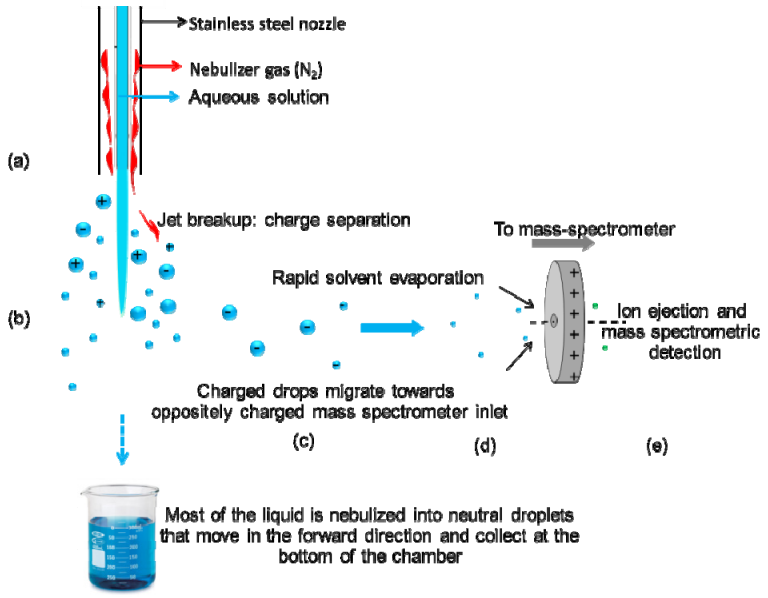

Figure 2.1: Schematic of an electrospray ionization mass spectrometer showing various stages to the best of our understanding: (a) a nebulizer gas shears the outermost layers of jet resulting in small droplets, (b) some of these resulting droplets carry excess charge(s), and change their trajectories under the influence of the electric field of the fragmentor plate, (c) solvent evaporation destabilizes droplets leading to smaller droplets via Coulomb explosions, (d) subsequent solvent evaporation leads to soft-ion ejection, and finally (e) ionic species undergo mass spectrometric detection.

Analyte solutions are pumped (50 μL min^{-1}) into the spraying chamber through an electrically grounded stainless steel capillary injector of 100 μm diameter (Figure 2.1). Surrounding this capillary injector is a coaxial sheath (250 μm internal diameter) releasing a nebulizer gas (usually boil-off N_2) at 13 L min^{-1} (Figure 2.1).

Pneumatic shearing of the surface of a slow moving (≈ 0.1 m s^{-1}) analyte jet by the nebulizer gas (~ 250 m s^{-1}) leads to smaller droplets. ***Why are some of the resulting droplets electrically charged?*** During the nebulization process, the kinetic energy of the nebulizing N_2(g) gas is consumed to shear the interfacial region into smaller droplets. Thus, following a normal distribution, some of the resulting droplets carry *excess* positive or negative charges as expected from a random process. While the nebulizer gas easily shears the initial jet of ≈ 100 μm size, it cannot further break the smaller droplets due to inadequate energy density and only aids evaporation thereafter. Thus, a constant fraction of the number of pre-existing ions in the interfacial layers is separated in this process.

How does ion-ejection take place? As shown in Figure 2.1, the jet emitted from the grounded nozzle proceeds in a direction orthogonal to the polarized inlet to the mass spectrometer. Due to electrostatic attraction, some of the charged droplets get preferentially deflected toward the polarized mass-spectrometer inlet. As the smaller charged drops progress towards the mass-spectrometer inlet, rapid solvent evaporation is accomplished via the nebulizer gas. Within ≈ 10 μs, the radii shrink to the Rayleigh limit, given by $q = 8\pi(\varepsilon \gamma R^3)^{1/2}$ at which the Coulombic repulsion between excess charges in the drop overwhelm surface tension, and the charged drop fissions into smaller droplets.[125] Here q is the charge on the droplet, ε is the dielectric permittivity, γ is the surface tension of the solvent and R, drop radius. Notice that these electrostatic Coulomb explosions do not separate negative from positive charges, but only the excess charges acquired during the jet break up by the nebulizer. It should be emphasized that anions may recombine with remaining counterions (or associate with neutrals) in shrinking charged droplets, but the net ions drawn per unit time from the initial jet (ions × $time^{-1}$) is conserved in sprays of non-interacting droplets. As the smaller droplets undergo further evaporation, eventually excess ions are ejected into the gas-phase amenable for mass spectrometric detection. The event of ion ejection may or may not coincide with complete solvent evaporation: two models—ion evaporation model (IEM) and charge residue model (CRM)—are based on those conditions, respectively.[126-128] In either case, the number of excess ions, finally ejected, remains conserved in a drop since the jet breakup and during solvent

evaporation. As a result, the mass spectral intensity of the ejected ions correlates to the excess charge at jet breakup event, which correlates to the interfacial concentrations in the jet before breakup.

In following sections, results of Cheng et al.,[108, 121] on anion fractionation, and recent results on proton transfer reactions at the air-water interface are compared against *bona fide* surface-sensitive techniques and theoretical predictions.

2.3 Ions at the Air-Water Interface

We start this section with a brief historical perspective: Based on the celebrated theory of liquids of Debye and Hückel[129, 130], which was furthered by Wagner[131], Onsager and Samaras[132] established a theoretical framework linking ion adsorption at the air-water interface to the surface tension. This theoretical framework considered only the electric field between ions, neglecting ion-dipole interactions with water molecules. The resulting paradigm was that the adsorption of ions at the air-water interface was impeded by (electrostatic) "image force" near the boundary. However, independent experiments of Heydweiller and Schwenker suggested presence of ions at the interface by measuring surface tension minima between low and high concentrations, but were ignored.[133] It was not until 1937, when Jones and Ray unambiguously established that the surface tension of aqueous electrolytes exhibited minima at a concentration ≈ 0.001N, and, thus, ions must be adsorbed at the air-water interface to relieve the surface tension.[133, 134] A molecular understanding of 'Jones-Ray effect' remains incompletely understood to date.[40, 90, 135-137] Recent application of complementary experiment and theory is expected to address it.[83, 121, 138, 139]

Thus, against the proposition of Onsagar and Samaras, anion fractionation at the air-water interface has been well established with a host of experimental techniques, including surface-specific nonlinear spectroscopy and electrokinetics. In fact, a recent phase-sensitive sum-frequency vibrational spectroscopy (PS-SFVS) study revealed that interfacial anion affinities of the following ions are in the order $I^- > NO_3^- > NH_4^+ > Cl^- > K^+ > Na^+$ in the concentration range 1 – 2 M.[140] Saykally and co-workers have applied resonant sum-frequency generation spectroscopy and confirmed the Jones-Ray effect and more recently suggested that capillary waves at the air-water

interface might explain the Hofmesiter effect (Also see Section 6.4.1 in Chapter 6).[83, 88] Though, SFVS and sum-frequency generation (SFG) platforms formally probe interfacial layers, they suffer from: (1) sensitivity limitations that require the use of concentrated (> 1 M) solutions, and (2) interpretational ambiguities that might make the molecular assignment of SHG or SFVS spectral features depend on certain assumptions.[76, 141, 142] Even the theoretical community has not been able to put anion fractionation on a quantitative basis so far, e.g., molecular dynamics predictions of anion fractionation at air-water interfaces are very sensitive to the use of electronic polarization function.[87, 143-146] Theoretical methods, such as molecular mechanics with (non)polarizable forcefields, Car-Parrinello metadynamics[138, 140, 147] have been applied to study this phenomenon, but quantitative insights remain elusive.

2.4 Investigating Anion Fractionation at the Air-Water Interface via ESIMS

Cheng et al., applied ESIMS to investigate the anion fractionation at air-water interface by analyzing a mixed aqueous electrolyte solution containing equimolar concentrations of sodium salts (NaX, X^- = Br^-, I^-, NO_3^-, IO_3^-, PF_6^-, SCN^-, BrO_3^-, BF_4^-) in the range 10 – 100 μM. If the ESIMS in our configuration did not sample only the interfacial region, resulting anion mass spectral signal strengths from the bulk solution would be similar in magnitude. On the contrary, Cheng et al., observed significantly varying mass spectral signal intensities in accordance with the Hofmeister series and in agreement with other surface-sensitive techniques for gas-liquid interface (Figure 2.2 (A)).[147-149] This experiment beautifully established the our ESIMS as a surface-specific platform. While the surface-sensitive ESIMS setup is also limited to relative quantification of interfacial ion abundances at the gas-liquid interface, it offers high sensitivity and unambiguous mass-to-charge ratio at concentrations as low as 1 μM. Normalized anion affinities, f_{X^-}, were calculated from the sum of mass spectrometric ion counts, $I_{m/z}$, for the isotopic variants of each anionic species [e.g., ($I_{99} + I_{101}$) for ClO_4^-] and the total ion count:

$$f_{X^-} = \frac{\sum I_{m/z}^{X^-}}{\sum I_{m/z}} \qquad (1)$$

Relative anion affinities, γ_{X^-}, calculated relative to f_{Br^-} (for bromide) as $\gamma_{X^-} = f_{x^-}/f_{Br^-}$, are shown in Figure 2.2(A).

What properties of the air-water interface do the uneven interfacial anion populations shown in Figure 2.2(A) correlate to? ESIMS data plots of $\ln f_{X^-}^-$ vs. a_X^- crystalline anion radii (Figure 2.2(B) were illuminating in this regard. Cheng et al., observed excellent linearity between $\ln f_{X^-}$ and gas-phase radii of ions (correlation coefficient, $R^2 = 0.97$) thus establishing that the fractionation of ions at the air-water interface was *strongly correlated* to their size, or the hydration energy. Interestingly, they also demonstrated that there was no correlation between ion fractionation and anion polarizability as claimed by a large number of theoretical predictions and agreed upon by experimental results (Figure 2.2(C)). [107, 109-111, 121, 122, 143, 146, 150-152] Thus, the ESIMS setup working as a surface-sensitive technique provided important clues towards understanding anion fractionation phenomenon.

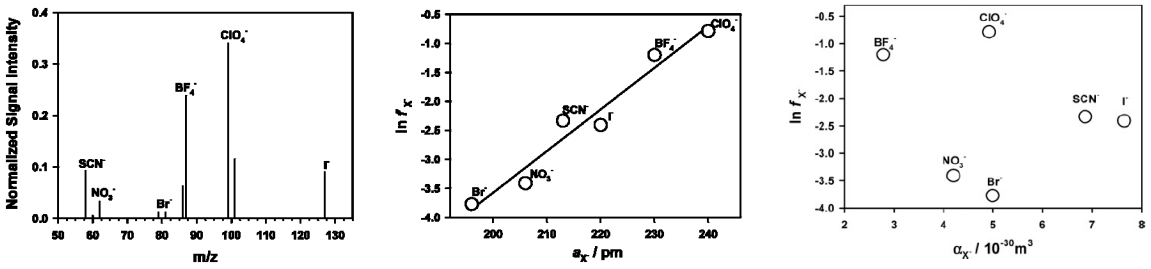

Figure 2.2(A): ESIM spectrum of a 100 μm aqueous solutions of the sodium salts of: Br^-, NO_3^-, SCN^-, I^-, BF_4^- and ClO_4^- at pH 6.5. Ion signal intensities normalized to the total ion intensity: $\sum I_x^- = 1$. $I_{SCN^-} = 0.097$, $I_{NO3^-} = 0.033$, $I_{Br^-} = 0.023$, $I_{BF4^-} = 0.301$, $I_{ClO4^-} = 0.455$, $I_{I^-} = 0.090$; Figure 2.2(B) Correlation between logarithmic normalized affinity and ion radii, from [153]. Solid line: linear regression: $\ln f_{X^-}, \alpha\ a_X^-$ ($R^2 = 0.956$); Figure 2.2(C): Correlation between anion polarizabilities and relative signal intensities of various anions: Br^-, NO_3^-, SCN^-, I^-, BF_4^- and ClO_4^- at pH 6.5 (no direct correlation)

2.5 ESIMS for Investigating Reactions at the Gas-Liquid Interface

To investigate reactions at the gas-liquid interface using ESIMS, Colussi and co-workers designed numerous experiments wherein composition-adjusted liquid jets were intersected with reactive gases before the jet breakup by a nebulizing gas (Figure 2.3).[31, 33, 34, 37, 40, 42, 43, 47, 51, 52, 54, 123, 154-159] For example, a 10% v/v solution of HNO_3 in deionized water at 278 K has a partial pressure, $p \approx 4.8 \times 10^{-8}$ atm due to nitric acid vapor.[160] Gaseous HNO_3 vapor was transported from a solution of dissolved HNO_3 by sparging 100 sccm N_2 gas at a fixed temperature. A detailed analysis [161] based on mass balance and application of the kinetic theory of gases to fast gas-liquid reactions suggesting that the thickness of the interfacial region sampled in these experiments is most likely < 1 nm follows: From the frequency of HNO_3 collisions on water's surface given by the kinetic theory of gases: $f[\mathrm{cm^{-2}\ s^{-1}}] = ¼\ \gamma\ c\ n$, where $\gamma \approx 1$ is the reactive uptake coefficient, $c = 3.2 \times 10^4$ cm s^{-1} is the mean speed of HNO_3 molecules at 300 K, and n is the number density (molecules cm^{-3}),[161, 162] we deduce that $f \times (\tau/\Delta) = 1.9 \times 10^{18}$ protons $cm^{-3} = 10^{-2.5}$ M must be delivered to interfacial layers of thickness Δ[cm] upon exposure to $n = 3.3 \times 10^{12}$ HNO_3(g) molecules cm^{-3} during τ[s] life times, i.e., $(\Delta/\tau) = 0.014$ cm s^{-1}. Previous experiments have shown that $\tau \sim 10$ μs [161]. Thus, we estimate that the thickness of the interfacial layers sampled in our experiments is: $\Delta \sim 1.4 \times 10^{-7}$ cm (Also see Section 3.4 in Chapter 3). Various spectroscopists have demonstrated that characteristic vibration spectra of the interfacial water merges into that of bulk water within a depth, $\delta \approx$ 1nm. [94-96, 163] Thus, we believe that our platform is ideally suited to probe the gas-liquid interface. Further, it must be noted that the gas-liquid collisions last for ≈ 5 ns, during which molecules can (de)adsorb or bounce off, while the aqueous jet has a life time of ≈ 10 μs after which it is sheared into smaller droplets. Within $t \approx 5$ ns, the molecules can sample depths, $\langle x \rangle = (D \times t)^{1/2}$, where $D \approx 10^{-9}$ m^2/s, leading to an average sampling of the interfacial region $\langle x \rangle \approx 1$ nm deep.

In all experiments described in this thesis, 50 μL min^{-1} of deionized water (or aqueous electrolyte solution) was injected into the spraying chamber of an ESIMS held at 1 atm, 293 K via an electrically grounded stainless steel pneumatic nozzle (100 μm) internal diameter. Note that the velocity at which the liquid jet emerges from the nozzle is ~ 500 times slower than that required for observing electrokinetic generation of H_2 gas as reported by Saykally and co-workers [164]. Other instrumental parameters were: drying gas (flow 6 L min^{-1}, temperature 340 ºC), nebulizer pressure (1.02 atm), fragmentor voltage (40 V), Gain 1, threshold 25, step size 0.1, and peak width 0.3. The pH of aqueous solutions was adjusted via concentrated NaOH or HCl.

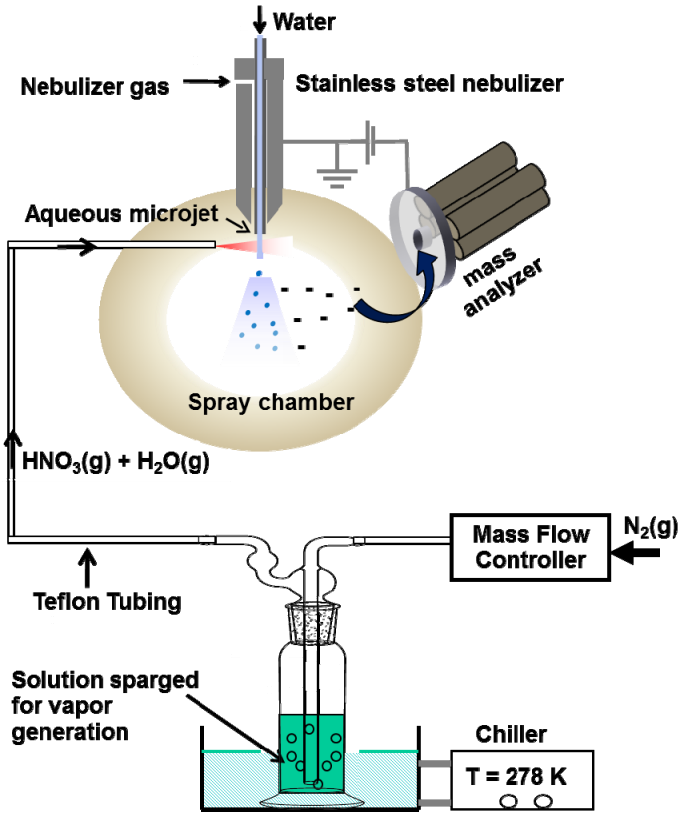

Figure 2.3: Schematic of our experimental setup for gas-liquid reactions. A microjet is created in the spraying chamber of an electrospray mass spectrometer by injecting water through an electrically grounded stainless steel nebulizer (100 μm internal diameter) and briefly exposed to nitric acid vapors before is broken up (after ≈ 10 microseconds) into charged droplets by the nebulizer gas. After subsequent solvent evaporation and successive Coulomb explosions, excess ion are ultimately ejected to the gas-phase via field desorption, and detected by mass spectrometry in < 1 millisecond. The spray chamber is at 1 atm of N_2, 293 K throughout.

Could increasing concentrations and curvatures of drops trigger/influence surface reactions? To address this concern it is critical to note that (1) in the life cycle of a jet emitted from the nozzle, the nebulizer gas shears it only once, because the hydrodynamic forces required to further break/shear the microscopic drops significantly exceed the energy density carried by the nebulizer gas, (2) the ion ejection process pertains only to excess ions which are acquired during jet break up, and (3) even though chemical reactions take place on the surface of a concentrated micro/nano droplet, such

acid-base reaction, the excess charge/species will remain unchanged. Indeed, there is a possibility that depending on the ionic species, there could be substitution of ions in concentrated drops leading to noise or false signal. But we have not observed it in our set of experiments. Indeed, the observation of standard titration curves for dissolved acids/bases reproduced from our ESIMS also testifies that the sampling process is affected by these effects (See Figures 2.4 and 4.2). With our experience so far, it can be concluded that the mass spectrum of an ESIMS setup adapted for investigating gas-liquid reactions, as described, directly correlate to the excess charge carried by the droplets which in turn is related to the interfacial ion concentrations.

2.5.1 Proton Availability at the Air-Water Interface

A clear understanding of aqueous interfaces is quintessential in understanding myriad (a)biotic processes and phenomena. Recently, there have been several conflicting reports—both theoretical and experimental—on the nature of surface acidity of air-water interface.[85, 165-167] Unfortunately, most estimates based on classical molecular dynamics simulations and surface-specific techniques can only predict "structures" of the air-water interface with known bulk acidity, but the "functional" information is not captured. In other words, presence of hydronium ions near the air-water interface does not render it "acidic": the surface is acidic if (and only if) it protonates a base. Recently, Enami et al., employed gas-phase trimethylamine (TMA) to evaluate the functional acidity (or the availability of protons) at the air-water interface by intersecting pH-adjusted aqueous jets with gaseous beams of TMA/N_2(g).[123] Compared to the proton affinity of the gas-phase water, PA(H_2O) = 165 kcal mol^{-1}, the proton affinity of gas-phase TMA is 227 kcal mol^{-1}. Further, the acidity constant of the conjugated acid of TMA in aqueous solution, pK_a ($TMAH^+$) = 9.8 suggests that TMA is a stronger base than H_2O in both the gas and liquid phases. Expectedly, the reaction R_1 is exothermic, ΔH = PA(TMA) – PA(H_2O)) = -62 kcal mol^{-1}, while R_2 becomes viable after extensive ion hydration.

$$H_3O^+(g) + TMA(g) \longrightarrow H_2O(g) + TMAH^+(g) \qquad (R_1)$$

$$H_3O^+(aq) + TMA(aq) \longrightarrow H_2O(aq) + TMAH^+(aq) \qquad (R_2)$$

Thus, the extent of protonation of TMA at the air-water interface provided functional insight into the surface acidity, or proton availability, at the air-water interface. Experiments were carried as described in the experimental section for gas-liquid collision reactions. Positive ion ESIM spectra produced by spraying pH-adjusted water jets crossed with 3.0 ppmv TMA/N_2(1 atm) mixtures display $TMAH^+$ (m/z=60) and $(TMAH)_2Cl^+$ (m/z=155, 157) signals. At constant concentration TMA(if), $TMAH^+$ signal intensities were found to vary with bulk pH, as shown in Figure 2.4 (blue downward triangles). Experimental data yielded pK_a = 3.0 ± 0.2 for interfacial protonation in striking contrast with $TMAH^+$ signals from pH-adjusted solutions of TMA in water which showed an equivalence point at pK_a = 9.96 ± 0.2, matching closely with the reported value for $pK_a(TMAH^+)$.

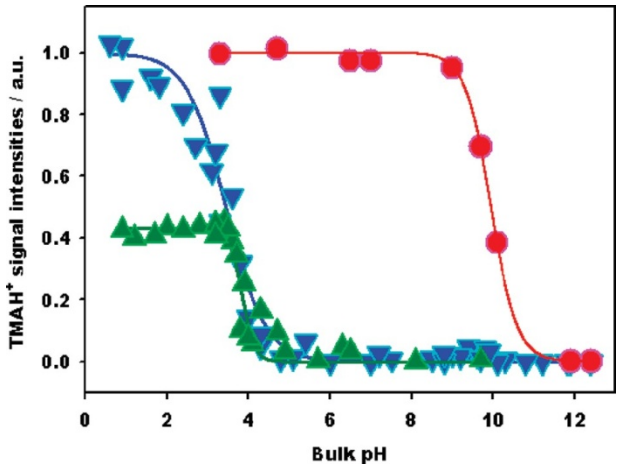

Figure 2.4: ESIMS $TMAH^+$ signal intensities versus pH_{BLK} on water microjets exposed to 1.00 – 3.0 (blue downward triangles) and 0.03 ppmv TMA(if) (green upward triangles) and on aqueous TMA/N_2(if) (red circles). Blue and red signal intensity data are normalized to $TMAH^+$ = 1 at pH_{BLK} = 1. Green data are relative to the blue data.

The investigation by Enami et al., employing the ESIMS tracking proton availability at the air-water interface, concluded that (1) TMA is more basic than water in the gas and bulk liquid phases but not at the interface, (2) the proton activity sensed by TMA(if) at the air/water interface is indirectly related to the bulk pH, (3) from a functional point of view the surface of water is not acidic unless bulk is acidified to pH < 3, (4) at pH < 3 air-water interface exhibits partial gas-phase behavior, thus

protonating hexanoic acid.[124] An isoelectric point at pH = 3.0 ± 0.2 for the water surface is in good agreement with the previous values derived from electrophoretic experiments on bubbles and droplets in water.[71-75] It must be made clear that this result was insufficient to prove that hydroxide, OH^-, ions selectively adsorb at air-water interface in that pH range; though, we will take up this issue in Chapter 4. At this point we also wish to point out that while it is true that the drops resulting from the pneumatic shearing of acidic jets in the range pH 4 – 7 become increasingly acidic as the solvent evaporates and $TMAH^+Cl^-$ may form on their surface. But the ESIMS did not detect $TMAH^+$ signal because the excess charge on the drop remains constant (zero) after pneumatic shearing process. This elucidates the importance of conservation excess charge formed during initial jet breakup. Protonation of TMA(if), and hence generation of some drops with excess charge only takes place on the surface of pH < 4 jets. We will again touch upon this in the next section.

2.5.2 Protonation of Organic Acids on the Surface of Mildly Acidic Water

How acidic is the surface of pH < 3 water? We applied acetic acid (RCOOH) and hexanoic acid (PCOOH) as molecular probes to investigate the surface of mildly acidic water as discussed in Section 2.5 and shown in Figure 2.3.[124, 168] Gas-phase proton affinity of both organic acids is ≈ 187 kcal mol^{-1}. Similarly, in the bulk solution the $pK = 4.8$ and $pK_{PCOOH2^+} = -3$ suggesting that they are both weak acids and bases. Thus, thermochemistry alone suggests that gas-phase acids (like TMA(if) in the previous section) might accept proton from H_3O^+(if) (reaction R_3), but in condensed phase would easily remain unprotonated above pH ≈ 1 (reaction R_4). We wish to find out the fate of interfacial PT reactions R_5.

$$H_3O^+(g) + PCOOH(g) \longrightarrow H_2O(g) + PCOOH_2^+(g) \quad (R_3)$$

$$H_3O^+(aq) + PCOOH(aq) \longrightarrow H_2O(aq) + PCOOH_2^+(aq) \quad (R_4)$$

$$H_3O^+(if) + PCOOH(if) \longrightarrow H_2O(if) + PCOOH_2^+(if) \quad (R_5)$$

We applied ESIMS in a series of experiments to monitor PT reactions during collisions of PCOOH(if) with the surface of pH-adjusted water as described in the experimental section and

Figure 2.3. As shown in Figure 2.5, we observed (1) protonation of organic acids coming from the gas-phase on the surface of pH < 3 water, and (2) protonation of acids already dissolved in water as PCOOH(aq) was insignificant in comparison.

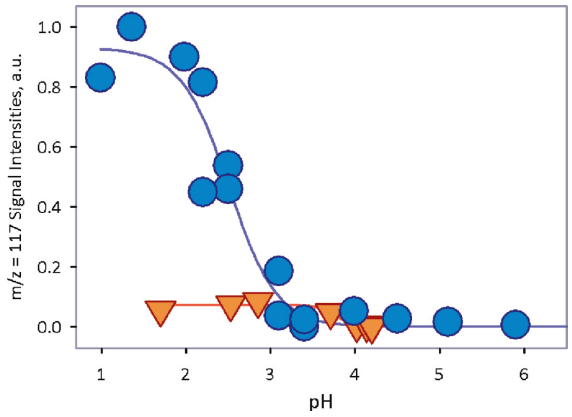

Figure 2.5: ESIMS $PCOOH_2^+$ signal intensities versus bulk pH on aqueous jets exposed to 77 ppbv PCOOH(if) (blue circles) and within 1mM PCOOH(aq) jets in pure N_2(g) (orange triangles). Data shows protonation of RCOOH at the surface of mildly acidic water, but not in the bulk.

ESIMS experiments tracking interfacial PTs at air-water interface clearly show that from a functional point of view (i) the air-water interface is not acidic in the range 4 < pH < 7, (b) the air-water interface exhibits superacidity at pH < 3, i.e., the proton activity of H_3O^+(if) vastly exceeds H_3O^+(aq) at same bulk acidity at pH < 3.

In subsequent chapters the reader will find several other proton transfer reactions at the air-water interface probed via the ESIMS, corroborated by theoretical predictions and contemporary surface-specific techniques.

2.6 Conclusions

With all the experimental results presented above, it is evident that the tunable parameter space of ESIMS functions renders it capable of investigating characteristics of the gas-liquid interface and reactions thereon. As a surface-sensitive technique, our ESIMS setup exhibits high sensitivity, flexibility, contamination resistance, and operability at ambient conditions, thus exponentially expanding its scope and application. Using this technique, experimental results on anion fractionation at the air-water interface are in close agreement with other surface-specific techniques and keenly underscore the role of ion size versus polarizability in this phenomenon.[121, 122, 138, 144, 146, 150, 169] While absolute quantification and exact details of ion enrichment and specific ion effects remain elusive, a rational approach for advancing scientific understanding would be to select robust correlations between experimental interfacial anion affinities and specific ion parameters and discard models that do not support such correlations and experimentally test the falsifiability of the ones that do support them.[121, 170] [171] Further, using the ESIMS setup we monitored gas-liquid reactions *in situ* and demonstrated that at the air-water interface protons do not become available to gaseous bases unless pH < 3. [123]Curiously, when pH enters the range pH < 3, the surface of water becomes acidic enough to protonate weak gas-phase acids, including acetic and hexanoic acids which requires extreme acidic conditions in bulk phase.[37] Finally, in light of our results and the multitude of challenges confronting current surface-specific techniques and the level of theory to investigate chemical physics at the gas-liquid interface, we hope that the chemical physics community might favorably consider ESIMS as a complementary surface-sensitive technique. Recent articles by Laskin et al., [172] and Saykally[100] show the community is favorably receptive of our platform.

Chapter 3

ANIONS DRAMATICALLY ENHANCE PROTON TRANSFER THROUGH AQUEOUS INTERFACES

Abstract

Proton transfer (PT) through and across aqueous interfaces is a fundamental process in chemistry and biology. Notwithstanding its importance, it is not generally realized that interfacial PT is quite different from conventional PT in bulk water. Deeper insight into interfacial proton transfers is the key to understand enzymatic catalysis, and heterogeneous chemistries implicated in the atmosphere-biosphere-oceanic coupling. It has been suggested that PT at aqueous events could be sensitively modulated by electrostatic fields of ions present at aqueous interfaces. In this chapter, we apply experiment and theory to assess the contrasting behavior of nitric acid (HNO_3) at the air-water interface versus the bulk water as a model system to elucidate this phenomenon. HNO_3 is a strong acid in bulk aqueous solutions, but behaves as a weak acid in the gas-phase. At the air-water interface, HNO_3 does not fully dissociate upon collisions (jet life-time, $\tau \approx 10$ μs) unless a few anions (> 1 per 10^6 H_2O molecules) are present therein. By applying surface-specific electrospray ionization mass spectrometry to monitor *in situ* the surface of aqueous jets exposed to HNO_3(g) beams we found that NO_3^- production increases dramatically on > 30 μM inert electrolyte solutions. We also performed quantum mechanical simulations showing that the barrier hindering HNO_3 dissociation on the surface of small water clusters is significantly lowered in the presence of anions. Anions effectively assist in pulling the proton away from a laggard NO_3^-, which stays behind at the interface because its incorporation into the cluster is hampered by the energetic cost of opening a cavity therein. Present results provide both direct experimental evidence and mechanistic insights on the relative slowness of PT at water-hydrophobe boundaries and its remarkable sensitivity to electrostatic effects.

3.1 Introduction

Proton transfers (PTs) at aqueous interfaces, such as aqueous boundaries with air [57, 173] or lipid membranes [174], mediate vital phenomena in the nature. Arguably, the most important PTs are those through and across water boundaries rather than in the bulk liquid. Interfacial PTs participate in the acidification of the ocean [175], the growth of atmospheric aerosols [57], the generation of the electrochemical gradients that drive energy transduction across biomembranes [174, 176, 177], and in enzymatic function [29, 178, 179] because the activation of neutral species in aqueous media is most generally accomplished via acid-base catalysis [180]. Interfacial PT, in contrast with conventional PT in bulk water, depends sensitively on the extent of ion hydration therein because the density of water vanishes across ~ 1 nm thin interfacial layers [97, 181]. The strength of hydronium at the interface, H_3O^+(if), is expected to bridge that of H_3O^+(aq), which protonates most non-alkane species in the gas-phase [182], and H_3O^+(aq), which neutralizes only relatively strong bases in solution. Critically controlled by ion hydration in thin yet cohesive interfacial water layers that resist ion penetration [183], PT 'on water' confronts unique constraints. Species that behave as strong acids 'in water' could become weak ones 'on water' if dissociation were hindered by kinetic and/or thermodynamic factors in the interfacial region [184, 185].

Herein we address these fundamental issues and report the results of experiments where we monitor the dissociation of gaseous nitric acid HNO_3(g) molecules in collisions with interfacial water, H_2O(if), reaction R_1

$$HNO_3(g) + H_2O(if) \rightarrow NO_3^-(if) + H_3O^+(if) \qquad (R_1)$$

3.2 The Technique

Experiments were conducted using our electrospray ionization mass spectrometer (ESIMS) wherein continuously refreshed surfaces of free-flowing aqueous jets were intersected with HNO_3(g)/N_2(g) beams at ambient temperature and pressure (see detailed description in Section 2.5 in Chapter 2 and reference [161]). The decisive advantages of online mass spectrometry over spectroscopic techniques are that (i) it operates *in situ*, is fast, mass-selective and has high sensitivity, (ii) naturally discriminates against a background of neutral AH reactants and (ii) provides unequivocal

information about the molecular composition of product ions A^-. We have previously demonstrated the surface-specificity of our experiments by showing that (i) anion signal intensities in the mass spectra of equimolar salt solutions adhere to a normal Hofmeister series (rather than being identical) [186, 187], (ii) we could detect the products of gas-liquid reactions that could only be formed at the air-water interface [188].

3.3 Experimental Results

Figure 3.1 displays mass spectral NO_3^- (m/z = 62) signal intensities, I_{62}, as a function of pH (of the bulk aqueous solution) on liquid jets exposed to HNO_3(if). I_{62} remains above detection limits on the surface of pH 4.5 to 9.5 jets, but sharply increases *both* on more basic and more acidic solutions to limiting values, I_{62}^{max}, above pH 11 and below pH 3. *Remarkably, we found that* I_{62}^{max} *values are uniformly reached at all pH values on > 1 mM NaCl jets*. Notice that the reported uptake coefficient of HNO_3(if) on deionized water, $\gamma > 0.1$, implies that only a fraction of the HNO_3(if) molecules colliding with the surface of water are incorporated into the bulk liquid where they become fully dissociated [$pK_a(HNO_3(aq)) = -1.4$]. [162, 189] Therefore, the small NO_3^- signals detected in our experiments on pure water jets indicate that we predominantly sample the outermost interfacial layers of the jet [190, 191], and most of the mass-accommodated HNO_3 can diffuse in undissociated form through such layers into bulk water. The fact that the production of NO_3^-(if) is dramatically enhanced by *inert* anions on water, starting at concentrations as low as 30 μM, hints at the possibility that the barrier preventing HNO_3 dissociation at the interface might be kinetic rather than thermodynamic [192, 193]. Thus, the results of Figures 3.1 and 3.2 provide evidence that (1) HNO_3(if) behaves as a weak acid on the surface of water, and (2) extrinsic inert ions significantly catalyze proton transfer between gas-phase HNO_3 and the air-water interface [185, 194].

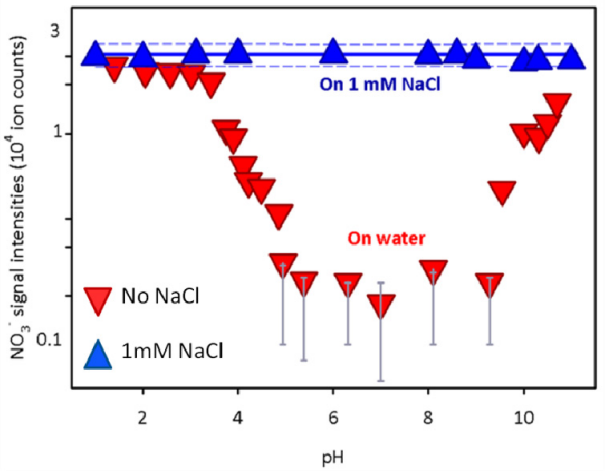

Figure 3.1: Electrospray mass spectral nitrate signal intensities (I_{62}) detected on water or 1 mM NaCl microjets exposed to 3×10^{12} molecules cm^{-3} of gaseous nitric acid for ≈ 10 μs as functions of pH. Solid, dashed lines are a linear regression and 95% confidence limits, respectively, to the data on 1 mM NaCl. Error bars estimated from reproducibility tests. All experiments under 1 atm of N_2 at 293 K.

It is well known that the air-water interface of electrolyte solutions is preferentially populated by anions. This is borne out by the negative surface potential of most electrolyte solutions [195], by surface-specific spectroscopic studies [196-199], and by theoretical predictions [193]. The saturation dependence of NO_3^- production on electrolyte concentration (Figure 3.2) can be formally ascribed to catalysis by anions A^- adsorbed to identical, non-interacting sites of the air-water interface, i.e.: $I_{62} = I_{62,max} [A^-]/(K_{½} + [A^-])$ [196]. The operation of long-range ionic effects on the surface of dilute electrolyte solutions was surmised long ago from the surface tension minima observed in electrolyte solutions at ~ 1 mM. Such effects were accounted for by electrostatic interactions among ions that saturate the surface of water at ~ 1 mM [200], i.e., in the concentration range where we observe a sharp increase of HNO_3 dissociation 'on water'. From Figure 3.2 we derive $K_{½}$ = 128 μM (NaCl) and $K_{½}$ = 77 μM ($MgSO_4$) (i.e., the concentrations at which the interface would be half-saturated with catalyzing anions), which are commensurate with the $[NaCl]_{max}$ = 400 μM and $[MgSO_4]_{max}$ = 200 μM values deduced from SHG experiments [196].

Although neither Cl^- nor SO_4^{2-} are as surface-active as I^- or ClO_4^- [198], they should approach the air-water interface closer than the $\langle R_{ion\text{-}ion} \rangle$ separations prevalent at the onset of catalytic effects.

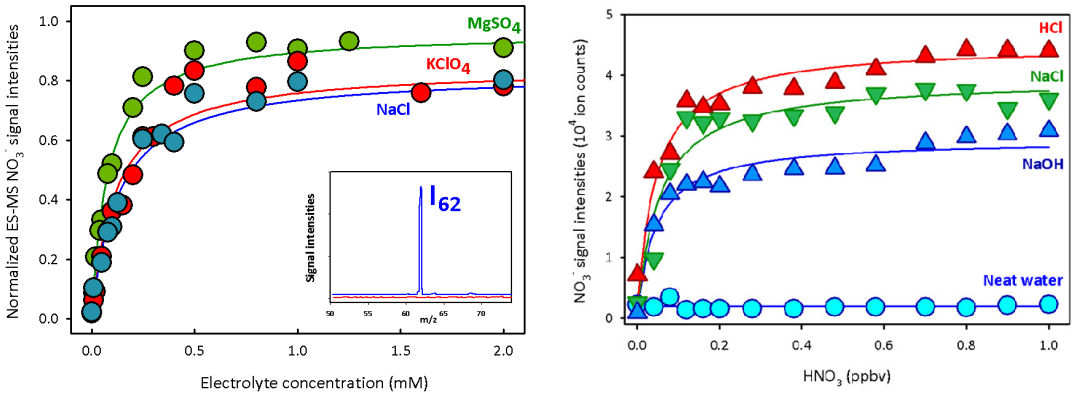

Figure 3.2: (A) Electrospray mass spectral nitrate signal intensities (I_{62}) detected on aqueous $MgSO_4$, $KClO_4$ or NaCl microjets exposed to 3×10^{12} molecules cm^{-3} of gaseous nitric acid for ≈ 10 μs as functions of electrolyte concentration. Solid curves fit experimental data with Langmuir adsorption functions: $I_{62} = I_{62}^{max}$ [electrolyte]×($K_{½}$ + [electrolyte])$^{-1}$; $K_{½}$ = 77 μM ($MgSO_4$), 117 μM ($KClO_4$) and 128 μM (NaCl). Inset shows ESIM spectrum (signal intensities in arbitrary units) on deionized water (red) and 1 mM NaCl (blue). All experiments under 1 atm of N_2 at 293 K. (B) Electrospray mass spectral nitrate signals (m/z = 62) detected on pure water, and on 1 mM HCl, NaCl or NaOH microjets exposed to gaseous nitric acid for ≈ 10 μs as function of HNO_3(if) concentration. All experiments in 1 atm of N_2 at 300 K.

3.4 Evidence for the Surface Specificity of Our ESIMS Platform

Interfacial Hydronium ion, H_3O^+(if), the counterpart of NO_3^-(if) in R_1, was tracked by using hexanoic acid (PCOOH) as a proton scavenger. PCOOH is both a weak acid and a weak base 'in water': pK_a(PCOOH)(aq) = 4.8, pK_a($PCOOH_2^+$)(aq) = -3. In Section 2.5, Chapter 2 we showed that the gas-phase hexanoic acid colliding with the surface of mildly acidic water could be protonated such that pK_a($PCOOH_2^+$)(if) = 2.5. Figure 3.3(A) is a schematic of the interfacial region of 1 mM PCOOH in 1:1/D_2O:H_2O microjets (at pH 8, adjusted by concentrated NaOH) exposed to either HNO_3(if) or DNO_3(if) is presented. Figure 3.3(B) displays I_{117} ($PCOOH_2^+$), I_{118} ($PCOOHD^+$) and

I_{119} ($PCOOD_2^+$) signal intensities from 1 mM PCOOH in 1:1/D_2O:H_2O jets as functions of gas-phase HNO_3(if) or DNO_3(if) concentrations. The inset in Figure 3.3(B) shows the corresponding I_{62} and I_{115} ($PCOO^-$) signal intensities versus HNO_3(if) concentration. It is apparent that: (1) $PCOO^-$ is promptly neutralized, along with the appearance of NO_3^- upon exposure to the lowest HNO_3/DNO_3(if) concentrations, whereas (2) the protonation/deuteration (hydronation) of the weaker base PCOOH requires exposure to at least $n > 2 \times 10^{12}$ molecules cm^{-3}. The fact that HNO_3(if) readily dissociates on water containing the anions of either a stronger acid [pK_a(HCl)(aq) = -7 versus $pK_a(HNO_3)$(aq) = -1.4] or a weaker one [pK_a(PCOOH)(aq) = 4.8] provides further support to the assertion that anions function as catalysts rather than proton acceptors. The appearance of hydronated species (($PCOOH_2^+$), ($PCOOHD^+$) and ($PCOOD_2^+$)) in fact reveals that the surface of the jet has been acidified (from pH 8) to pH < 2.5. In Figures 3.3 B andC, the ratios $\alpha = I_{117}/I_{118} = PCOOH_2^+/PCOOHD^+$, $\beta = I_{118}/I_{119} = PCOOHD^+/PCOOD_2^+$ report the H/D composition of the interfacial layers of 1 mM PCOOH in 1:1/D_2O:H_2O microjets exposed to either HNO_3(if) or DNO_3(if). The statistical protonation/deuteration (hydronation) of $PCOO^-$ in interfacial layers of proton molar fraction x_H leads to: $\alpha = \frac{x_H}{2\,(1-x_H)}$; $\beta = \frac{2x_H}{1-x_H}$. From the asymptotic ratios: α = 1.92, β = 6.0 measured under [HNO_3(if)] > 7×10^{12} molecules cm^{-3} we derive: x_H = 0.77 ± 0.02. Similarly, from α = 0.93, β = 3.4 under [DNO_3(if)] > 6×10^{12} molecules cm^{-3}, we obtain: x_H = 0.64 ± 0.01. As a reference, the α = 1.31 ratio measured in 1 mM PCOOH in 1:1/H_2O:D_2O at pH ≈ 3.0 microjets *not* exposed to gaseous nitric corresponds to x_H^0 = 0.72 (rather than x_H^0 = 0.50). Therefore, the fraction of protons in interfacial layers increases from x_H^0 = 0.72 to x_H = 0.77 under HNO_3(if) and decreases to x_H = 0.64 under DNO_3(if). Since x_H^0 is perturbed to similar but opposite extents (by ± 9% on average) upon exposure to HNO_3(if) or DNO_3(if), we infer (1) a small KIE for the interfacial dissociation of H(D)NO_3(if), (2) a ~ 90 % contribution by the 1:1/D_2O:H_2O solvent to the isotopic composition of interfacial layers under present experimental conditions. Since ~ 0.6 mM hydrons are delivered under $n = 7 \times 10^{12}$ H(D)NO_3(if) molecules cm^{-3}, we infer that the effective water concentration in the interfacial layers is ~ 0.03 M. In other words, since these results are achieved under conditions where the number of hydrons delivered by HNO_3/DNO_3(if) on interfacial layers is ~ 10^3 times smaller than those carried by the 50 μL min^{-1} 1:1/D_2O:H_2O aqueous jet, the former must be confined to thin (Δ[cm]) interfacial layers during the lifetime of the jet.

Interestingly, the fact that the relative abundances of the $PCOOH_2^+$, $PCOOHD^+$, $PCOOD_2^+$ isotopologues are appreciably different under HNO_3(if) or DNO_3(if) (Figure 3.3A and B) confirms that hydrons delivered by gaseous nitric acid remain (i.e., do not diffuse into and rapidly scramble their isotopic labels with the bulk solvent) in the interfacial layers sampled by our technique (See Figure 3.4).

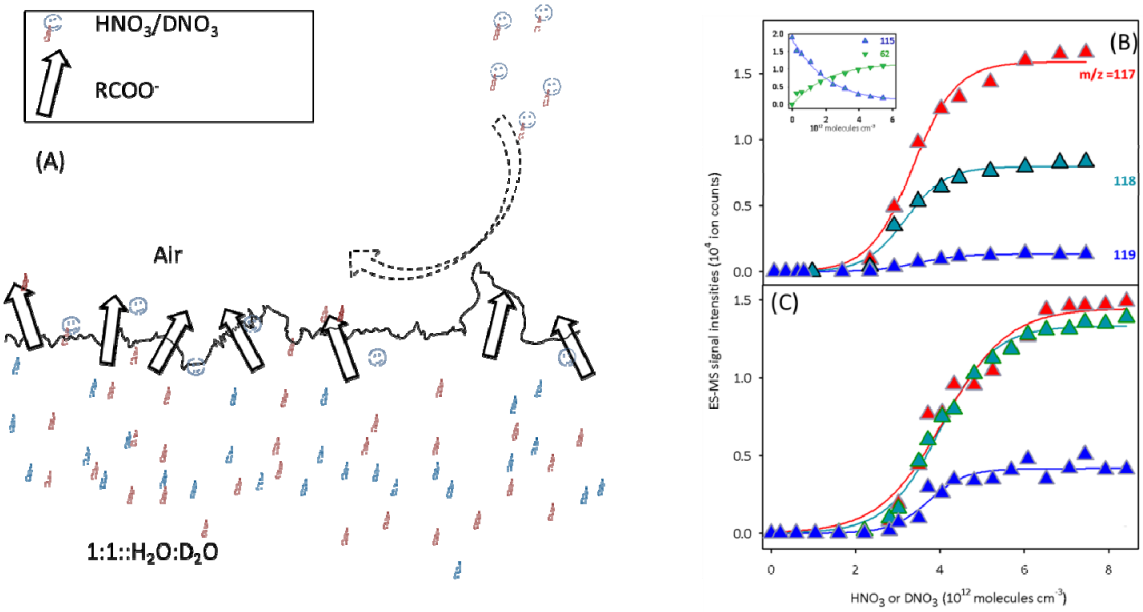

Figure 3.3(A): Schematic of our experiment wherein gas-phase HNO_3/DNO_3 molecules alight the surface of 1mM hexanoic acid solution in 1:1::H_2O:D_2O mixture maintained at pH 8 by addition of concentrated NaOH. Presence of OH- and hexanoate ions (arrows) at the surface facilitate proton transfers from the incoming nitric acid molecules, leading to protonation of the air-water interface exhibited as hydronation (i.e., addition of two H^+, or two D^+, or one H^+, and one D^+) of hexanoate ions and detected via mass spectrometry. Figure 3.3(B): Electrospray mass spectral signal intensities of protonated isotopologues of hexanoic acid (PCOOH): m/z = 117 ($PCOOH_2^+$), m/z = 118 ($PCOOHD^+$) and m/z = 119 ($PCOOD_2^+$) detected on 1 mM PCOOH solutions in 1:1/D_2O:H_2O microjets exposed to variable concentrations of gaseous HNO_3 (a) or DNO_3 (b). The inflection point corresponds to $pK_a(PCOOH_2^+)$(if) = 2.5.[52] The inset in Figure 3.3 (B) shows the evolution of the $PCOO^-$ (m/z = 115) and NO_3^- (m/z = 62) signals detected in negative ion mode. All experiments under 1 atm of N_2 at 293 K.

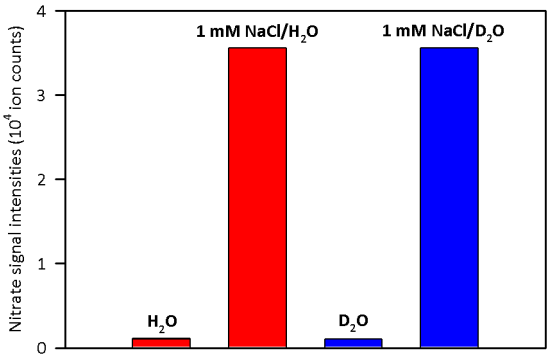

Figure 3.4: Electrospray mass spectral nitrate ($m/z = -62$) signal intensities detected on microjets of deionized H_2O, 1-mM NaCl/H_2O, D_2O, and 1-mM NaCl/D_2O exposed to 4-ppbv gaseous nitric acid for approximately 10 μs at pH of approximately 8. It is apparent that the extent of dissociation of gaseous nitric acid is nearly independent of reactant or solvent deuteration KIEs. All experiments in 1 atm of N_2(if) at 293 K.

These observations raise a straightforward question: *Why do the protons/deuterons delivered at the air-water interface not penetrated interfacial region, to be solvated in the bulk right away?* In fact, recent experiments of Pohl and co-workers investigating the lipid-water interface also made the same observation, but a clear reasoning underlying the presence of ~ 10 k_BT kinetic barrier for protons to re-enter the bulk remains unclear.[201] These observations are also in sync with the previous work of Mulkidjanian and co-workers investigating proton dynamics at protein-water interfaces.[17, 18] These results also remind us of the chemiosmotic phosphorylation implicated in bioenergetic transduction at lipid-water interface.[19, 202-206]

3.5 Theoretical Predictions

What is the minimum number of additional water molecules *m* that renders reaction R_1 exoergic? The free energy required to produce a hydrated contact ion pair at the air-water interface, ΔG^0_1, can be estimated as the sum of the gas-phase process: $\Delta G^0_2(HNO_3(g) + H_2O(g) \rightarrow NO_3^-(g) + H_3O^+(g))$ = 160 kcal mol^{-1} [182], plus the electrostatic energy released as the infinitely distant gas-phase point charges reach a ~ 3.3 Å separation in the contact ion pair: E_{el} = - 100 kcal mol^{-1}, plus the free energy of hydrating $H_3O^+(g)$: $\Delta G^0_3(H_3O^+(g) + m\ H_2O(aq) \rightarrow m\ H_2O{\cdot}H_3O^+(aq))$: $\Delta G^0_1 = \Delta G^0_2 + E_{el} + \Delta G^0_3$ =

60 kcal mol^{-1} + ΔG^0_3. Extant thermochemical data on (m $H_2O{\cdot}H_3O^+$) clusters [207] show that $\Delta G^0_3(m \geq 4) < -60$ kcal mol^{-1}, i.e., R_1 *is thermodynamically allowed for* $m \geq 4$*, even if* NO_3^-*(if) were not hydrated at all* [208]. The hydration of NO_3^-*(if)* will, of course, contribute to the exoergicity of the whole process. Since HNO_3 should be able to interact with at least four water molecules upon impact with the surface of water [194], the barrier hindering reaction R1 may not be thermodynamic. Its origin, however, is not immediately apparent. It has been proposed that acid-base equilibria at the air-water interface might be shifted (relative to bulk water) toward neutral species by ≈ ± 2 pK_a units [209]. In the case of nitric acid, $pK_a(HNO_3(aq)) = -1.4$, this proposal would make HNO_3*(if)* a strong acid at the interface: $pK_a(HNO_3(if)) \sim 0$, at variance with our observations. We wish to emphasize that in our experiments, in contrast with most other studies [210], HNO_3 approaches the air-water interface from the vapor instead of the water side. Hence, gas-phase ion thermochemistry [182, 207] provides a more realistic framework for analyzing our results.

Against this background, we performed density functional theory (DFT) simulations on water decamers W_{10} ($W \equiv H_2O$) interacting with HNO_3 in the absence and presence of Cl^- to ascertain the molecular basis of our experimental observations. Two model water clusters were considered as surrogates for the air-water interface: one with ten water molecules, and another with twenty at X3LYP[211-213] and B3LYP[214, 215] levels of theory, respectively. Gibbs free energies (ΔG) at 298K were computed from calculated enthalpies (ΔH) and entropies (S) according to $\Delta G = E_{elec} + ZPE + H_{vib} - TS_{vib}$. Geometries of energy minima and transition states were optimized using the 6-31G**basis for light atoms [216], and 6-311G**++ for Cl^- [217]. Hessians at these geometries provided harmonic zero-point energies, vibrational enthalpies and entropies. Neglect of anharmonicity effects (< 1 kcal mol^{-1}) may not affect the main conclusions. Calculations of nitric acid interactions with water/electrolyte clusters were initialized by positioning a nitric acid molecule close to one of the waters of the cluster, and to the five waters nearest to chloride in $(Cl{\cdot}W_{10})^-$ (Figure 3.5). Product structures created out of the three lowest-energy adducts by separating the proton from nitrate with none, one or two waters were then energy-minimized. We found stable zwitterion products separated by one and two waters in the presence of chloride, and by two waters in its absence. The lowest-energy products in each case correspond to ion pairs separated by two waters. Transition states, TS, for transforming adducts into stable products were then searched by optimizing structures in which the six O-H bonds connecting nitrate with hydronium were

constrained, until the chosen set of constraints led to an imaginary frequency vibration. The path of steepest ascent is then followed by tracking the eigenvector of the motion associated with the imaginary frequency, until an energy maximum is found. Full Hessian harmonic calculations were then performed for the TS structures. We also investigated whether nitric acid would transfer a proton through rather than assisted by chloride. For a W_{10} system, structures in which nitric acid was hydrogen-bonded or fully transferred its proton to chloride, were found to lie G = 1.6 kcal/mol (H = 4.1 kcal/mol) and G = 9.0 kcal/mol (H = 8.38 kcal/mol) above the aforementioned lowest-energy adduct. Thus, chloride assists rather than relay proton transfer in this system. After geometry optimization, the electronic energy E_{elec} was evaluated with the 6-311G**++ basis on all atoms. The free energies of nitric acid and nitrate at 1 atm were calculated using statistical mechanics for ideal gases. Figures 3.5A and B display the calculated Gibbs free energy (ΔG^0) and enthalpy (ΔH^0) profiles at 300 K.

We confirmed that HNO_3 embedded in W_{10} clusters dissociates spontaneously, in accordance with common knowledge, thermodynamics and Car-Parrinello molecular dynamics (CPMD) calculations [184, 185]. HNO_3 molecule alighting on the surface of water weakly binds via two hydrogen bonds with ΔH^0 = - 13.0 kcal mol^{-1} and (by losing translational and rotational entropy) ΔG^0 = -1.2 kcal mol^{-1}. The free energy barrier for transferring a proton from adsorbed HNO_3 into the cluster, while leaving a NO_3^- on its surface, is quite large: ΔG^- = 14.1 kcal mol^{-1}, or 12.9 kcal mol^{-1} above the reactants (Figure 3.5).

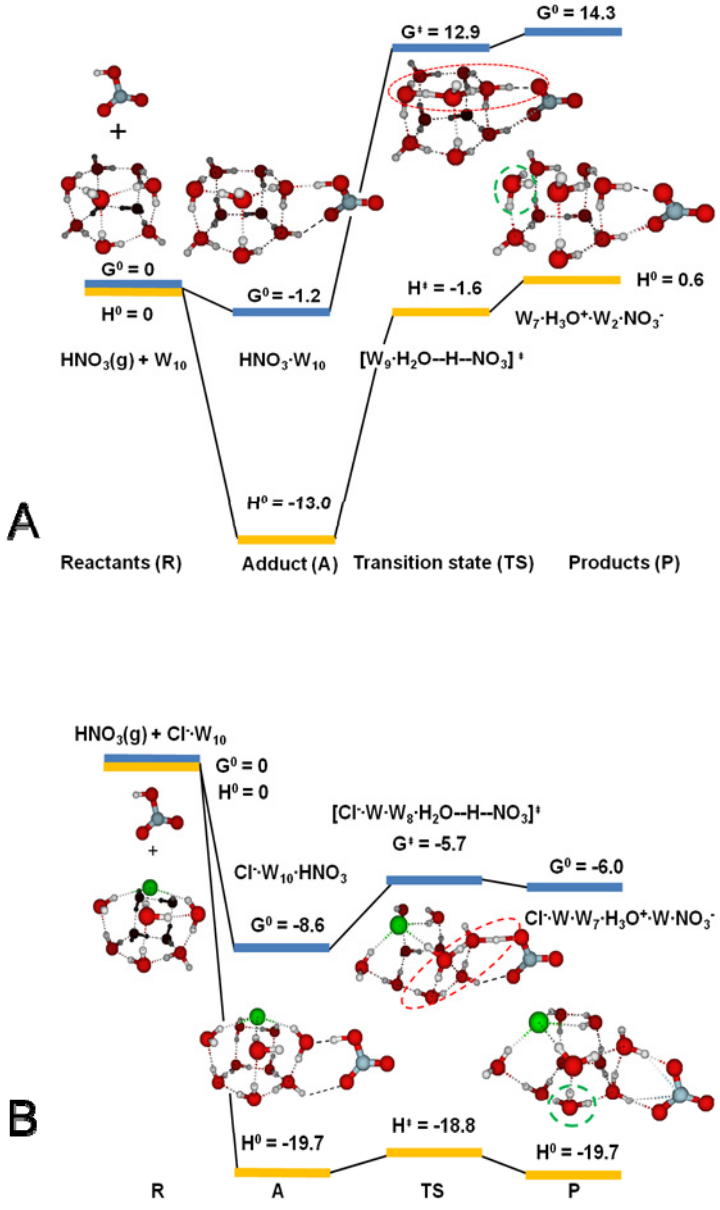

Figure 3.5: Calculated Gibbs free energies (ΔG^0) and enthalpies (ΔH^0) of reactants, adducts, transition states, and products of optimized water clusters in contact with nitric acid in the absence **(A)** and in the presence (**B)** of interfacial chloride. Proton wires highlighted. Energies in kcal mol^{-1}.

These results are in complete agreement with the exhaustive theoretical work of Hynes and co-workers on the dissociation of HNO_3 at the air-water interface.[48, 218-223] The main contribution of our work is the investigation of the catalytic effects of anions in the proton transfer process.

Remarkably, when a Cl^- ion is present at the air-water interface, HNO_3 not only binds more strongly (ΔH^0 = - 18.6 kcal mol^{-1}, ΔG^0 = - 6.9 kcal mol^{-1}) to the surface, but the free energy barrier for transferring a proton from adsorbed HNO_3 to $W_{10}{\cdot}Cl^-$ is dramatically reduced: $\Delta G^{\ddagger}$ = 1.2 kcal mol^{-1}, or 5.7 kcal mol^{-1} below the reactants. (Figure 3.5 B)

To test for limitations in the W_{10} cluster, we repeated the calculations for a W_{20} cluster, which could provide a more accurate molecular framework to investigate local gas-water interactions. We used the energy optimized cluster of twenty water molecules, W_{20}, composed of overlapping ten-membered planes to represent the air-water interface. Several low-energy W_{20} cluster structures are within a 1.0 kcal mol^{-1} free energy range. The structure chosen here is amongst the lowest-energy ones.[224, 225] We found that the results obtained for W_{20} and W_{10} clusters are in close agreement. Thus, we consider that our W_{20} model is adequate to capture the interfacial chemistry of our system; to be described next.

To represent an air-electrolyte interface we optimized the $(Cl{\cdot}W_{20})^-$ adduct produced by adding a Cl^- to the optimized W_{20} cluster. Since our motivation is to find a mechanism to explain our experimental results obtained on ~ 1 mM NaCl solutions, we consider that the inclusion of a Na^+ counterion within a W_{20} cluster would be unrealistic, since this would correspond to 2.8 M NaCl solution. In 1 mM solutions, counterions are separated by distances much larger than those accessible by our QM calculations on small clusters. We find that the Cl^- is stabilized at the surface of W_{20} by accepting five H-bonds from surrounding water molecules. Our observation of anion 'floatation' on water is in agreement with previous experimental[111, 121, 140, 226, 227] and theoretical[138, 145, 227, 228] work on anion fractionation. B3LYP-level DFT [214, 215] was applied towards capturing the phenomenon of anion affinity for the air-water interface, at least on a qualitative level. We tested several structures comprising a Cl^- embedded into water clusters ranging from W_{10}, W_{15}, W_{16} and W_{20} (not shown here). For $W_{20}.Cl^-$ the most stable geometry was chosen for studying proton transfer from HNO_3(if) (Figure 3.6). These results are all consistent with Figure 3.5B. Our conclusion that Cl^- accumulates at the surface of W_{20} implies that the potential of the surface becomes more negative than the cluster interior, thereby enhancing proton

transfer from HNO_3. There is experimental evidence that addition of electrolytes does increase the potential at air-water interfaces.[226] Figure 3.6B shows the free energy and enthalpy landscapes for dissociation of nitric acid on $(W_{20}.Cl)^-$ at 298 K. In contrast to pure water case shown in Figure 3.5A, we observe that:

1. Gas-phase HNO_3 forms stronger H-bonds with the surface of water. The adduct A is more stable than the reactants by $\Delta G^0 = -5.6$ kcal mol^{-1} and $\Delta H^0 = -16.2$ kcal mol^{-1},

2. The free energy and enthalpy barriers for transferring a proton to $W_{20}{\cdot}Cl^-$ are reduced dramatically relative to the pure water case above: $\Delta G^- = 4.5$ kcal mol^{-1} and $\Delta H^- = 0.6$ kcal mol^{-1}. The free energy and enthalpy of the product state after proton transfer were found to be $\Delta G^0 = 2.2$ kcal mol^{-1} higher and $\Delta H^0 = -12.4$ kcal mol^{-1} below than the corresponding values for the reactants. It should be pointed out that the electronic energy of the TS configuration is higher than that of product by 0.17 kcal mol^{-1}, but the addition of zero-point energy corrections and temperature effects nearly equalize their free energies, thereby rendering the reverse ion recombination a diffusionally controlled process, as expected.

By increasing the size of the water cluster, we expect that enhanced solvation of NO_3^- ion should further stabilize the products. Thus, we expect that calculations on much larger clusters will still reflect significant anion effects on HNO_3 dissociation at the surface of water. From these results we envision the process of nitric acid dissociation on aqueous electrolyte surface as follows:

1. A gas-phase HNO_3 molecule collides with the surface of dilute aqueous electrolyte solution at sites that may be, on average, far removed from dissolved Cl^- sticks to it by forming H-bonds with $\Delta H^0 = -4.7$ kcal mol^{-1}.

2. This weakly H-bonded, shallow HNO_3 then diffuses' across the surface for ≈ 1 picosecond eventually approaching a Cl^-, thereby falling into a deeper well followed by proton transfer to nearby waters. Or, the surface-bound HNO_3 desorbs back into the gas-phase.

3. Alternatively the HNO_3 could diffuse undissociated into the bulk liquid where it will dissociate spontaneously a suggested by previous calculations [185, 229] and confirmed by us.

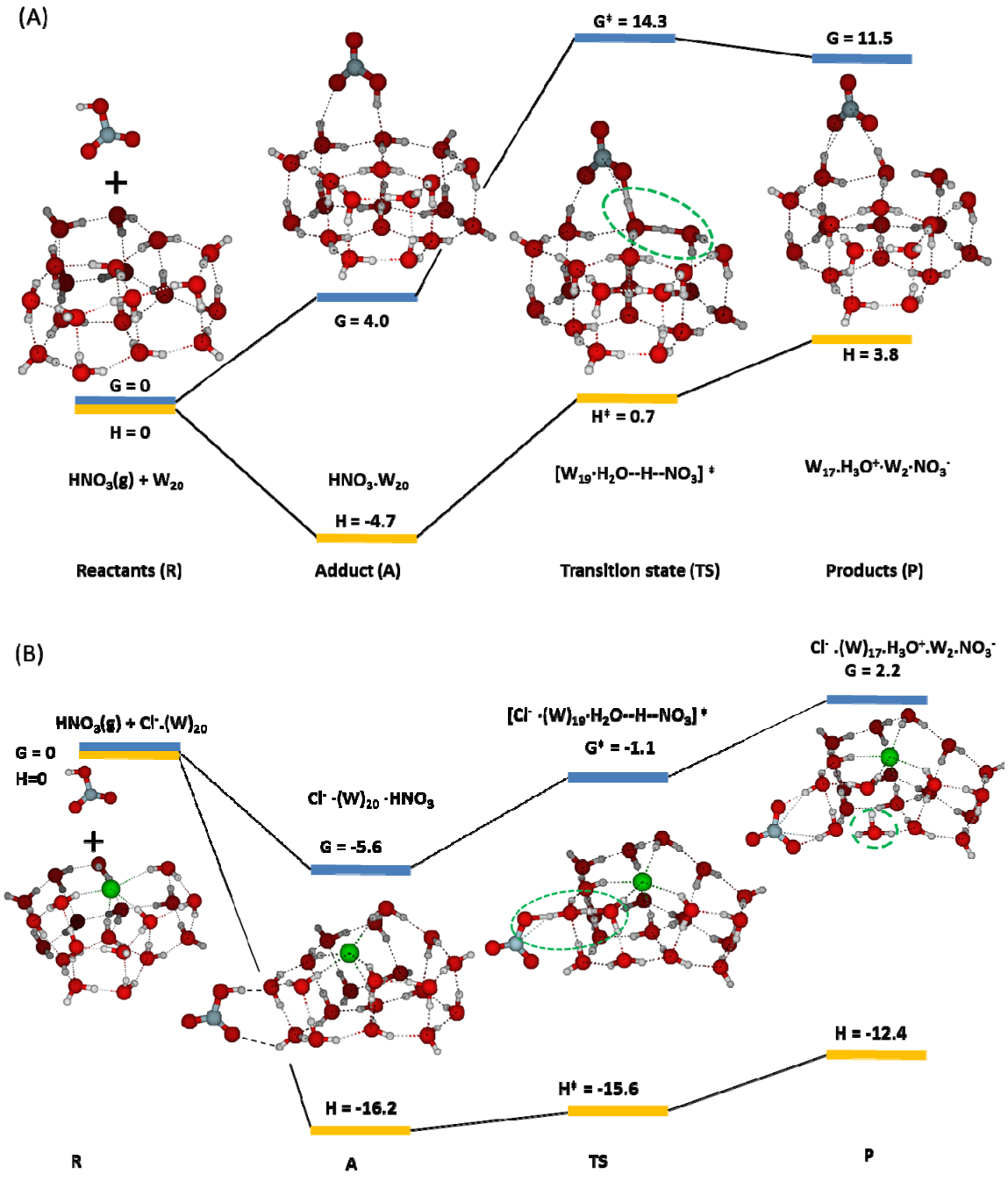

Figure 3.6: Calculated Gibbs free energies (G^0) and enthalpies (H^0) of reactants, adducts, transition states, and products of optimized water clusters in contact with nitric acid in the absence **(A)** and in the presence **(B)** of interfacial chloride. Concerted proton transfer process highlighted. Energies in kcal mol^{-1}.

3.6 Discussion

What is the origin of the barrier for dissociation of the gas-phase HNO_3 on the surface of pure water, and how do interfacial Cl^- ions catalyze this reaction? The answer depends critically on the solvation status of the interfacial NO_3^-. There have been extensive theoretical and experimental investigations of dissolved NO_3^- at air-water interface, but it is not entirely unclear whether NO_3^- resides at the interface or in the bulk.[109, 230-232] We hypothesize that the large size of NO_3^-, which is incompatible with the tetrahedral network of water, and the surface tension of water may conspire against its direct incorporation into water. Thus, after HNO_3 transfers its proton to the surface of water producing an interfacial close ion pair, any further inward proton displacements will both entail moderate stabilization via enhanced H_3O^+ hydration and a large electrostatic destabilizations, unless NO_3^- follows in concert behind. For the aqueous electrolyte case, the interfacial chloride ion attenuates the electrostatic bias on hydronium, H_3O^+, generated by NO_3^-, thereby reducing the barrier. Theoretical simulations provide significant clues about the origin of the barrier to HNO_3 dissociation 'on water'. HNO_3 binds to the surface of water both as a H-bond donor and acceptor, but the NO_3^---H^+ proton, an intrinsic water ion, cannot readily slip into cluster leaving NO_3^- behind (Figure 3.6A). The barrier to PT on the surface of water seems therefore associated with the fact that both (1) overcoming the electrostatic attraction in a disjoint [$NO_3(if)^-$---H^+] ion pair or (2) opening a cavity for NO_3^- to follow after the proton into the cluster, entail significant energy costs. Calculations involving larger water clusters do not eliminate such barrier, as reported by Bianco et al. [194]. Clearly, the presence of chloride, primarily by countering the electrostatic bias imposed on H_3O^+ by laggardly NO_3^- lets H_3O^+ advance into the cluster. We also noticed that the atomic rearrangements involved in binding HNO_3(if) to the air-water interface are largely uncorrelated to those required for subsequent PT. In contrast, the stronger interaction between HNO_3(if) and $(Cl{\cdot}W_{10})^-$ clusters also propitiously primes $(Cl{\cdot}W_{10}{\cdots}HNO_3)^-$ for PT. The reaction coordinate for PT on pure water is a combination of six internal modes involving displacements of heavy oxygen atoms, whereas in the presence of chloride PT proceeds adiabatically along a three-link proton wire between quasi-degenerate solvent states (See Figures 3.7A and B and their animation at http://www.wag.caltech.edu/catalysis/projects/PT.html) [233].

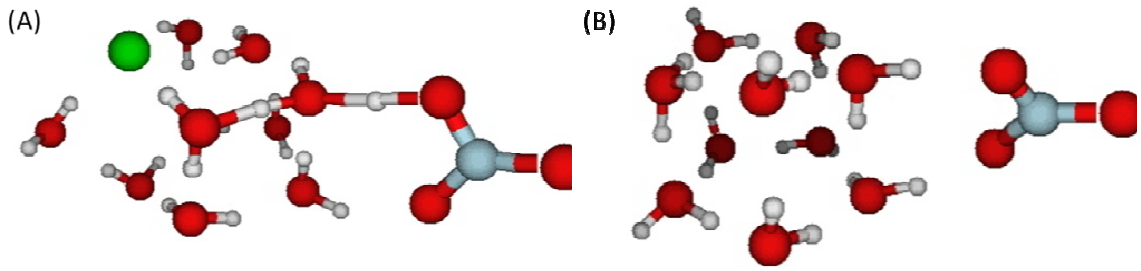

Figure 3.7: Vibration modes of atoms during the proton transfer process: (A) heavy atoms vibrate, (B) heavy atoms vibrate much less. Thus, concerted proton transfer process is amenable in the presence of interfacial anion. Please see the animation of these vibration modes at http://www.wag.caltech.edu/catalysis/projects/PT.html

After establishing the role of electrostatics in the catalysis of HNO_3 dissociation on small water clusters, we need to understand why catalytic effects are observed in > 30 μM electrolytes, i.e., at $\langle R_{\text{ion-ion}} \rangle$ < 120 nm separations that vastly exceed the size of such clusters. On the basis of our calculations we envision that HNO_3(if), after alighting on water, roams rather freely over its surface as HNO_3(if) until approaches an interfacial Cl^-, whereby falls into a deeper potential well and undergoes prompt dissociation. Consider a disk of interfacial water of radius R_S, depth $\Delta = 1.4 \times 10^{-7}$ cm (from Section 3.4), and volume $V_S = \pi R_S^2 \Delta$, centered at a chloride ion. At 30 μM (by assuming uniform concentration throughout) there is 1 Cl^- per $N_W = 2 \times 10^6$ H_2O molecules of volume $V_W = 3 \times 10^{-23}$ cm^3. Therefore, $R_S = (V_W \times N_W \times \Delta^{-1} \times \pi^{-1})^{1/2} = 117$ nm. Thus, a HNO_3 molecule hitting the surface of a > 30 μM solution will have to diffuse on average $R_S < 1.2 \times 10^{-5}$ cm to reach a Cl^- and undergo barrierless dissociation. By assuming that the frequency of diffusional jumps between surface wells of depth E_D can be estimated from transition-state theory as ν_D (s^{-1}) approximately 10^{13} $\exp(-E_D/k_BT)$, we obtain: ν_D approximately 7×10^{10} s^{-1}, with $E_D \sim 3$ kcal mol^{-1} at 300 K. The time to make 376 jumps of length 3×10^{-8} cm to cover the distance $R_S = 1.2 \times 10^{-5}$ cm is therefore $376/\nu_D$ approximately 5 nanoseconds, which is comparable to the residence time of adsorbed gases on the surface of water (11). Thus, we estimate that average number of hops required by HNO_3(if) to reach a Cl^- on the surface of > 30 μM solutions would take a few nanoseconds, i.e., in a time scale and is commensurate with half-times towards back desorption into the gas-phase [161, 234, 235]. Thus, present experimental results substantiate a key role for electrostatics in the mechanism of HNO_3 dissociation at water-hydrophobe interfaces, and suggest that even sparse anions can effectively catalyze this process.

Chapter 4

BRØNSTED BASICITY OF THE AIR-WATER INTERFACE

Abstract – Variations in the protonation of functional groups on either side of water-hydrophobe interfaces are essential to atmospheric aerosol-gas exchanges, enzymatic catalysis, molecular recognition, and bioenergy transduction. The sign and range of such variations, however, are essential to understand remain to be established experimentally. Herein we report experiments showing that gaseous carboxylic acids RCOOH(g) begin to deprotonate on the surface of water more acidic (by ≈ 2 pH units) than that supporting the deprotonation of the same acids dissolved in water. Thermodynamic analysis indicates that > 6 H_2O molecules must participate in the deprotonation of RCOOH(g) on water, but quantum mechanical simulations on a model air-water interface predict that such event is hindered by a significant kinetic barrier unless OH^- ions are present therein. Thus, by detecting $RCOO^-$ on pH > 2 water exposed to RCOOH(g) we demonstrate the presence of OH^- on the aerial side of water. Furthermore, because in similar experiments the base $(Me)_3N$(g) is protonated only on pH < 4 water (See Section 2.5.1 in Chapter 2), we infer that the outer surface of water is Brønsted neutral at pH ≈ 3 (rather than at pH 7 as bulk water), a value that matches the isoelectric point of bubbles and oil droplets determined in independent electrophoretic experiments. The OH^- densities sensed by RCOOH(if) on the aerial surface of water (~10^9 cm^{-2}) are 100 times smaller than those at the (> 1 nm) deeper shear planes probed in electrophoresis thereby implying the existence of OH^-gradients in the interfacial region, which could account for the weak OH^- signals detected by surface-specific spectroscopies. Lastly, detection of pH ≈ 3 OH^- at the air-water interface on the surface of pure water within $\tau < 10$ μs also indicates a faster autodissociation rate of water therein.

4.1 Introduction

Acid-base chemistry at aqueous interfaces lies at the heart of major processes in chemistry and biology. Changes in the degree of dissociation of the acidic/basic residues upon translocation between aqueous and hydrophobic microenvironments orchestrate enzyme catalysis [236] drive proton/electron transport across biomembranes [237, 238] and mediate molecular recognition and self-assembly phenomena [239-241]. In spite of its importance, the characterization of acid-base chemistry at aqueous interfaces remains shrouded with unknowns [73, 166, 242-244].

Air-water interface is characterized by fluctuations and sharp discontinuities in hydrogen-bonding network and density. The dielectric behavior of water within the interfacial region is also found to be anisotropic. Further, along with varying standard states on either side, chemical and physical phenomena at air-water interface have unique thermodynamic, kinetic and dynamic constraints, absent in bulk water. As a result several counterintuitive phenomena appear at the surface of water, such as (1) negative electrical potential/charge of the air-water interface at pH = 7, (2) specific Hofmeister effects, and (3) inability of HNO_3 to dissociate at the air-water interface, though it is a strong acid in bulk water. Basic questions linger about the thickness of interfacial layers [97], how acidity changes through the interfacial region [245] and the mechanistic differences between proton transfer (PT) in interfacial (if) versus bulk (B) water [244, 246]. Since aqueous surfaces are usually charged relative to the bulk liquid [247], the thermodynamic requirement of uniform electrochemical activity throughout (including the interfacial regions) implies that the chemical activity of protons (pH) in interfacial(if) water can be different from that in the bulk (B) liquid. Reduced hydration of ionic species at the interface could force acids and bases toward their undissociated forms [209].

Some of these fundamental issues have been extensively investigated via electrostatic [195] and electrokinetic experiments [73], surface tension studies (and analysis) [248, 249] surface-specific spectroscopies [77, 141, 243, 250] and theoretical (quantum mechanical and molecular dynamics) calculations [242, 251-253]. Some experimental [243] and theoretical [242, 253, 254] results were interpreted to signify that the air-water interface is more acidic than bulk water, whereas others reached the opposite conclusion [73, 77, 166, 251, 255]. The impasse stems in part from the failure to recognize that (Brønsted) acidity is a relative concept describing the extent of proton sharing between two conjugate acid/base pairs under specified conditions. Theoretical predictions and

surface-specific spectroscopies on the *structure* of interfacial water are therefore moot about its *functional* acidity. By definition [256], W is a Brønsted base *if and only if* it can accept protons from Brønsted acids AH, reaction R_1

$$AH + W \longrightarrow A^- + WH^+ \qquad (R_1)$$

An operational measure of the basicity of W as a medium is given by the acidity constant of AH therein: $K_A = [A^-]\,[WH^+]/[AH]$. If W is bulk water, the acidity constant $K_{A,B}$ can be derived from experimental data on the degree of dissociation: $\theta_B = [A^-]/([A^-]+[AH])$, as a function of pH via equation E_1

$$\theta_B = 1/(1 + 10^{\,pKA - pH}) \qquad (E_1)$$

A formal extension of Eq. E_1 to interfacial water would require (θ_{IF}, pH_{IF}) rather than experimentally accessible (θ_{IF}, pH) data. This is an essential difficulty because the estimation of pH_{IF} from pH_B [209, 257] necessarily involves assumptions about ion distributions and the dielectric properties of water in double layers of molecular dimensions [258-261]. Lacking a thermodynamic pH_{IF} scale based on independent measurements, interfacial acidity constants $K_{A,IF}$ become constructs circularly defined from estimated pH_{IF} values. These simple considerations should make it clear that conventional concepts on acidity in bulk phases may be meaningless in connection with interfaces.

It is however meaningful, and consequential, to ask whether the Brønsted basicity of water is different on either side of water/hydrophobe interfaces. Here we sought to answer this question by performing appropriate experiments. Experiments had to ensure that the acidic probe, AH, would exchange its proton with the interface immediately prior to the detection of ($A^- + XH^+$) products. Mapping interfacial layers of molecular thicknesses further calls for static molecular probes locked at specified depths, or dynamic ones that interact with the interface during intervals shorter than characteristic diffusion times through the interfacial region. Below, we report experiments in which the production of A^- is monitored as a function of pH via online electrospray ionization mass spectrometry (ESIMS) of the interfacial layers of injected aqueous jets containing dissolved AH(aq) versus those collided with gaseous AH(if) molecules. [244, 262]

4.2 Experimental Method

Gas-liquid experiments were conducted by intersecting free-flowing aqueous jets with $C_5H_{11}COOH(g)/N_2(g)$ beams in a chamber held at 1 atm, 293 K, and detecting the formation of $C_5H_{11}COO^-$ therein via electrospray ionization mass spectrometer (ESIMS). Our ESIMS has been described in detail in Chapter 2 and references [37, 40, 123].

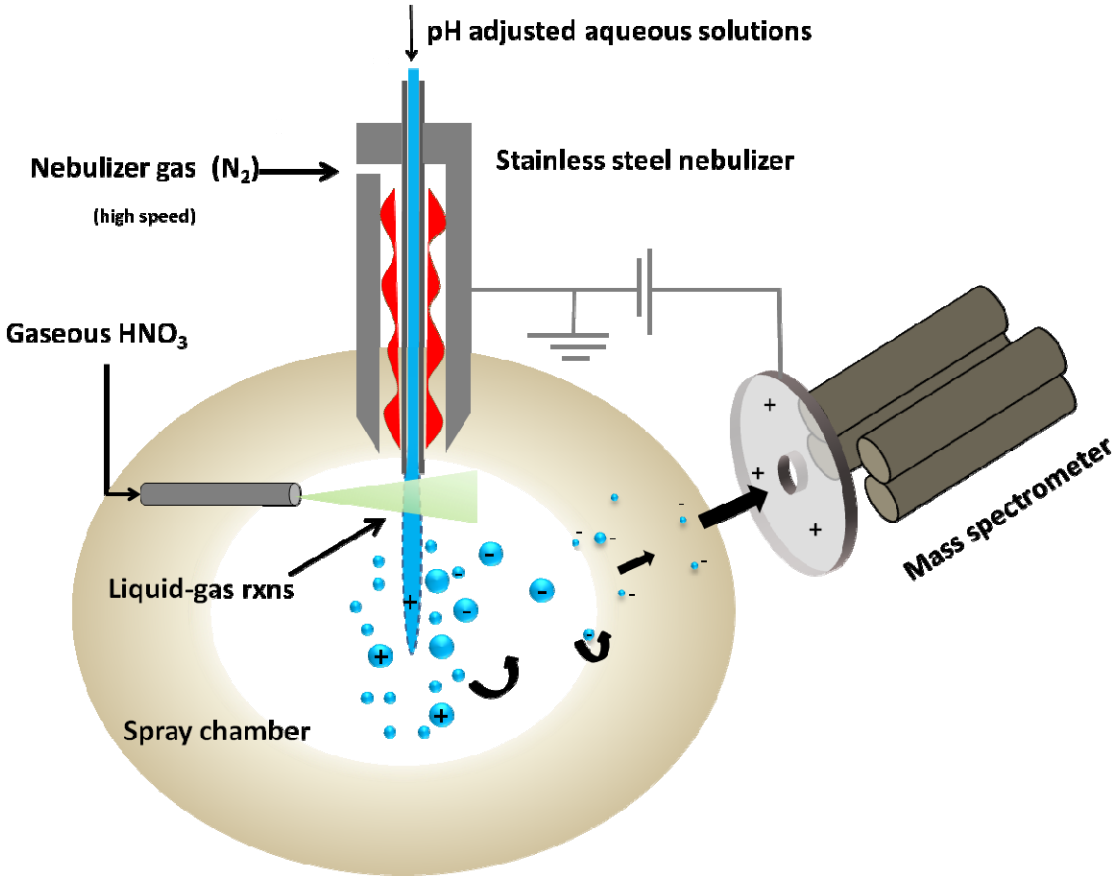

Figure 4.1: Schematic of our ESIMS platform tracking proton transfer events during gas-liquid collisions.

4.3 Experimental Results

The results of a typical experiment are shown in Figure 4.2, in which the formation of hexanoate ($RCOO^-$, $R \equiv C_5H_{11}$, m/z = 115, detected by online ESI-MS and reported as I_{115} signal intensities) on the surface of aqueous jets (1) containing dissolved RCOOH(aq) or (2) externally exposed to RCOOH(if), is plotted as a function of pH. Throughout, pH is the pH of the injected solutions, adjusted with HCl/NaOH and measured with a calibrated pH meter prior to injection. We found that 50% of the injected RCOOH(aq) dissociates into $RCOO^-$ at $pH_{½} = 4.8 \pm 0.2$ (the inflexion point of the I_{115} versus pH titration curve), which is identical to the acidity constants, pK_A, of short-chain alkyl carboxylic acids determined by conventional analytical procedures [263].

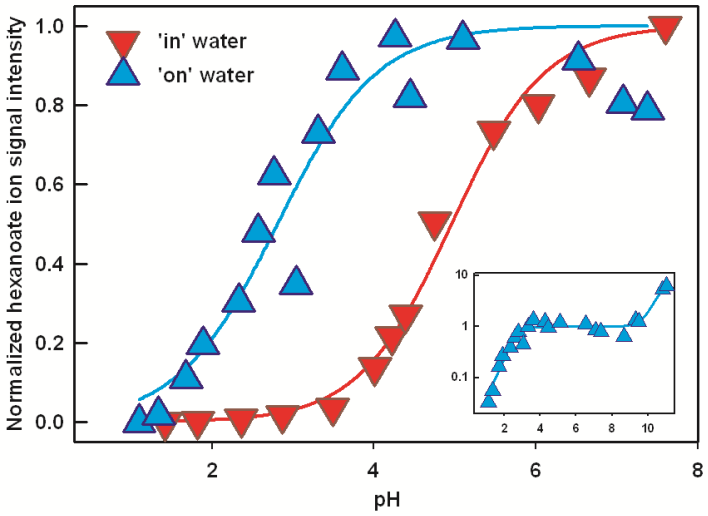

Figure 4.2: Normalized electrospray ionization mass spectral signal intensities of hexanoate ion $RCOO^-$ ($R = C_5H_{11}$, m/z = 115) on the surface of water jets (1) containing 1 mM RCOOH(aq) (downward triangles), (2) exposed to 770 ppbv RCOOH(if) (upward triangles) for ≈ 10 μs (1 ppbv = 2.4×10^{10} molecules cm^{-3} at 1 atm, 293 K) as functions of the pH of jet water. Midpoints at (1) $pK_A = 4.8 \pm 0.2$, (2) $pH_{½} = 2.8 \pm 0.2$. The inset shows the results of case (2) experiments carried over a wider pH range. Detection of interfacial hexanoate ions via our ESIMS setup on-water (blue) and in water (red). Experimental procedure described in detail in Section 2.5 of Chapter 2.

This result corroborates the reliability of our experimental setup and provides a calibration set-point for our measurements. The key finding, however, is that RCOOH(if) dissociates upon colliding on the surface of water jets that are ≈ 2 pH units more acidic than in case (1), leading to a titration curve with a $pH_{½} = 2.8 \pm 0.2$ midpoint (Figure 4.2). The second major difference between both experiments is that the limiting I_{115} signals reached above pH ~ 5 only extend to pH ~ 9, before increasing again about fivefold above pH ~ 10 (see inset, Figure 4.2). This fact indicates that the nature of the W/WH^+ conjugate pair presented by the surface of water to incoming RCOOH(if) changes above pH ~ 10. To sum up, the results of Figure 4.2 represent unambiguous evidence that RCOOH(if) and RCOOH(aq) are deprotonated to significantly different extents on either side of the air-water interface at the same pH. They also confirm that the $RCOO^-$ detected in case (2) are produced on the aerial side of the interface, i.e., prior to the dissolution of RCOOH(if) in bulk water, because otherwise we should have obtained the same titration curve in both cases. The addition of inert electrolytes, such as NaCl, in the sub-millimolar range has little effect on these results (Figure 4.3). Present results, which are the counterpart of the observations we made in similar experiments involving the protonation of the strong-base trimethylamine (See Section 2.5.1, Chapter 2) on aqueous jets [244], represent, to the best of our understanding, *the first experimental determination of the functional basicity of the air-water interface*.

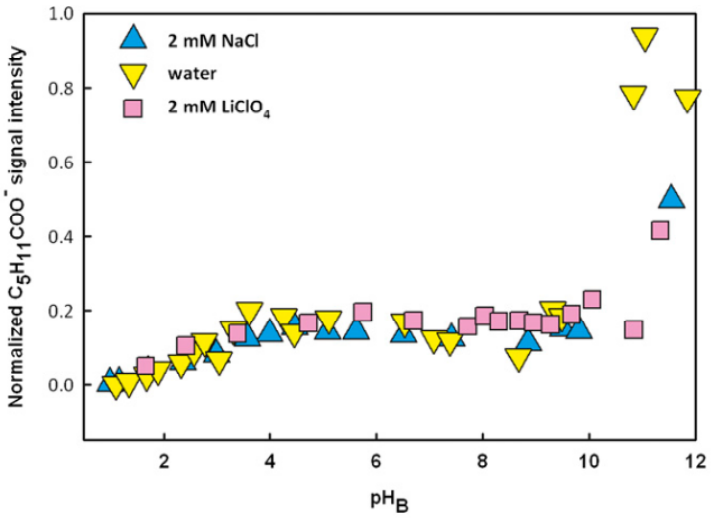

Figure 4.3: Dissociation of gaseous hexanoic acid vapors at the air–water interface as a function of the pH of bulk water in the absence and presence of inert electrolytes. Unlike the case of the strong HNO_3 (as seen in Chapter 3, Figure 3.1), inert anions are unable to catalyze the dissociation of a weak carboxylic acid. All experiments in 1 atm of N_2 at 293 K.

Figure 4.4 shows how $RCOO^-$ increases as a function of the concentration of RCOOH(if) on water jets of three different acidities. Notably, $RCOO^-$ production plateaus above ≈ 300 ppbv RCOOH(if) both at low (pH 2.1) and high (pH 10.1) acidities, but still increases at ~ 800 ppbv RCOOH(if) over pH 5.1 water. It is apparent that (i) RCOOH(if) does not transfer its proton directly to the aerial side of water, i.e., W in reaction R1 is not H_2O but a more reactive basic species, probably interfacial OH^-, OH^-_{IF}, (ii) the production of $RCOO^-$ on the surface of water is limited by the availability of OH^-_{IF} at pH 2.1 and 10.1, and by [RCOOH(if)] (up to and beyond 800 ppbv) at midrange pH values.

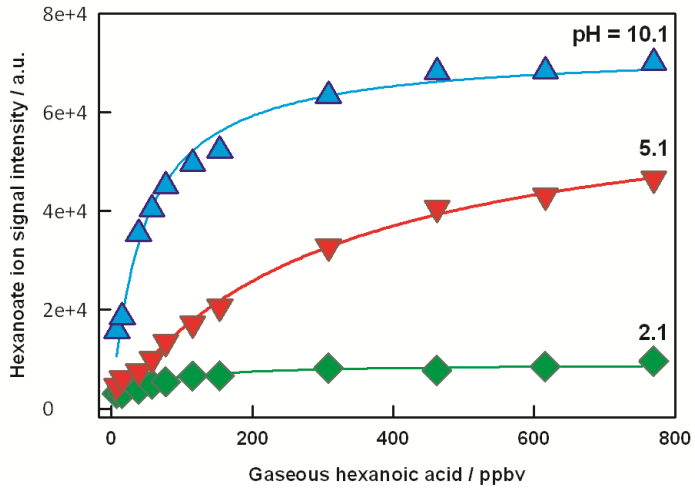

Figure 4.4: Normalized electrospray ionization mass spectral signal intensities of hexanoate ion $RCOO^-$ ($R = C_5H_{11}$, m/z = 115) on the surface of water jets exposed to variable concentrations of RCOOH(if), at pH 2.1, 5.1 and 10.1. Curves correspond to data regressions to Langmuir adsorption isotherms: $\Gamma = \Gamma_{MAX} \times [RCOOH(if)]/(K_{½} + [RCOOH(if)])$ $\Gamma_{MAX} = I_{115,MAX} = 9.1 \times 10^3$, 6.5×10^4, and 7.2×10^4 (in arbitrary units); $K_{½} = 42$, 308 and 46 ppbv at pH 2.1, 5.1 and 10.1, respectively.

Regression of the data of Figure 4.4 to a Langmuir adsorption functional: $\Gamma = \Gamma_{MAX} \times [RCOOH(if)]/(K_{½} + [RCOOH(if)])$, yields: $\Gamma_{MAX} = I_{115,MAX} = 9.1\times 10^3$, 6.5×10^4, and 7.2×10^4 (in arbitrary units), $K_{½}$ = 42, 308, and 46 ppbv at pH 2.1, 5.1 and 10.1, respectively. The physical implications of these results are that (i) the surface becomes saturated with OH^-_{IF} at pH > $pH_{½}$ = 2.8 (because $\Gamma_{MAX}(10.1) \sim \Gamma_{MAX}(5.1) >> \Gamma_{MAX}(2.1)$) and (ii) OH^-_{IF} is ~ 7 times less reactive at pH 5.1 than at pH 10.1 (because $K_{½}(5.1)$ is ~ 7 times larger than $K_{½}(10.1)$). In other words, it is the reactivity of OH^-_{IF} toward RCOOH(if), rather than its concentration, that increases above pH 10.1. The higher reactivity of OH^-_{IF} above pH 10.1 is consistent with its closer approach to an increasingly screened negatively charged interface in more concentrated solutions.

The OH^-_{IF} surface density, $\sigma_{OH\text{-}IF}$, sensed by RCOOH(if) molecules on the aerial side of water could be estimated from the frequency of RCOOH(if) collisions with the surface of the jet given by the kinetic theory of gases: $f[cm^{-2}\ s^{-1}] = ¼\ \gamma\ c\ n$. We obtain: $\sigma_{OH\text{-}IF} \sim (3 – 15) \times 10^9\ OH^-\ cm^{-2}$, at pH 5.1 and 10.1, i.e., a surface-charge density of: $\sigma_{qOH} \sim (0.5 – 2.5)$ nC cm^{-2}. We notice that the estimated value of σ_{qOH} is ~ 10^3 times smaller than the surface-charge densities $\sigma_\zeta > 1$ μC cm^{-2} deduced from the ζ-potentials measured in the electrophoretic of bubbles and oil droplets in water of pH higher than their isoelectric point pI ~ 3 [73, 166]. The discrepancy exceeds the combined stated uncertainties of σ_{qOH} and σ_ζ and is deemed significant. This issue is analyzed later in Section 4.6 and 4.7.

4.4 Thermochemical Considerations

The above observations are conveniently framed in terms of the thermodynamics of proton transfer from the prototypical carboxylic acid CH_3COOH to X = H_2O or OH^- [208, 246, 264, 265] reactions R_2 and R_3

$$CH_3COOH(g) + H_2O(g) \longrightarrow CH_3COO^-(g) + H_3O^+(g) \qquad (R_2)$$

$$CH_3COOH(g) + OH^-(g) \longrightarrow CH_3COO^-(g) + H_2O(g) \qquad (R_3)$$

viz.: $\Delta G_2° = 182$ kcal mol^{-1}, $\Delta G_3° = -43$ kcal mol^{-1} [264]. The large endoergicity of R_2, in which infinitely separated ions are created from neutral species, is reduced by ~ 100 kcal mol^{-1} if products

are brought to the contact ion-pair separations (~ 3 Å) reached in the early stages of proton transfer [208]. The participation of six additional H_2O molecules, leading to partially hydrated $[CH_3COO^-\cdot(H_2O)_3 + H_3O^+\cdot(H_2O)_3]$ contact ion pairs, is sufficient to render R_2 exoergic [265]. Exoergic proton transfer, however, could nevertheless be hindered by a significant kinetic barrier that would prevent R_2 from proceeding fast enough during $CH_3COOH(g)$ collisions with the surface of water [126, 266]. Reaction R_3, in contrast, is exoergic as written, spontaneous both in gas-phase and in aqueous solution and therefore expected to proceed readily at the interface. To provide a molecular underpinning to these anticipated behaviors we carried out quantum mechanical calculations on model water clusters.

4.5 Quantum Mechanical Calculations

We applied the M06 level DFT with 6-311G**++ diffuse basis set to analyze our experimental results. M06 is a hybrid meta-GGA functional that contains kinetic energy density and exact exchange energy on top of a GGA formulation.[103, 267] Various groups, including ours, have confirmed that M06 provides a better description of hydrogen bonding, internuclear distance and chemical kinetics of water clusters than other GGA-, dispersion- corrected GGA, meta-, and hybrid-GGA functionals.[103, 268] Furthermore, we have shown recently that such small water clusters could indeed provide insight into interfacial processes at air-water interface.[40, 269] Gibbs free energies (G) at 298K were computed from calculated enthalpies (H) and entropies (S) according to $G = E_{elec} + ZPE + H_{vib} - TS_{vib}$. Geometries of energy minima states were optimized using the M06 functional [270] and 6-311G** basis [271] for all the atoms. After geometry optimization, the electronic energy E_{elec} was evaluated with the 6-311G**++ basis[272] The Hessians at these geometries were used to determine that the minima and transition states led to 0 and 1 imaginary frequency, respectively. Vibrational frequencies provided zero-point energies and vibrational contributions to enthalpies and entropies. The free energies of acetic acid at 1 atm were calculated using statistical mechanics for ideal gases.

Here we considered clusters of water containing twenty molecules, W_{20} ($W = H_2O$), and clusters containing an additional OH^- ion, $W_{20}.OH^-$. For the $W_{20}.OH^-$ cluster we find that the excess OH^- ion prefers to be at the surface of the cluster. Thus, our model system provides the OH^- at the air-water

interface required to explain the interfacial chemistry observed in our experiments. For pure water, we found that (i) CH_3COOH coordinates to the surface of W_{20} producing weakly bound adducts [$CH_3COOH\cdots W_{20}$], (ii) for a variety of [$CH_3COO^-\cdots W_{19}\cdot H_3O^+$] initial structures in which CH_3COO^- is placed on the periphery of $W_{19}\cdot H_3O^+$ we find that all relax spontaneously to [$CH_3COOH\cdots W_{20}$] (Figure 4.5). These results indicate the existence of a significant barrier for CH_3COOH dissociation on the surface of pure water, which is not lowered by the presence of strong acid anions such as Cl^- ($pK_A(HCl) = -7 << 4.8$).

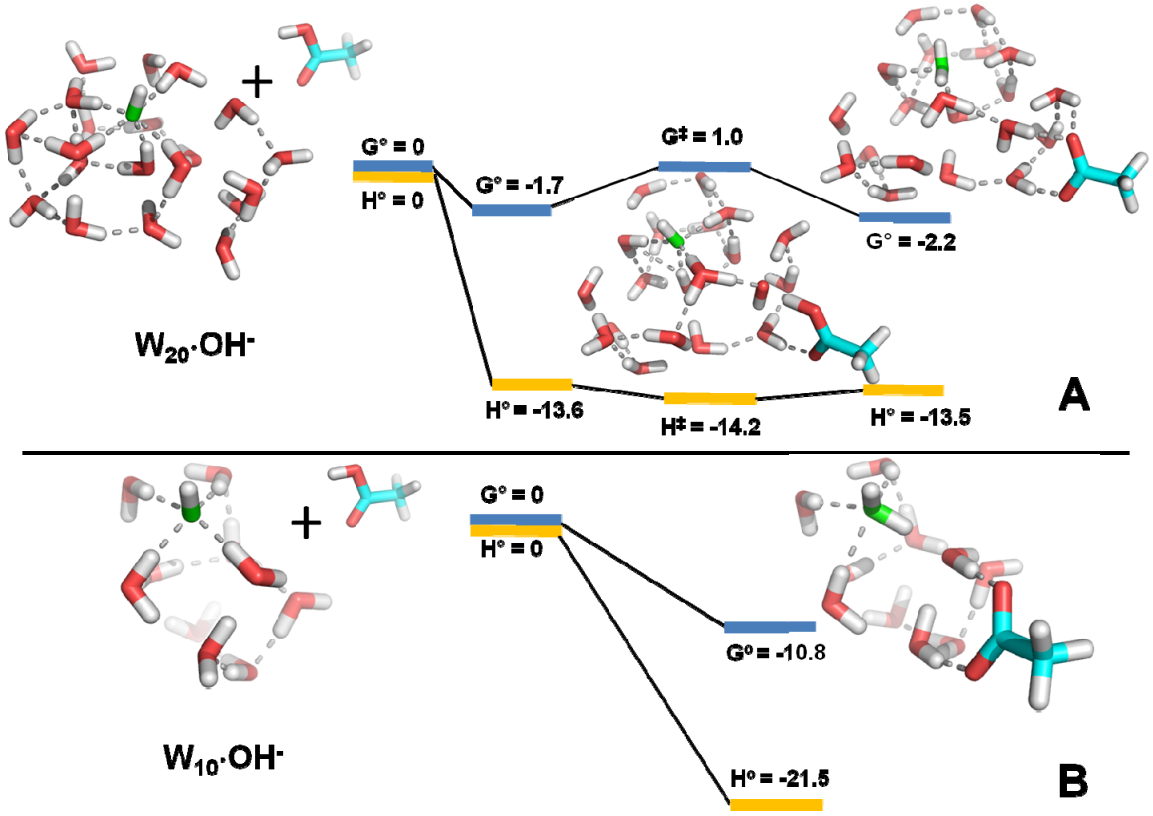

Figure 4.5: (A) Calculated Gibbs free energies (G) and enthalpies (H) (in kcal mol^{-1}) of reactants, adducts, transition states, and products of optimized water clusters containing hydroxide, $W_{20}\cdot OH^-$ in contact with acetic acid. Calculations in the absence of OH^- did not yield stable [CH_3COO^- + H_3O^+] dissociation products. (B) With $W_{10}\cdot OH^-$.

Interestingly, this behavior contrasts with our observations on the dissociation of the strong HNO_3 at the air-water interface, described in Chapter 3 and reference[40, 41]. This dissociation of the weak CH_3COOH on the surface of water is hindered both by the intrinsic kinetic barrier limiting this process 'in water' (a process previously investigated via Car-Parrinello QM metadynamics with the HCTH/120 density functional [266]), and by the additional cost of creating a cavity to accommodate the resulting CH_3COO^- inside the bulk liquid . In the case of a $W_{20}{\cdot}OH^-$ water cluster, the reaction coordinate for proton transfer from CH_3COOH to $W_{20}{\cdot}OH^-$ involves 3 or 4 water molecules, leading to a negligible ($\Delta G° = 2.7$ kcal mol^{-1}, ($\Delta H° = -0.6$ kcal mol^{-1} kinetic barrier and stable reaction products on both free energy and enthalpy surfaces (Figure 4.5). We find that these results depend little on the various close-lying energy minima or the anharmonicity of low frequency vibrations in $W_n{\cdot}OH^-$ clusters [273]., Since $\Delta G_3° = -43$ kcal mol^{-1}, it is quite plausible that an OH^- near the interface would induce barrierless PT.

The mechanism by which anions (including OH^-) are driven to the interfacial region, however, falls outside the scope of this study, which is to investigate the pH dependence of RCOOH dissociation on both sides of the air-water interface. The hierarchy of the interactions (which include electrostatic, inductive, hydrogen-bonding and dispersive interactions) responsible for driving OH^- to the interface are not fully resolved by current density functionals [103, 104, 270, 274-279].

4.6 Discussion

Our reactive gas-liquid experiments demonstrate that OH^-_{IF} ions become available to RCOOH ($pK_A = 4.8$ in bulk water) on the aerial side of pH > 2 water. We conclude that the pH at which $[H_3O^+_{IF}]$ and $[OH^-_{IF}]$ balance each other on the aerial side of water, the point-of-zero-charge, is $pH_{PZC} \sim 3$. Quite significantly, this value coincides with the isoelectric point of water, pI ~ 3, measured at the shear plane of air bubbles [280] and of hydrophobic oil drops [73] in electrophoretic experiments [281]. The 'shear plane' is the outer surface of the water shells that move along with migrating bubbles and drops, and lies a few nm away from the interface proper [73, 166]. Since RCOOH(if) is a specific probe for OH^-_{IF} (recall that PT from RCOOH(if) to the surface of water is kinetically hindered regardless of the orientation of water molecules therein) whereas electrophoretic measurements report net electric charge, the essential coincidence of pH_{PZC} and pI values suggests

that the negative charge of the air-water interface above pH ~ 2.5 should be ascribed to the presence of excess interfacial OH^-_{IF} [73, 166]. This view is consistent with the fact that negative ζ-potentials of colloidal drops and bubbles in the static electric fields of electrophoretic experiments require the presence of negatively charged discrete entities that can migrate independently of their counterions, such as OH^-, rather than of inward-pointing water dipoles or charge transfer [$H_2O^- \cdots H_2O^+$] moieties [282-285]. A potential role for hydrated electrons, $H_2O{\cdot}e^-$, as discrete carriers can be discarded because its formation via: $3\ H_2O = H_2O{\cdot}e^- + H_3O^+ + {\cdot}OH$, is thermodynamically forbidden under ambient conditions [283, 286, 287].

Some surface-specific non-linear spectroscopic studies [199, 243], most theoretical calculations [242, 288, 289], and the ion partitioning analysis of surface tension data on electrolyte solutions [249] have predicted the accumulation of H_3O^+ at and the exclusion of OH^- from the air-water interface. On the basis of such evidence it has been argued that 'water surface is acidic' [242, 253]. It should be apparent by now that 'acid' and 'basic' qualifiers designate the ability of certain bodies, the air-water interface in this case, to exchange protons with other entities under specific conditions and, therefore, strictly apply to chemical reactions rather than to structural features.

4.7 Implications on the Extant Research Literature

The finding that the charge density on the aerial side of the interface, σ_{qOH}, estimated from our reactive gas-liquid experiments is significantly smaller than that detected at the shear hydrodynamic plane,σ_ζ, suggests the existence of non-monotonic OH^-_{IF} vertical profiles. We have recently shown that different anions populate interfacial layers at depths that are inversely correlated with their relative surface affinities [290]. The emerging picture is that surface affinities reflect how close anions approach the interface rather than their relative concentrations within a single subsurfacial layer. Thus, the possibility arises that ion profiles within interfacial double layers could not follow monotonic distributions [259] and, as a result, experiments probing water basicity at different depths can lead to dissimilar results. As a consequence, the low affinity of OH^- for the air-water interface predicated by some calculations [242, 253] and implied by some surface-specific spectroscopies [243] is not in principle incompatible with the sizable charge densities deduced from electrophoretic experiments [166]. Note that these implications are necessarily conditional because

the reported σ_ζ values against which the comparison is made are derived from experimental ζ-potentials by using a continuous Gouy-Chapman model for the double layer based on the dielectric constant of bulk water [259, 260], which may undergo revision.

4.8 Implications on the Autodissociation of Water at the Air-water Interface

The experimental results presented in this chapter were based on sampling the composition of the surface of nascent water jets exposed to RCOOH(if) within ≈ 10 μs after emerging from an electrically grounded nozzle. Thus, our finding that $pH_{PZC} \sim pI$ seems to suggest that equilibrium is established in both cases. However, since our molecular probes find OH^- ions at the air-water interface even at pH = 7, within reaction time < 10 μs, they must be produced at faster rates than those estimated from the dissociation of bulk water, whose characteristic time, $\tau_{dissociation} = k_{forward}^{-1} = (K_w\, k_{backward})^{-1} \sim (10^{-14} \times 10^{11}\ M^{-1}\ s^{-1})^{-1} = 10^3$ s [291, 292], vastly exceed the lifetimes of our water jets [242]. Water autolysis concurrent with OH^- diffusion and binding at the interface may effectively shorten relaxation times into the sub-millisecond timescale [38, 39, 281], but other explanations are possible [293]. We consider that the resulting difference in the concentration of OH^- ions at the air-water interface and bulk gives rise to the negative potential as shown in the Figure 4.6.

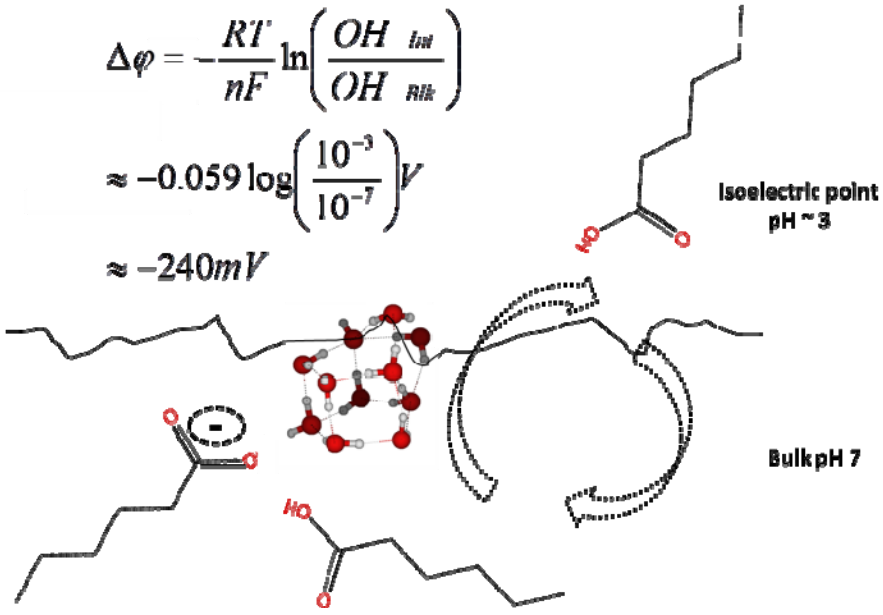

Figure 4.6: Schematic of the air-water interface with an interfacial OH^- ion surrounded by water molecules. Applying Nernst's equation to the concentration of OH- at the air-water interface and the bulk yields a surface potential of -240 mV as measured by Fawcett and co-workers[247].

We are currently exploring this issue in further detail (See Section 6.4.3 in Chapter 6).

Chapter 5

HETEROGENEOUS CHEMISTRIES ON THE SURFACE OF WATER: IMPLICATIONS IN GREEN CHEMISTRY AND ENVIRONMENTAL SCIENCE

Abstract

Recent reports on the acceleration of various organic reactions in aqueous emulsions have spurred a drive to step up the application of green chemistry and engineering.[62] Indeed, the prospect of employing water as a co-solvent is tantalizing due to its environmental benevolence, economy, non-toxicity, and excellent thermophysical properties. These findings also bear heavily on heterogeneous chemistries prevalent in the environment, such as interactions of isoprene and monoterpenes with mildly acidic drops of water in clouds, fog, and dew drops. However, the mechanism(s) underlying chemical activation and reactions at the interface of water with hydrophobic media, such as air, lipids and several biomaterials, remain unclear. Various mechanisms based on hydrophobicity, hydrogen bonding, and acid-base catalysis have been proposed. By applying our surface-specific electrospray ionization mass-spectrometer (ESIMS) setup, it was demonstrated that the gas-phase isoprene (2-methyl buta-1,3-diene, ISO) could be protonated (as $ISOH^+$) and oligomerized into $(ISO)_2H^+$, $(ISO)_3H^+$ during collisions with the surface of pH < 4 water drops during life time of ≈ 10 μs.[42] Based on these observations, we expected the probability of protonation per collision ($\gamma \sim 10^{-5}$) corresponding to a process hindered by E ~ 7 kcal mol^{-1} kinetic barriers. We also applied quantum mechanics to explore the interactions of ISO with $(H_2O)_n \cdot H_3O^+$ clusters as surrogates for the air-water interface with excess hydronium (H_3O^+) ions. We found that ISO weakly binds to $(H_2O)_2 \cdot H_3O^+$ clusters, whereupon $ISO \cdots (H_2O)_2 \cdot H_3O^+$ rearranges into $(H_2O)_3 \cdot ISOH^+$ via a $\Delta G^{\ddagger}$ = 6.9 kcal mol^{-1} barrier. A second ISO alighting on $(H_2O)_3 \cdot ISOH^+$ readily yields an acyclic C_{10}-oligomer via a $\Delta G^{\ddagger}$ = 2.1 kcal mol^{-1} barrier, in accordance with our experiments. Surprisingly, the rate-controlling proton transfer in a fully coupled larger cluster, viz.: $ISO \cdots (H_2O)_{35} \cdot H_3O^+ \rightarrow (H_2O)_{36} \cdot ISOH^+$, has a prohibitively high barrier: $\Delta G^{\ddagger} \sim 17$ kcal mol^{-1}. We infer that the catalysis 'on-water' is extremely sensitive to the extent of hydration of H_3O^+(if),[294, 295] and the protonation of hydrophobic species (like ISO) on the surface of water involves minimally hydrated interfacial H_3O^+ species along trajectories that avoid the free energy penalties associated with disrupting extended water domains. These findings should aid development of strategies in green synthesis and realistic modes in atmospheric chemistry.

5.1 Introduction

Molecular activity and reactivity depend crucially on the extent of solvation. As a result, reactions spontaneous in the aqueous phase are thermodynamically forbidden in the gas- phase, and vice versa.[296] In anisotropic interfacial layers separating water from hydrophobic media, steep hydration gradients and unbalanced long-range forces may lead to unique thermodynamic and kinetic constraints that remain poorly understood.[83, 100, 102, 154, 278] Continuum physical models, based on concepts such as dielectric constant, density, surface tension, and hydration, cannot capture phenomena at heterogeneous aqueous interfaces.[295, 297, 298] Indeed, several unintuitive physical and chemical phenomena manifest at the air-water interface, including enhanced ionic products,[38, 154] negative surface potentials,[154, 278] Hofmeister effects,[136] unequal fractionation of ions,[121] contact electrification,[7] anion-catalyzed chemistries,[40] and the Jones-Ray effect[90]. It has been suggested that enzymes exploit heterogeneity at the protein-water interface to tune the acidity/basicity of functional groups via subtle conformational adjustments.[28, 29] But whether this process is causative or subsidiary to their function is still controversial. The unique characteristics of interfacial processes are also essential in the atmospheric chemistry of marine aerosols,[32, 36, 44, 47] cloud acidification,[32, 40, 41, 44, 47] secondary organic aerosol formation,[34, 35, 42, 123, 158] and to ‘green chemistry’ in general.[299]

In 1980s, Breslow and co-workers discovered that several Diels-Alder cycloaddition reactions, such as between cyclopentadiene and butenone proceed orders of magnitude faster and exhibiting stereospecificity, if carried out in a homogeneous aqueous phase rather than a standard organic solvent, like isooctane.[59, 61] Other important reactions that experienced rate accelerated in aqueous environment over organic phase included, aldol condensation, Mannich reaction, Claisen rearrangement, Michael addition, aldol condensation, benzoin condensation and Grignard-type additions.[300, 301] Employing hydrophobic pockets of β-cyclodextrin, several researchers attributed this phenomenon to the hydrophobic aggregation of reactants;[58, 61, 302, 303] though, other theorists and experimentalists proposed that hydrogen bonding between solutes and solvents played a key role in stabilizing transition states leading to rate acceleration.[301, 304, 305] More intriguingly, researchers have recently discovered even higher enhancements in rates of similar organic reactions in aqueous emulsions when carried out with vigorous shaking.[62-65] Since the reacting hydrocarbons are practically insoluble in water, the drivers for enhancement in rates must

reside at the surface of water; hence these reactions are referred to as ‘on-water’. Further, since hydrophobic effects in aqueous emulsions cannot be higher than in the homogeneous aqueous phase, other effects have been proposed to account for this unanticipated phenomenon, such as favourable stabilization of polar transition states by the dangling OH groups ‘on water’ versus those interlocked ‘in water’,[45, 66, 67] strong adsorption of the hydroxide ion at aqueous interfaces,[69, 306] and the superacidity of hydronium ions at the air-water and oil-water interfaces.[32, 37]

5.2 Review of Various Mechanisms Proposed to Explain the Catalysis ‘On-Water’

An important outstanding question relates to the minimum number of water molecules needed to simulate these reactive processes ‘on water’. For example, Jung and Marcus investigated interfacial cycloaddition reactions via transition-state theory, and U-B3LYP/6-31+G* level density functional theory.[67] They employed three explicit water molecules to represent the oil-water/air-water interface, and concluded that the preferential stabilization of the transition states via free dangling OH bonds (as shown by Shen and co-workers)[80, 82] of polar organic reactants at aqueous interfaces could explain the observed effects.[67] Subsequently, they validated these results on a larger slab of water (1264 molecules) via a mixed quantum mechanics/molecular mechanics study.[66] Ensconced within the framework of hydrogen bonding, while their model explained rate accelerations quite well, it was unable to account for the **significant kinetic isotope effects** observed in the experiments.[42, 62, 67, 69] Jorgensen and co-workers also studied Diels-Alder additions between cyclopentadiene with 1,4-napthoquinone on a slab of 1220 water molecules by applying QM/MM calculations using Monte Carlo simulations and free energy perturbation theory (semiempirical PDDG/PM3 molecular orbital theory and TIP4P water model).[68] They found that (1) transition-state structures for reactions at the air-water interface were less stable than in the bulk, and concluded that (2) “consideration of the possible role of interfacial hydronium ions” was “warranted” to explain the experimental result.

Providing an alternative hypothesis based on the specific adsorption of OH^- ions ‘on-water’ (and free H_3O^+ ions), Beattie and co-workers pointed out that most of the reactions investigated ‘on water’ were acid-catalyzed, i.e., involved molecular activation via protonation; though did not observe a correlation between the catalysis and the bulk pH.[69, 306] Indeed, proposals based on hydrogen bond stabilized transition states versus acid-base catalysis could be subjected to scrutiny

by investigating 'on-water' reactions of (non-polar) hydrophobic molecules, such as hydrocarbons, that would gain minimal stabilization via dangling OH bonds at the aqueous interface. Herein we analyze these proposals in the light of our experimental and theoretical results.

5.3 Thermochemical Considerations

We chose isoprene (ISO) as the test candidate because (1) it is a hydrophobic molecule and should put the hydrogen-bonding theory to test, and (2) it is an important player in atmospheric chemistry, though it remains unclear how much of it gets converted to secondary organic aerosol. In dealing with Brønsted acidity, A is a stronger Brønsted acid than B if protons would bind preferentially to B therein.[256] Because the proton affinity of water (PA = 165 kcal mol^{-1}) is lower than ISO (197 kcal $mole^{-1}$), [182] hydronium, $H_3O^+(g)$, protonates it in the gas-phase (reactions R_1, R4 and Figure 5.4). In contrast, aqueous $H_3O^+(aq)$ can protonate only relatively stronger bases in bulk water (reaction R_2)

$$B(g) + H_3O^+(g) \longrightarrow BH^+(g) + H_2O(g) \qquad (R_1)$$

$$B(aq) + H_3O^+(aq) \longrightarrow BH^+(aq) + H_2O(aq) \qquad (R_2)$$

$$B(if) + H_3O^+(if) \longrightarrow BH^+(if) + H_2O(if) \qquad (R_3)$$

Thus, ion hydration might play a crucial role in controlling the extent of proton transfers between Brønsted acids and bases on the surface of water (reaction R_3). Considering that the density of water changes by a thousand-fold from the bulk to the vapor phase within a nanometer, the nature of proton transfers in interfacial layers is expected to be an extraordinarily sensitive function of depth. In fact, Morokuma,[294] and more recently Doi et al.,[295] have investigated the role of microhydration on model S_N2 reactions $X^- + CH_3I \rightarrow XCH_3 + Y^-$ via application of both theory and experiment. They found drastic variations ranging over 10^4-10^{20} times enhancement in rates of reactions as a function of interfacial hydration in clusters. Thus, our working hypothesis, which we validate via theory herein, is that under conditions of vigorous shaking, interfacial H_3O^+ ions could exhibit partial gas-phase behavior.[37, 42]

5.4 Experimental Section

As noted in Section 2.5.2 in Chapter 2, we recently found that certain organic gases could be protonated on pH < 4 aqueous surfaces.[37, 123] This unforeseen phenomenon is ascribed to the *superacidity* of weakly hydrated hydronium ions at the air/water interface.[37, 307]Although ISO has been shown to polymerize on extremely acidic surfaces, the possibility that it might do so on less acidic environmental surfaces has never been considered before.[308, 309] Experiments were conducted by intersecting continuously refreshed, uncontaminated surfaces of free-flowing aqueous jets with ISO(g)/hexane(g)/N_2(g) beams at ambient temperature and pressure, and detecting the formation of carbocations, such as $ISOH^+$(if) (see reaction R_4 below) by our ESIMS setup. Conditions in typical experiments were: drying gas flow rate: 10 L min^{-1}; drying gas temperature: 340 ^oC; inlet voltage: - 3.5 kV relative to ground; fragmentor voltage: 17 or 26 V. Isoprene (> 99 %, Sigma-Aldrich) was used as received. All solutions were prepared in purified water (Resistivity = 18.2 MΩ cm) from a Millipore Milli-Q gradient water purification system. Solution pH_{BLK} was adjusted by adding HCl and measured with a calibrated pH meter (VWR).

5.5 Experimental Results

Figure 5.1 shows a positive ion ESIM spectrum of the surface of water microjets at pH 2.3 exposed to dilute ISO(g)/hexane(g)/N_2(g) mixtures for ≈ 10 μs. Note the intense ESIM spectral signals at m/z = 69, 81, 137, and 205 Da. No other signals were detected at lower or higher masses. The gaseous carrier, hexane, is not protonated on these microjets at any pH (see blue trace in Figure 5.1) as expected from its low gas-phase proton affinity PA(hexane) = 159 kcal mol^{-1} < PA(H_2O) = 165 kcal mol^{-1}.[182]In accord with this rationale ISO (PA = 197 kcal mol^{-1}) is readily protonated in interfacial layers giving rise to the carbocations $ISOH^+$, $(ISO)_2H^+$ and $(ISO)_3H^+$.

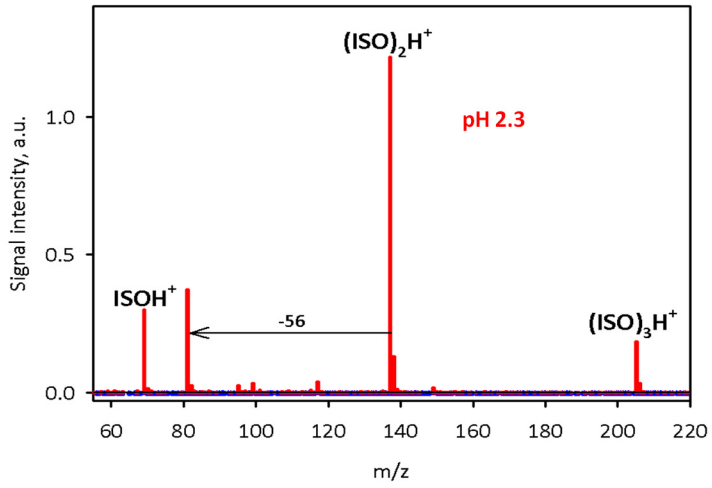

Figure 5.1: Positive ion ESIM spectra of pH 2.3 water microjets exposed to 88 ppmv isoprene/hexane/N_2 gas mixtures for $\tau \approx 10$ μs (red trace). Blue trace corresponds to experiments without isoprene. 1 ppbv = 2.4×10^{10} molecule cm^{-3} at 1 atm, 293 K experimental conditions.

The m/z = 81 and 95 signals are typical fragments of the collisionally induced decomposition of protonated monoterpenes $C_{10}H_{17}^+$ (m/z = 137) into $C_6H_9^+$ (+C_4H_8) and $C_7H_{11}^+$ (+ C_3H_6), respectively.[310] This assignment is in sync with the reciprocal evolution of m/z = 81 and 95 versus m/z = 137 and 205 signal intensities as functions of fragmentation voltage (not shown here). Notice that present evidence establishes the molecular formula but not the molecular structure of our $(ISO)_2H^+$ and $(ISO)_3H^+$ oligomers. The absence of any such signals from the ESIM spectra of 1 mM ISO in water:acetonitrile (50/50) solutions at 1.9 < pH < 4.3, *which contain the same components present in the gas/liquid experiments*, demonstrates that ISO can be protonated at the gas/water interface, but not in bulk solution, in this pH range.[37]In other words, the carbocations detected in these experiments are produced at the ISO(if)-water jet interface rather than in deeper liquid layers, in accordance with the body of evidence gained in previous experiments from our laboratory.[35, 37, 123, 158]

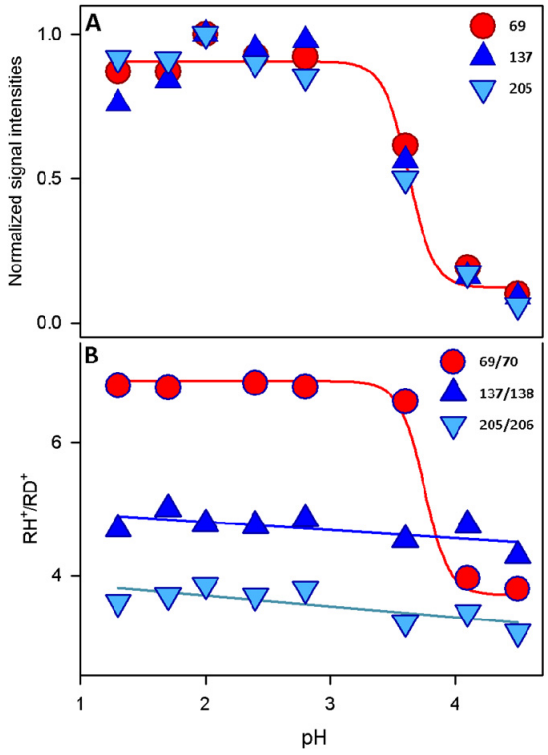

Figure 5.2: (A) Normalized $ISOH^+$ (m/z = 69), $(ISO)_2H^+$ (m/z = 137) and $(ISO)_3H^+$ (m/z = 205) ES mass spectral signal intensities, (B): Ratios of M/(M+1) ES mass spectral signal intensities as a function of bulk pH, in experiments performed on H_2O:D_2O (50/50) microjets exposed to 88 ppmv gaseous isoprene(if) for $\tau \approx 10$ μs contact times. All experiments in 1 atm N_2(g) at 293 K.

Figure 5.2A shows that all species appear below pH ≈ 4 and evolve along a steep saturation curve possessing an inflection point at $pH_{½} = 3.63 \pm 0.05$. It also confirms our previous reports on the emergence of strongly acidic hydronium species, H_3O^+(if), to the surface of water in this pH range.[37, 123] H_3O^+(if) behaves as a partially hydrated species that, like H_3O^+(g), can protonate gases having proton affinities larger than that of gaseous water.[182] Most non-alkane gases meet the latter requirement and might be similarly protonated on the surface of mildly acidic water.[182] It is important to note that, although thermodynamics ensures that the chemical potential of the jet (adjusted to ± 0.1 pH units prior to injection) is the same throughout (i.e., in the bulk as at the surface of the liquid) [311] the protonating ability of H_3O^+(if) toward gas-phase species impinging on the surface is quite different from that of H_3O^+(aq) toward the same species after they become

fully hydrated in bulk water.[37, 123] The chemical potential at the surface of the jet should be minimally affected by ISO(if) at the low exposures employed in these experiments. Since the $pH_{½}$ = 3.6 derived from Figure 5.2A nearly matches the $pH_{½} \approx 3$ previously measured in experiments using the much weaker base hexanoic acid gas (PA = 187 kcal mol^{-1}) as proton acceptor, (Section 2.5.2 in Chapter 2 and reference [37]) we infer that the curve of Figure 5.2A reflects an equilibrium established on water rather than in the gas-phase. The steepness of the saturation curves is consistent with the emergence of H_3O^+(if) to the air-water interface and excludes unspecific ion effects. A common saturation curve for all carbocations further implies that the rate-determining step is the protonation of ISO, i.e., that the rate constants for:

$$H_3O^+(if) + ISO(if) \longrightarrow ISOH^+(if) \qquad (R_4)$$

$$ISOH^+(if) + ISO(if) \longrightarrow (ISO)_2H^+(if) \qquad (R_5)$$

$$(ISO)_2H^+(if) + ISO(if) \longrightarrow (ISO)_3H^+(if) \qquad (R_6)$$

are in the order: $k_1 < k_2 \sim k_3$. We ascribe the fact that oligomerization stops at $(ISO)_3H^+$ to the small exposures (exposure = $x_{ISO} \times \tau$, x_{ISO} is mixing ratio, τ is contact time) prevalent in our experiments. The fact that cationic polymerization proceeds at all under these conditions, i.e., in the presence of a nucleophile, is a remarkable confirmation of the low activity of water at the gas-liquid interface.[312] Figure 5.2B displays the isotopic ratios RH^+/RD^+ measured in experiments on H_2O:D_2O (50/50) microjets as functions of pH. Notably, $RH^+/RD^+ = ISOH^+/ISOD^+$ (69/70) follows a saturation curve similar to that of Figure 5.2A, whereas $(ISO)_2H^+/(ISO)_2D^+$ (137/138) and $(ISO)_3H^+/(ISO)_3D^+$ (205/206) vary linearly as functions of pH. We infer that $ISOH(D)^+$ preserves the isotopic labeling generated by a direct kinetic H-isotope effect in the protonation of ISO by H_3O^+(if), and $(ISO)_2H(D)^+$ and $(ISO)_3H(D)^+$ scramble their isotope labels with the solvent prior to detection. Figure 5.2B Observation of large kinetic isotope effect (> 1.4) as noted by Sharpless and co-workers confirms our hypothesis that interfacial H_3O^+ ions play a key role in catalysis 'on-water' whereas the role of hydrogen bonding might secondary, such as in the stabilization of carbocations.

Figure 5.3 shows the dissimilar dependences of $ISOH^+$, $(ISO)_2H^+$ and $(ISO)_3H^+$ signal intensities as functions of ISO(if) exposure. Recall that reactant conversion is proportional to exposure rather than to mixing ratio alone. Thus, exposures of 1 ppbv × s are realized by exposing water to 1 ppbv ISO(if) for 1 s or to 1 ppmv ISO(if) for 1 ms (1 ppbv = 2.4×10^{10} molecule cm^{-3} under 1 atm, 293 K

experimental conditions). It is apparent that both $ISOH^+$ and $(ISO)_2H^+$ are produced with non-zero initial slopes, i.e., as primary products. The implication is that the relatively smaller $ISOH^+$ signals correspond to an intermediate formed in a rate-determining protonation reaction at the gas/water interface, which is rapidly converted to $(ISO)_2H^+$. Accordingly, $ISOH^+$ signals approach steady-state whereas $(ISO)_2H^+$ and $(ISO)_3H^+$ production accelerates at larger exposures. Taken together, these findings represent direct evidence that ISO(if) undergoes cationic

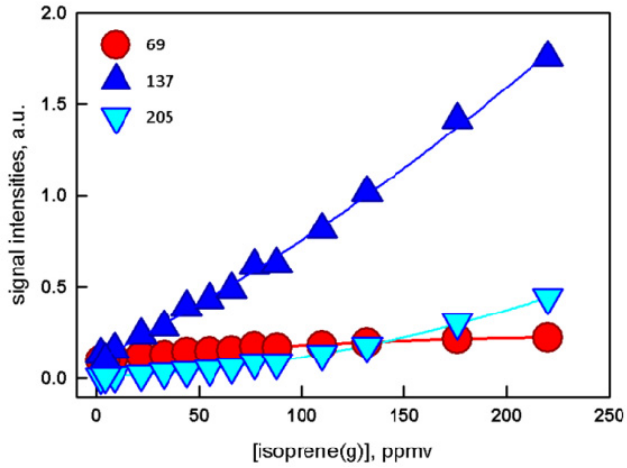

Figure 5.3: ES mass spectral signal intensities from aqueous microjets at pH 2.3 exposed to gaseous isoprene for ≈ 10 μs contact times as a function of exposure (exposure ≡ mixing ratio × contact time). Note the inverse curvatures of $ISOH^+$ versus $(ISO)_2H^+$ and $(ISO)_3H^+$ curves, and the non-vanishing initial slopes of both $ISOH^+$ and $(ISO)_2H^+$ curves, as expected for a stepwise oligomerization process. 1 ppbv = 2.4×10^{10} molecule cm^{-3} at 1 atm, 293 K experimental conditions.

polymerization upon impact on gas/mildly acidic water interfaces.[37, 123, 307] It should be pointed out that if the surface of water were already saturated with ISO(if) at the ppmv concentrations employed in our experiments, the degree of polymerization, i.e., the relative concentrations of $ISOH^+$, $(ISO)_2H^+$ and $(ISO)_2H^+$, would depend on ISO concentration rather than exposure and, therefore, might be different under typical atmospheric conditions. The probability of ISO(if) protonation in collisions with water is, of course, independent of ISO concentration.

5.6 Theoretical Approach

To gain deeper insight into the catalysis 'on-water', we also applied quantum mechanics on model systems. We carried out density functional theory (DFT) calculations at M06 level shown to provide an accurate description of clusters of ground-state thermochemistry and thermochemical kinetics of ISO and water.[103, 313-315] Calculation of transition-state structures and energies of a series of organic reactions with M0-6 have been found in good agreement with experimental data.[103, 316] Bryantsev et al., evaluated binding energies of water clusters, W_n, (range n = 2 – 8, 20) along with hydration and neutralization energies of hydroxide and hydronium ions using DFT functionals (M06, M06-2X, M06-L, B3LYP, X3LYP), and compared against high-level theory (CCSD(T)/aug-cc-p VDZ level).[313] They found the results from M0-6 to be in excellent agreement with high-level theory, with and without the basis-set superposition error correction. Here we used the 6-311G** basis set for H, C and O atoms.[317] Geometries were minimized and single point electronic energy E_{elec} was evaluated with the diffuse 6-311G**++ basis set for all atoms.[318] The Hessians at these geometries were used to determine that the minima and transition states led to 0 and 1 imaginary frequency, respectively. Transition-state structures were obtained by following the steep ascent/descent along the vibration mode with imaginary frequency till the saddle point was reached. The vibrational frequencies from the Hessians were also used to provide zero-point energies, and the vibrational contributions to enthalpies and entropies. The free energies of isoprene at 1 atm were calculated using statistical mechanics for ideal gases.

5.7 Theoretical Results

As a starting point, our simulations predict that the gas-phase proton transfer between H_3O^+(g) and ISO(g) (reaction R1, B ≡ ISO)) is exothermic with ΔG^0 = - 30 kcal mol^{-1}, in accordance with the difference between the gas-phase basicities (GB) of H_2O (GB = 157.7 kcal mol^{-1}) and ISO (GB = 190.6 kcal mol^{-1}): ΔGB = 32.9 kcal mol^{-1}.[182] (Figure 5.4) Adding trans- or cis-ISO(if) to ($ISOH^+$ + H_2O) spontaneously leads to cyclic (ΔG^0 = - 40 kcal mol^{-1}) or acyclic monoterpenes (ΔG^0 = - 9 kcal mol^{-1}) (Figures 5.5A, B).[312, 319]

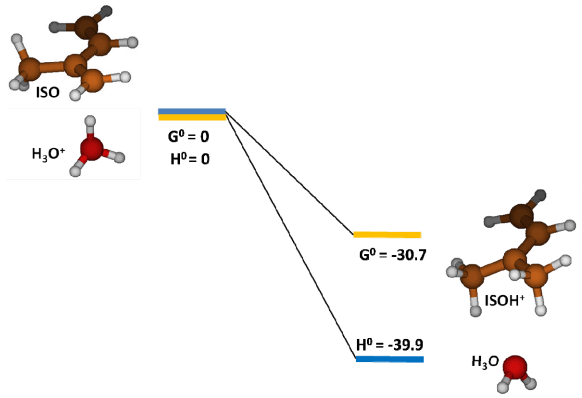

Figure 5.4: Protonation of gas-phase isoprene (ISO(if)) with gas-phase hydronium ion (H_3O^+(if)). Theory at M0-6/6-311g**++ level accurately predicts change in energy

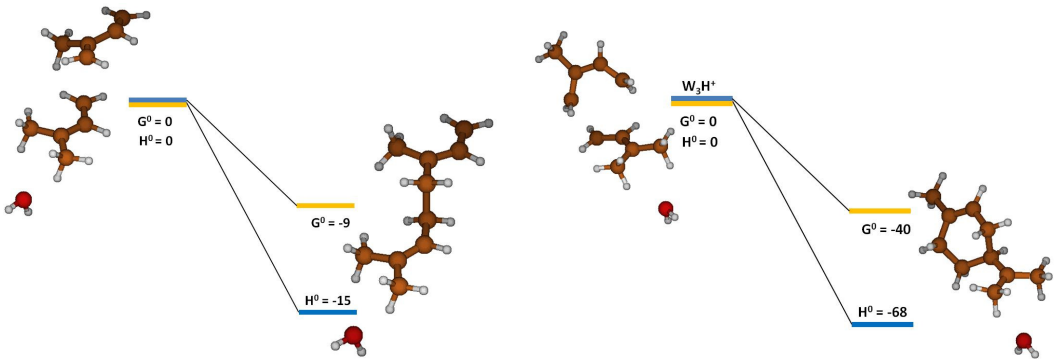

A. B.

Figure 5.5: (A) Oligomerization of a trans-isoprene (ISO(if)) molecule with a protonated trans-isoprene leading to a linear product; (B) Oligomerization of gas-phase cis-isoprene (ISO(if)) with a protonated trans-isoprene molecule leading to a cyclic product.

It has been reported that protons at the lipid-water interface might be impeded by a kinetic barrier > 8 k_BT toward entering the bulk water.[17, 201] Further, vigorous shaking protocol in the experiment could render H_3O^+ ions minimally hydrated.[102] Thus, our model air-water interface with an excess proton is represented by a $(H_2O)_2.H_3O^+$ cluster. In this configuration, the H_3O^+ ion is a

proton donor. In 1 mM aqueous solutions (pH = 3), ions are separated by distances much larger than the size of our water clusters, thus the inclusion of a counterion, say Cl^-, within $(H_2O)_3H^+$ cluster was unrealistic. We found that ISO(if) interacted strongly with the cluster via H-bond donation to C1 with ΔH^0 = - 14.2 kcal mol^{-1} while losing 43.7 cal K^{-1} mol^{-1} of translational and rotational entropy (Figure 5.6). The H-bonded adduct underwent proton transfer over a $\Delta G^{\ddagger}$ = 5.8 kcal mol^{-1} barrier, which is consistent with our experimental results.

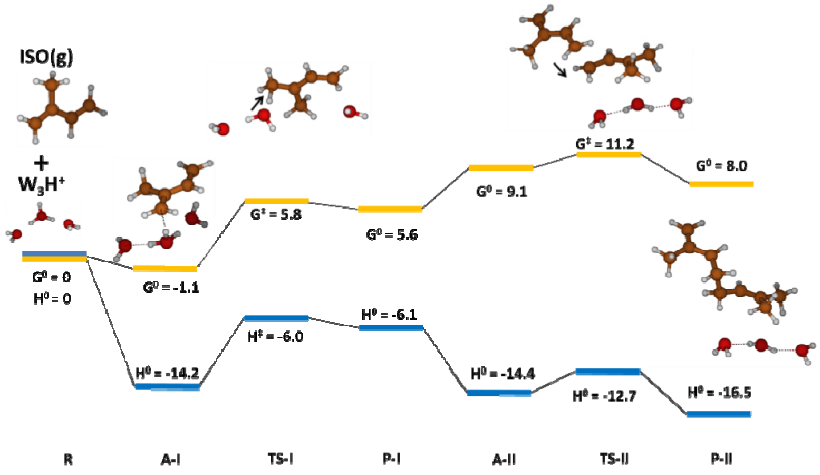

Figure 5.6: Free energy and enthalpy landscape for the oligomerization process of isoprene on a $(H_2O)_3H^+$ cluster. Kinetics of the predicted mechanism is commensurate with our experimental results.

The addition of a second ISO(if) was also exothermic. Our results (Figure 5.6)are summarized as follows:

1. ISO(if) interacted with $(H_2O)_2{\cdot}H_3O^+$ leading to an [ISO---$(H_2O)_3H^+$] adduct (A-I) that is ΔG^0 = -1.1 kcal $mol^{-1}$and ΔH^0 = -14.2 kcal mol^{-1} more stable than the reactants (R).

2. The overall kinetic barrier for transferring the proton from $(H_2O)_2{\cdot}H_3O^+$ to ISO leading to marginally stable products (ΔG^0 = 5.6 kcal mol^{-1}, ΔH^0 = - 6.1 kcal mol^{-1}) was $\Delta G^{\ddagger}$ = 6.9 kcal mol^{-1} ($\Delta H^{\ddagger}$ = 8.2 kcal mol^{-1}) (Figure 5.7).

3. A Mulliken population analysis showed that the tertiary C2 carbon in $(H_2O)_3 \cdot ISOH^+$ acquired a partial + 0.2 positive charges. C4 also gained a smaller positive charge due to resonance.

4. The kinetic barrier for C-C bond formation between the two ISO units in A-II was $\Delta G^{\ddagger}$ = 2.1 kcal mol^{-1} ($\Delta H^{\ddagger}$ = 1.7 kcal mol^{-1}) leading to products with ΔG^0 = -3.2 kcal mol^{-1} ($\Delta H^{\ddagger}$ = -3.5 kcal mol^{-1}) below the transition state. (Figure 5.6)

5. Note that the entire process takes place downhill over an exothermic surface, but was hindered by the entropy losses resulting from restricting the external motions of polyatomic gas-phase species.

6. From the computed free energy landscape we estimated an uptake coefficient, $\gamma = e^{-\frac{\Delta G^{\circ}}{k_B T}} = 10^{-5}$, which is consistent with our experimental estimates.[42]

Remarkably, similar calculations on larger $(H_2O)_{35} \cdot H_3O^+$ clusters, which should presumably provide more realistic models of the surface of water, led to unrealistically large kinetic barriers (Figure 5.7). In the larger cluster containing an excess proton, $(H_2O)_{35}.H_3O^+$, the hydronium ion resided at the surface, thus allowing us to investigate interfacial reactions. But unlike the smaller cluster ($(H_2O)_2.H_3O^+$), wherein H_3O^+ donated two hydrogen bonds to nearby water molecules and third to the isoprene molecule, the interfacial H_3O^+ in $(H_2O)_{35}.H_3O^+$ donated three hydrogen bonds to three surrounding water molecules (Figure 5.7). Thus, an incipient ISO(if) molecule accepted a proton via a proton wire connecting the H_3O^+ ion to a water molecule at the edge of the cluster. It is this difference in structure, state of hydration, and coordination environment of the interfacial H_3O^+ that aggravated the kinetic barrier. The calculated kinetic barriers for protonation and C-C bond formation were: $\Delta G^{\ddagger}$ = 16.6 kcal mol^{-1} and $\Delta G^{\ddagger}$ = 25.4 kcal mol^{-1}, respectively (Figure 5.7). Such barriers would be insurmountable in the time scale (τ < 10 μs) of our experiments conducted under ambient conditions.[42] Furthermore, calculations with larger clusters led to protonated alcohols, ISO-OH_2^+ and $(ISO)_2$-OH_2^+, rather than the $ISOH^+$ and $(ISO)_2H^+$ that we detected by mass spectrometry.[42] Our calculations substantiate the observations that the condensed-phase chemistry of ISO dissolved in 30 – 50% sulfuric acid solutions leads to short-chain alcohols instead

of the olefinic and aliphatic hydrocarbon polymers produced by in > 65% sulfuric acid.[312, 319, 320]

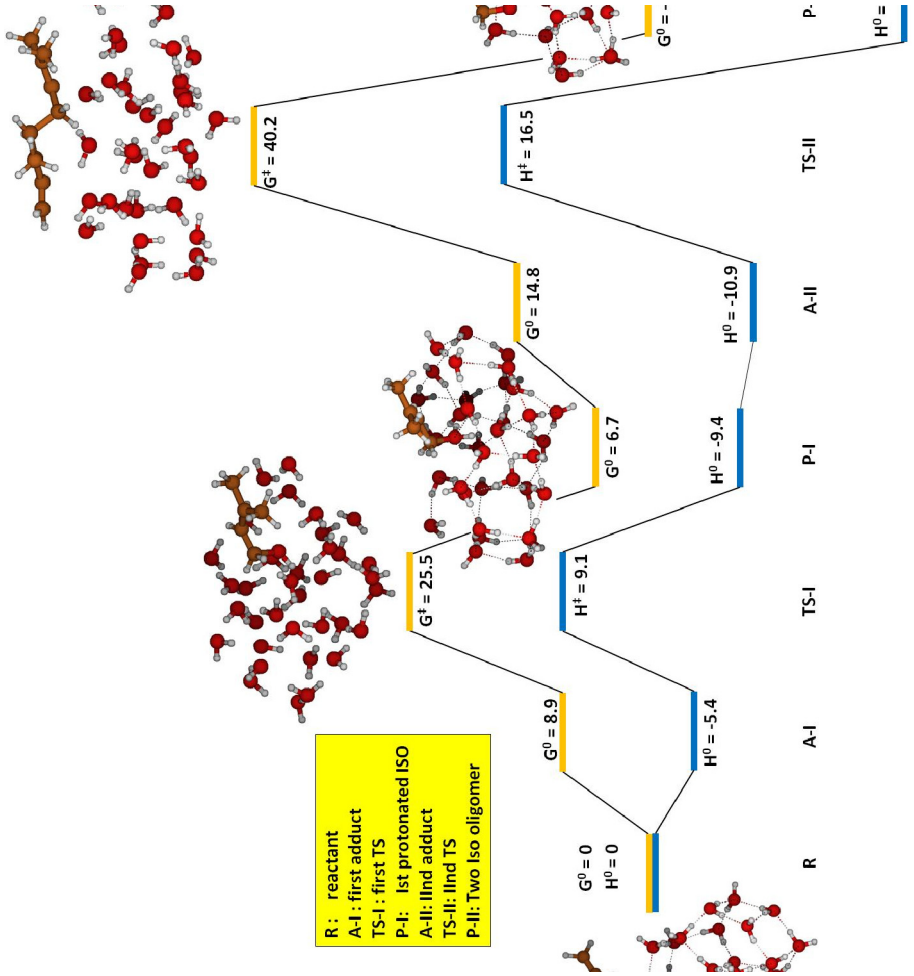

Figure 5.7: Protonation and oligomerization of gas-phase isoprene (ISO(if)) on a larger water cluster (W_{35}) with an excess proton leading to a linear product. The predicted kinetic barriers are insurmountable under ambient conditions, and at variance with our experimental results.

5.8 Discussion

At present, it is not clear what interfacial properties or processes are influenced by short- versus long-range interactions; whether density functionals created to fit thermodynamic properties of bulk water could be confidently applied to predict the rates of interfacial reactions, or whether the optimal sizes of the water ensembles used to simulate different phenomena are comparable. Molecular simulations of surface tension and surface excesses, which, by definition, involve integration of distribution functions over semi-infinite slabs, may not be generally invoked as references for the description of localized dynamical interfacial processes. Thus, the protonation and oligomerization of ISO(if) on the surface of mildly acidic pH < 4 water detected during ≈ 10 μs contact times [42] involves a subset of interfacial H_3O^+ ions that remains uncoupled from surrounding waters. It should be emphasized that olefinic ISO lacks hydrogen bond acceptors and, therefore, its cationic oligomerization 'on water' must be due to the 'superacidity' of interfacial H_3O^+. Since the interfacial protonation and oligomerization of all the olefins we studied exhibit the same pH dependence, the rate-determining step is the initial protonation in all cases. This observation underscores the role dynamic microhydration in tuning the activity of reactants in the interfacial layers, we infer that our reactive gas-liquid collisions involve less abundant $(H_2O)_2{\cdot}H_3O^+$, rather than lower energy $(H_2O)_{35}{\cdot}H_3O^+$ interfacial species, because they lead to lower energy pathways for proton transfer. Vigorous shaking during experiments might lead to minimally solvated H_3O^+ ions that would drive this reaction. We are currently designing a more elaborate theoretical framework to capture such effects

While this work answers some questions pertaining to catalysis 'on-water', it also highlights important questions to be addressed surrounding the nature of interfacial protons. We hope that application of theory and experiment could answer the following questions (1) how does the interplay of enthalpy of hydration and entropy drives H_3O^+ ions to the air-water interface,[80, 169, 201, 276] (2) how to probe acidity at the air-water interface as a function of bulk acidity,[37, 40, 154] and (3) what is the origin of kinetic barrier(s) impeding the migration of interfacial H_3O^+ ion into bulk water,[17, 18, 201]. While slower protonation/oligomerization of ISO on the surface of pure water remains to be demonstrated, this work presents an alternative mechanism for 'on-water' catalysis.

5.9 Environmental Implications

The rapid decay of ISO observed in and atop canopies after sunset, i.e., in the absence of photogenerated OH or NO_3 radicals [321-325]has remained unclear for some time based on homogeneous chemistries operating in the environment. Among the first to study this phenomenon, Jacob and Wofsy[321]pointed out that 'nighttime losses of ISO exceed rates of reaction with NO_3 and O_3 and appear to reflect dry deposition processes'. Zimmerman et al.,[325]reported ISO vertical profiles up to 400 m altitude above ground that revealed the existence of 'a strong ISO sink near the surface at night'. Hurst et al.[323]noticed that 'essentially every evening, ISO concentrations fall from several ppbv to levels below 100 pptv, with an average lifetime of 2.7 hours. Since this decay rate exceeds that expected from established nighttime chemistry, other possible mechanisms (may be operative)'. Remarkably, Hurst et al. argued that 'since ISO is a non-polar species, dry deposition is an unlikely candidate for the ISO sink' and postulated a dark source of OH radicals at nighttime to account for their observations.[323]

Thus, all indications suggest that current atmospheric chemistry models underpredict secondary organic aerosol (SOA) mass both in the boundary layer and aloft. This negative bias has been variously ascribed to: (1) gross uncertainties in emission inventories of precursor VOC emissions, (2) missing physical and chemical processes that contribute to SOA formation in the aerosol phase, (3) errors associated with the extrapolation of laboratory data to atmospheric conditions,[326](4) uncertain meteorological inputs, or (5) errors in the measurement of ambient aerosol loads.[326] Our experimental results support the notion that ISO emission inventories may have been overestimated due to missing heterogeneous losses. Atmospheric chemical models that incorporate enhanced canopy reduction factors driven by interfacial acid-catalysis may approach resolution on the fate of biogenic gas emissions.

5.10 Conclusions

Our experimental and theoretical results, in conjunction with other independent experimental and theoretical reports, support the notion that 'on-water' catalysis is driven by interfacial H_3O^+ due to fluctuating hydration levels at the air-water and lipid-water interfaces.[31, 42, 68, 69, 123] In the proposed mechanism for catalysis 'on-water', explicit proton transfers are involved, thus, significant KIEs (> 1.4) could be explained. Specifically, the kinetic barrier for protonation and oligomerization of ISO at the air-water interface predicted by our theoretical investigation corresponds to uptake coefficients, ~ 10^{-5}, which are commensurate with our experimental

results.[31, 42] These results have direct implications on green chemical synthesis and heterogeneous chemistry of biogenic isoprene and monoterpenes in the atmosphere.

Chapter 6

CONCLUSIONS AND FUTURE WORK

In this chapter the key ideas of this thesis are summarized, which are, (1) the role of anions in catalyzing interfacial proton transfer (PT) reactions, (2) the origin of the negative surface charge of the air-water interface, and (3) protonation and oligomerization of inert organic species on the surface of pH < 4 water. Our application of both experiment and theory in this regard has provided complementary insights into molecular underpinnings of these phenomena. During the process, we also furthered the understanding of electrospray ionization mass spectrometry (ESIMS) as a surface-sensitive platform for liquids. In the section dedicated to future work, we will discuss several new sub-projects that arose during the course of this dissertation and are being pursued.

6.1 Anion-Catalyzed Proton Transfer Reactions at Aqueous Interfaces

Applying our surface-specific electrospray ionization mass spectrometer (ESIMS) platform, we discovered the catalytic role of inert anions in proton transfer (PT) reactions at the air-water interface, a model water-hydrophobe interface. We employed gas-phase nitric acid (HNO_3), a strong acid in bulk water, as a molecular probe for the aerial side of the interface. As a first step, our experiments and theory confirmed previous results regarding the weakness of HNO_3 as a Brønsted acid at the air-water interface.[40, 41, 48, 218-222, 327] Our density functional theory (DFT) calculations at a B3LYP/6-311G**++ level employing a twenty water cluster as a surrogate for the air-water interface provided insights at the molecular level. We found that, though, the proton of HNO_3 could readily slip into water, further inward displacement is favored by hydration of the H_3O^+, but opposed by the electrostatic attraction from the NO_3^-. Thus, kinetic barriers of $\Delta G^{\ddagger} = 10$ kcal mol^{-1}, and $\Delta H^{\ddagger} = 4$ kcal mol^{-1} on the free energy, and enthalpy landscapes, respectively, appear due to the expense of opening a cavity for the NO_3^- ion in the interfacial aqueous layers. Curiously, while investigating the effects of pH on the PT process via our ESIMS setup, we serendipitously found dramatic enhancement in the rate of PTs when inert anions, such as Cl^-, SO_4^{2-}, ClO_4^-, and $CH_3(CH_2)_4COO^-$ were present at the air-water interface.[40, 41] Subsequently, our DFT simulations showed that the presence of interfacial anions at the air-water interface led to a significantly stable hydrogen-bonded adduct, that was structurally similar to the transition state [Figure 3.5 and 3.6]. Thus, the reaction coordinate for PT on pure water was a combination of internal modes involving displacements of heavy oxygen atoms, whereas in the presence of chloride PT proceeded quasi-adiabatically along a proton wire leading to a significantly lower kinetic barrier [Figure 3.7].

6.1.1 Implications in Atmospheric Chemistry

Our finding that PT across water-hydrophobe interfaces is catalyzed by anions has important implications in many fields. Whether HNO_3 dissociates on aqueous surfaces, for example, bears on various environmental issues [328]. Whereas NO_3^- is a sink for active nitrogen in the atmosphere because it can be removed by dry and wet deposition, undissociated HNO_3 may be react via: $2HNO_3 + NO \rightarrow 3\ NO_2 + H_2O$, thereby sustaining the atmospheric impact of nitrogen oxides[329]. Adsorption of HNO_3(g) on ice also depends critically on whether HNO_3 dissociates therein, i.e., whether coverage is a function of P or $P^{½}$ ($P \equiv HNO_3$(g) partial pressure)[330]. Our results suggest that HNO_3(if) will dissociate upon impact on most environmental aqueous surfaces, including pre-melted films on ice that contain electrolytes impurities at least at millimolar levels.

6.1.2 Implications in Enzymatic Catalysis and other Membrane Phenomena

Insights derived from our work should hold at the lipid-water interface due to thermophysical similarities, especially in the dielectric composition, and the dominance of entropic effects at water-hydrophobe interface.[331] Thus, our demonstration of PT across water-hydrophobe interface catalyzed by electrostatics is intimately related to the concept of anion-mediated water bridges for PT in proteins [236, 332-334]. It also accounts for the fact that inert anions, such as chloride, acetate, and hexanoate, could catalyze proton transfers along membrane surfaces [283, 335]. In regards to proton diffusion along membrane surfaces between sites of proton release and consumption, it is crucial to identify whether the migrant proton proceeds via binding and unbinding events with anions (such as PO_4^{3-}), or simply cruises through proton wires facilitated via interfacial water molecules under the influence of such anions. Our simple model of the water-hydrophobe interface (presented in Section 3.4 in Chapter 3) suggested the latter mechanism could be significant and has been independently confirmed by elegant experiments of Pohl and co-workers.[201] These results are at variance with theoretical predictions on the large stabilization of protons in vicinity of PO_4^{3-} and $RCOO^-$ ions at the lipid membrane-water interface, such that their release is at the same time scale as the motion of the membrane.[336-338] Lastly, our experiments

also demonstrated that hydrons (protons or deuterons) delivered at the water-hydrophobe interface do not scramble with the protons in the bulk (See Section 3.4, Chapter 3), as verified by Pohl and co-workers[201], and Mulkidjanian and co-workers[17, 18, 30] at the lipid-water and protein-water interfaces, respectively.

6.2 Brønsted Basicity of the Air-Water Interface

Recent debate on the acidity versus basicity of the surface of water has generated lot of excitement in the chemical physics community, but it is not a new problem. In fact, since the nineteenth century a number of experimentalists investigating electrokinetics, electricity, colloidal chemistry, and tribology, had reported on charging and electrification phenomena at the aqueous interface.[70-72, 133-135, 339, 340] Meteorologists have also been keenly investigating the physics and chemistry of thunderstorms due to clouds and volcanoes, and the role played by precipitation and wind in the process.[340-348] Physicists and physical chemists have analyzed spraying[349, 350], bubbling[351] and splashing[352] of water with a variety of experiments, ranging from Millikan oil-drop experiments[353], to bubble-bursting[351]. Effects of relative humidity (RH) in contact electrification was found to be critical: Diaz and co-workers reported on dramatic decrease in contact electrification at 0% RH, compared to maximum at 30% RH.[7, 354] It was proposed that formation of a "water-bridge", of thickness ~ 1 – 2 nm < Debye length facilitated ion diffusion via change in entropy, along with electrostatics.[354] Measurement of electrophoretic mobilities of xylene, dodecane, hexadecane and perfluoromethyldecalin drops in water as a function of pH concluded excess hydroxide ions, OH^-, at the oil-water interface.[73] Similar, measurement of the zeta-potential of air bubbles in electrokinetic experiments, under ambient conditions, also confirmed a negative surface charge alluded to OH^- ions adsorbed at the interface.[74] Most recently, same results have been confirmed by electrophoresis cells and via electroacoustic methods; further, with the addition of concentrated acid the isoelectric point (also the point of zero charge) of the oil-water interface was found to be at pH ≈ 3 (at which bubbles became stationary, i.e., the aqueous interface became charge neutral). [75, 355-360] The overall consensus was that the negative charge was due to the specific adsorption of hydroxide ions at the water-hydrophobe interface, releasing hydronium ions in the bulk. Thus, the air-water interface thought to be basic in nature.

However, at variance with the 150 years of experimental evidence, Jungwirth and co-workers claimed that "water surface is acidic" based on their *ab initio* molecular dynamics (AIMD) calculations employing the BLYP functional with DZVP basis set.[165] While BLYP functional has been known to inaccurately capture dispersion forces, especially the hydrogen bonding, [103-105] this article sparked an acrimonious debate between the theorists and the experimentalists [85, 89, 100, 152, 337, 338, 356, 361-367]. In fact, ignoring previous advances in the area, researchers (re)started arguing whether the negative potential of the air-water interface was due to specific

alignment of water dipoles therein; though, if that was the case, the observed electrophoretic mobility and negative zeta-potential of bubbles/drops could not be explained.[278, 368, 369] Even the role of solvated electrons was also evoked, but rejected due to magnitude of energies associated in exciting electrons in water.[367] Since there is confusion regarding the depth of the shear plane associated with the zeta-potential measurements, and its being representative of the interfacial phenomenon, surface-specific spectroscopy was expected to quantitatively resolve the issue.[85] But, unfortunately, it was not possible due to interpretational ambiguities, and experimental constraints, especially when probing H_3O^+ ions.[76, 79, 80, 85, 100] In fact, recent AIMD predictions have not been unanimous when applied to understand the propensity of OH^- at air-water interface. For example, while Mundy and co-workers[276] observe only 1 k_BT potential well for OH^- by potential of mean force calculations, Kudin and Car[279] observed that near a water-hydrophobic interface OH^- behaved as an 'amphiphilic' surfactant more so than H_3O^+. Most recent multistate empirical valence bond (MS EVB)[370, 371] based calculations by Wick reported "no free energy minimum at the air-water interface", except for a shallow -1.5 kcal mol^{-1} minima observed if polarizability was added "on the hydronium ion alone" in the model.[169] We posit, that all molecules are ions are polarizable. Also, it is interesting to note that despite all the disagreement most of these models capture the radial distribution function (RDF) of water perfectly. Thus "accurate" RDF should not be seen as primary metric when judging the molecular models, but it is most heavily employed.

We sought to investigate the nature of the negative surface potential (and charge) of the air-water interface with our ESIMS-based surface-specific platform. We employed gas-phase carboxylic acids (hexanoic and acetic acids) for the molecular reconnaissance of the air-water interface from either side: (1) *aerial side* via gas-liquid collisions, and (2) *water side* via dissolving organic acid in water, and analyzing ESIMS spectra (described in detail in Section 4.2 in Chapter 4). Thus, with a completely different setup than those used in previous electrokinetic experiments, we confirmed (1) presence of interfacial hydroxide ions at the aerial side of the air-water interface at pH > 2.5, (2) isoelectric point observed ≈ pH 2.5 in sync with electrophoretic experiments, and (3) enhanced autodissociation rate of water at the air-water interface. While the first two findings were not shocking to us, the third result is and we are exploring its details and implications(See Section 6.4.2 in Chapter 6). Two recent articles that have caught our attention in this regard are listed as references [38, 39].

It is curious to estimate the surface-charge density due to interfacial OH^- ions at the air-water interface. Applying electrokinetic measurements on aqueous emulsions, Beattie and co-workers have found this value to be "one hydroxide about every nm^2", which amounts to a surface density of about 1600 nC/cm^2.[75] Our measurements with a surface-specific electrospray ionization mass spectrometer, detailed in Chapter 2, could also be employed to estimate the surface density of the OH^- ions. With an uptake co-efficient, $\gamma \sim 0.05$, and the average speed of gaseous molecules (at 298 K), $c \sim 30{,}000$ cm/s, and the flux of incoming gaseous molecules to be, $n \sim 10^{12}$ molecules/cm^3, we get the number of proton transfer events to be, $N = \gamma \times c \times n/4 \approx 1.5 \times 10^{15}$ molecules/cm^2s. If the time duration for these collisions at the aqueous surface is, $\tau \approx 5$ μs, we get a surface density of OH^- ions to be, $N_{OH^-} = N \times \tau = 7.5 \times 10^9$ molecules/cm^2 ($= 7.5 \times 10^{-5}$ molecules/nm^2) leading to a surface-charge density to be: $\sigma \approx N_{OH^-} \times q \sim 1.2$ nC/cm^2. This estimate is $\sim 10^3$ times lower than the value reported by Beattie and co-workers. However, it is interesting to note that the isoelectric point reported in our experiments matches with other macroscopic electrokinetic measurements. We like to point that the zeta-potential measurement is not at the interface, but, in fact, at the slip-plane of the interface, that moves along with the air bubbles, or oil drops.[85] Thus, estimation of the interfacial charge may not be straightforward.

We also applied density functional theory simulations to gain deeper insight into our experiments. The theory predicted that the presence of interfacial OH^- ions was required for transferring protons from a gas-phase acetic acid to the surface of pure water, and the accepted proton neutralized the basic OH-at the surface (described in Section 4.5 in Chapter 4).[100, 154] In the absence of an interfacial anion, OH^- in this case, we could not find a stable geometry after proton transfer, i.e., the proton hopped back to the carboxylate anion. Unfavorable electrostatics and the large size of acetate ion underlie the nature of the kinetic barrier, similar to the dissociation of nitric acid on water described in the Section 3.6 in Chapter 3; further, acetic acid is also a much weaker acid (pKa = 4.8) than nitric acid (pKa = -1.3). Thus, with a complementary application of experiment and theory not only were we able to ascertain the surface density of the OH^- ions at the air-water interface, but also gain molecular insight in the process. It is hoped that these results will settle the debate on the acidity versus basicity of the air-water interface.[100]

6.3 Heterogeneous Chemistries on the Surface of Mildly Acidic Water

Nearly 0.01 % of the entire water on the planet Earth exists in the atmosphere. While this fraction appears tiny compared to ~ 97% in oceans, and ~ 2.1% in polar ice caps, and 0.6% in aquifers, the net surface area of water drops in clouds exceeds the surface area of our planet by a factor of ~ 50.[9] Thus, it is imperative to quantitatively realize the scope of heterogeneous chemistry on the surface of water, especially with gases capable of forming hydrogen bonds, such as, for example, HNO_3, NO_x, and SO_x.[9] During our investigation of the pH dependence of acid-catalyzed reactions at the air-water interface, via the surface-specific ESIMS, it was found that the surface of pH < 3 water could protonate most non-alkane organics with gas-phase proton affinity > 165 kcal/mol.[37, 42] We were surprised to find that coming from the gas-phase, inert hydrophobic molecules of isoprene (ISO) could be protonated ($ISOH^+$) and oligomerized ($(ISO)_nH^+$, n < 4) at the air-water interface (See Figure 5.2, Chapter 5). Our theoretical calculations with density functional theory showed the role of hydration in the process, i.e., the hydration status of hydronium, H_3O^+, ions could be such that it could exhibit thermochemistry akin to the gas-phase. In fact, the recent work of Doi et al.,[295] and previous findings of Morokuma et al.,[294] confirm the key role of microhydration in controlling the thermodynamics and kinetics of chemical reactions. These findings should have implications in both atmospheric chemistry, and green chemistry.

6.3.1 Environmental Implications: Heterogeneous Chemistry of Biogenic Isoprene

It is estimated that an annual flux of ~ 0.6×10^{15} grams of gaseous isoprene (ISO) is emitted by the biosphere.[326] To put the magnitude in perspective, it represents half of total volatile organic compound (VOC) emissions and amounts up to 10 % of photosynthetically fixed carbon.[372]In spite of the magnitude of these numbers and the anticipated response of this process to global warming and anthropogenic perturbations, it is not entirely how and how much of it is converted to aerosol.[326, 373] We considered that our experimental and theoretical findings could help solve the puzzle. In Chapter 5, we reported on protonation and oligomerization of ISO(g) on the surface of mildly acidic water. But how common are such surfaces in the environment is a pertinent question.

It is known that all environmental surfaces, including leaves, foliage, soil, buildings, and materials, have molecular layers of water molecules physisorbed on them.[55, 374] Key interactions at these interfaces include, hydrogen bonding, electrostatics, dispersion, induction, and repulsion.[375] Interestingly, several independent studies, some of which are listed herein, confirm that the water-lining on arboreal surfaces could contain proton concentrations equivalent to pH < 3 water. Water films produced by the condensation of ambient moisture on the cuticles of leaves are ~ 10 μm thick (determined from the weight gained by dried leaves of known surface area after they reach equilibrium in 90% relative humidity air) and persist down to low relative humidity.[376, 377]These waxy cuticles are polyelectrolytes with isoelectric point $pH_{IP} \approx 3$ and have low proton conductance. [378, 379]The intrinsic acidity of such polyelectrolyte cuticles can be inferred from the additional weight gained by the leaves saturated in 90% relative humidity upon exposure to NH_3(g). van Hove and Adema performed these experiments and found[376] that 50 μmoles of NH_3 cm^{-2} were absorbed irreversibly[380]by the ~ 10 μm thick water films, thereby leading to ~ 5 mM NH_4^+ solutions. Thus, it could be inferred that the water films produced by condensation of water vapor on leaves are not pristine water but (at the time they were exposed to NH_3(g)) acidic water at pH ~ 2.3. The detection of gas-phase hyponitrous acid, HONO(g), with $pK_a = 2.9$ [381]in the forest air by independent groups provides compelling evidence that these ecosystems, as a whole, are indeed at pH < 4. Further, HONO(g) emissions are largely the result of microbial activity in forest soils that are verifiably acidic (i.e., the pH of soil extracts, as measured using calibrated pH-meters, is acidic).[382] Notice, in passing, that reported soil pH values are actually upper limits (i.e., soils are actually more acidic than their extracts) because extracts are produced by lixiviating 1 g soil samples with 1 g of water.[383, 384] In addition to the leaves, and foliage, perhaps not coincidentally, forest soils have been reported to be sinks for ISO.[385] Given the large surface-to-volume ratios (LAI) of typical forest foliages, we inferred that the overhead foliage cannot be much less acidic than the soil beneath, for otherwise it would efficiently scavenge HONO(g) soil emissions (pK_a 2.9). In this context, it should be emphasized that the pH sensed by ISO upon contact with undisturbed leaves in a pristine forest during dry, sunny conditions is unrelated to the pH of dew or rainwater collected from such leaves at dawn or after rainfall. In addition to the intrinsic acidity of foliage, vegetation, even in remote locations, is exposed to acidic deposition. Notice moreover that the acidity of fog, rain or aerosol droplets just fallen on canopies is actually a lower bound to the acidity that ensues upon water evaporation.[386-388] For example, fine aerosol particles consisting of NH_4HSO_4 eventually deliquesce and reach pH = -0.5 in ambient air at 80%

relative humidity.[389]Particles containing excess (non-volatile) oxalic acid would approach pH = 0.3 under similar conditions.[389]Thus, our observations indicate that environmental surfaces could provide a heterogeneous sink for isoprene as significant (50-70%) as the gas-phase reactions.[42]

6.3.2 Implications in Green Chemistry

Sharpless and co-workers reported on the dramatic acceleration in rates of organic reactions, including aldol condensation, Mannich reaction, Claisen rearrangement, Michael addition, benzoin condensation and Grignard-type additions, when carried out in aqueous emulsions rather than pure organic phase.[62-65] The use of water in organic synthesis has obvious benefits owing to its abundance, non-toxicity, and non-corrosiveness, and thus has led to much excitement. However, despite its potential, underlying mechanisms for 'on-water' catalysis are not entirely clear. Various proposals have been put forth to account for this unanticipated phenomenon, such as favorable stabilization of polar transition states by the dangling OH groups 'on water' versus those interlocked 'in water',[45, 66, 67] strong adsorption of the hydroxide ion at aqueous interfaces,[69, 306] and the superacidity of hydronium ions at the air-water and oil-water interfaces.[32, 37] Our recent report on protonation and oligomerization of inert and hydrophobic isoprene at the surface of mildly acidic water (pH < 3) suggests that stabilization of transition states via hydrogen bonds at the air-water interface may not suffice an explanation.[66, 67] Based on the pH dependence of the experimental results, and our theoretical calculations (Section 5.5 and 5.7 in Chapter 5), we have demonstrated that the hydration gradient of hydronium ions at the air-water interface control the thermodynamics and kinetics of proton transfer reactions 'on-water'. We found that minimally hydrated interfacial hydronium ions at the surface of pH < 3 water are implicated in protonation and oligomerization of gas-phase isoprene at the air-water.[42] Recently, Enami et al., have confirmed these results on biogenic monoterpenes, such as limonene, α-pinene and β-pinene.[31] We consider that these superacidic hydronium ions can protonate most gas-phase non-alkane hydrocarbons according to the trends in the gas-phase thermochemistry.[37] We consider that vigorous shaking during the experiments reported by Sharpless and co-workers might play a crucial role in enabling the formation of minimally hydrated $H_3O^+(H_2O)_n$ clusters, but it remains to be demonstrated theoretically. In the future, we plan to apply a reactive forcefield, ReaxFF,[390] developed by

Goddard and Duin to investigate acid-catalyzed oligomerization of isoprene on a realistic aqueous system *in silico*. Our initial attempts have not been successful in this regard, i.e., we did not observe proton transfer or oligomerization during a time of 1 ns at elevated temperature (100 ºC) to expedite the kinetics (results not presented here).

6.4 Future Work

Presented below are new scientific inquiries that arose during the course of this dissertation.

6.4.1 How Do Interfacial Phenomena Manifest at Low Salt Concentrations?

A natural, but profound, observation during our experimental investigation of anion-catalyzed proton transfer reactions at the air-water interface was the emergence of the catalytic activity at electrolyte concentrations as low as 30 μM (Debye length ~ 10 nm, ion-ion separation ~ 100 nm). How could the effect of anions pervade through such long distances and influence the propensity of faraway interfacial water molecules towards accepting protons from HNO_3(if)? Indeed, these findings are reminiscent of the Jones-Ray effect, wherein a depression in the surface tension of water is observed in the < 1 mM concentration range, followed by monotonic increase.[133, 134] Jones-Ray effect falls out of the scope of the theory of surface tension developed by Wagner, and Onsager and Samaras, based on interionic electrostatics.[131, 132] In their classic article, Jones and Ray concluded with the rational speculation of McTaggart[71, 72], "If we add a salt to water in such great dilution that the interionic forces are negligible, there must nevertheless be a disturbance of the normal arrangement of the water molecules in the vicinity of the ions. The electric forces between the water dipoles would oppose this disturbance and tend to thrust the disturbing ions out into the surface, thus causing positive adsorption. In view of the electrically unsymmetrical character of the water molecules, this force may well be different for positive and negative ions, thus accounting for the effects described by McTaggart". Inspired by the insightful work of Frumkin, Dole invoked the idea of dynamic "active spots" at the air-water interface, one per ~ 25,000 water molecules, such that negative ions from the interior followed Langmuir adsorption statistics enforced via electrostatic attraction.[135] For completeness, while this model could account for the Jones-Ray effect, it fails to account for the specific-ion effects at the air-water interface.[15, 136] In particular, the observation of the Hofmeister effect has remained unexplained, wherein ions influence each other specifically at the air-water interface at micromolar dilutions. A recent review article by Marcus provides an in depth account of "structure making and breaking effects" of ions in/on water.[98]

An alternative way for propagating (electrical) signals across interfacial water molecules via sparse anions could be via a joint effect of (1) vectorial rotation of anion-bound water dipoles, and (2)

electrodynamic percolation network of hydrogen bonds propagating across long distances (See Appendix I). Since anions attract the hydrogen-end of a water molecule, the dipolar vector could perturb adjacent dipoles and propagate perturbation to long distance (Figure 6.1). Note that this is not possible in the case of interfacial cations as they attract the central oxygen atom of a water molecule, thus locking its azimuthal orientation (Figure 6.1). We present some of our ongoing work in this direction.

Figure 6.1: (Left) Schematic of interactions between water-dipoles and cations at the air-water interface; (Right) Schematic of interactions between water-dipoles and anion at the air-water interface.

6.4.1.1 Experiments

Recently, Enami and co-workers investigated specific ion effects at the vapor-liquid interface of water, methanol, and isopropanol. Remarkably, they found that water and methanol exhibited long-range specific ion effects, while IPA did not.[137] By applying molecular dynamics simulations, we are currently simulating the extent of percolation networks of hydrogen bonds in methanol and isopropanol. Our initial results are as follows:

6.4.1.2 Theoretical Approach

Our simple model of the liquid-vapor interface consisted of a 200 molecules of methanol (or isopropanol, or water or acetonitrile) in a cube of size determined by the bulk density (methanol: 792 Kg/m^3, isopropanol: 786 Kg/m^3). The methanol slab was a cube of edge ≈ 3nm, while the IPA slab was a cube of edge ≈ 2.4 nm. To simulate the liquid-vacuum interface, the z-dimension of a slab was extended into vacuum by 40 Å. A harmonic potential wall of stiffness 10 kcal mol^{-1} was placed at a distance of 5 Å from the liquid-vacuum interface to preempt the loss of atoms during the course of dynamics. With periodic boundary conditions in place, each slab had 6 – 8 layers of the solvent, thus affording a gradual transition from the bulk phase to vacuum. To describe methanol and isopropanol, we used a Dreiding forcefield, that has been demonstrated to provide an accurate description of structures and energetic of organics.[391] We consider that this model is adequate to capture the percolation network of the hydrogen bonds; there are no charges in our current systems.

6.4.1.3 Molecular Dynamics procedure

Energy minimization was carried out by a conjugate gradient algorithm, wherein at every step the force gradient is combined with the previous iteration information to compute a new search direction perpendicular to the previous search direction. Iterations terminated when one of the stopping criteria (energy or force tolerance) was satisfied. The local energy minimum afforded a good starting point for the dynamics. As a starting point, all atoms were assigned velocities following a Gaussian distribution with a mean situated at T = 10K. Following this, time integration on Nose-Hoover style non-Hamiltonian equations of motion, designed to generate positions and velocities sampled from the canonical (NVT) ensemble, was applied to ramp the temperature of the system up to 298 K. The time step was chosen to be 1fs, and the equations of motion used were those of Shinoda et al.,[392] which combine the hydrostatic equations of Martyna et al., [393] with the strain energy proposed by Parrinello and Rahman[394]. The time integration schemes closely followed the time-reversible measure-preserving Verlet and rRESPA integrators derived by Tuckerman et al[395]. AT 298 K, the system explored different configurations in an NVT ensemble for 1 ns and the data for analysis was extracted from the last 20 ps.

6.4.1.4 Percolation network analysis

For equilibrated slabs of methanol and isopropanol, the top 6 Å region was investigated for percolation networks of the hydrogen bonds. Two molecules were regarded to belong to a cluster if they were connected via a hydrogen bond. For every oxygen atom within the top 6 Å region, at the liquid-vacuum interface, hydrogen atoms within a range of 0.9 Å < d < 2.0 Å were evaluated. For statistical efficacy, several snapshots of the 20 ps dynamics trajectory (post NVT equilibration at 298 K) were analyzed. Our results consistently indicated that methanol surface was connected by long-range percolating hydrogen bond network, whereas the surface of isopropanol was marked by sporadic, small clusters connected via hydrogen bonds (Figure 6.2). Intuitively, it makes sense because of the steric hindrance due to the methyl groups and the van der Waals attractive interactions between them. In the past, reports on the percolation network of hydrogen bonds at the surface of water have appeared, and agree with our findings.[396, 397] Thus, the long-range effects may not be crucially influenced solely due to the pinching of capillary waves as suggested recently by Geissler and co-workers. [83]

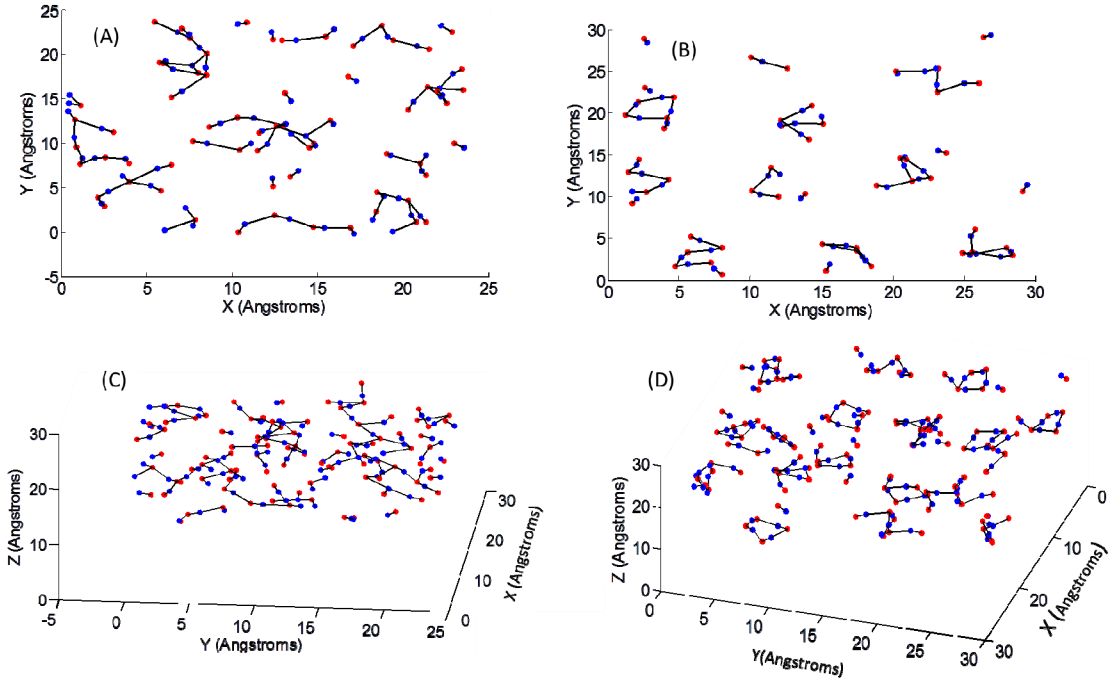

Figure 6.2 (A) Hydrogen bond percolation networks at the vapor-liquid interface of methanol; (B) Hydrogen bond percolation networks at the vapor-liquid interface of isopropanol; (C) Depth profile of the methanol slab; (D) Depth profile in the case of isopropanol. This simple model suggests that in the case of methanol the percolation network of hydrogen bonds is denser and longer.

In the future, it would be interesting to add charges and consider them via polarizable forcefields to see the effect of long-range percolation networks on translocation of partial charges via fluctuations, and induced dipole-dipole interactions. Another interesting direction would be to study the mixtures of isopropanol and water and analyze the extent of resulting percolation networks. Insights derived should have implications across natural and applied sciences.

6.4.2 CO_2 Uptake and Release from the Ambient Atmosphere by Controlling Hydration at the Gas-Solid Interface

As seen in Chapter 5, hydration could play a crucial role in interfacial chemistries. Herein, we propose to understand, and develop materials capable of absorbing CO_2 gas from the ambient atmosphere. Indeed, global concern over carbon dioxide (CO_2) emissions from unsustainable consumption of fossil fuels requires CO_2 capture and sequestration.[398-400] Desired processes should be sustainable, cost-effective and scalable.[401] Traditional methods for trapping CO_2 from industrial waste gases have been dominated by aqueous alkanolamines and alkali solutions (reactions R_1 and R_2) leading to carbamates and carbonates, respectively.[402] The problems impeding their global acceptance are threefold: (i) corrosive nature [403], (ii) formation of stable carbamates and carbonates (bond strengths > 50 kcal mol^{-1}) requiring intense thermal kick to desorb CO_2 for sequestration[399, 401, 404], and (iii) globally distributed CO_2 emission sources call for a pragmatic CO_2 capture technique that could capturing CO_2 from the air anywhere.[399, 401, 405] Recent reports by Lackner and co-workers on the prospect of using commonly available, low cost anion-exchange resins to this end have sparked optimism. [401, 406-408]

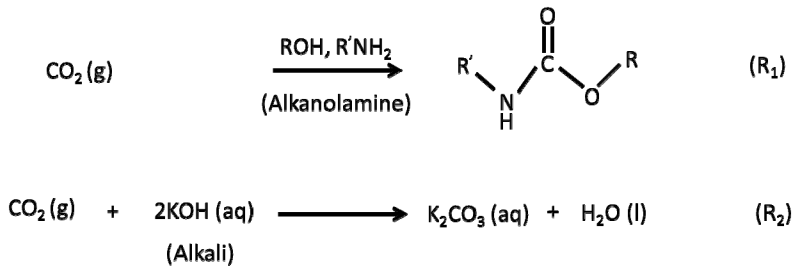

Reaction scheme I: (R_1) for gaseous CO_2 capture with alkanolamine leading to formation of carbamates, and (R_2) for alkali solutions forming strong carbonate bonds.

6.4.2.1 Ion-Exchange Media as Gas-Sorbents

As early as 1960s, ion-exchange resins were investigated for molecular sieving of industrial pollutants like SO_2, NO_x and H_2S.[409] Operating on an entirely different binding mechanism than alkanolamine solutions, these solid sorbents seem to offer an effective solution to the CO_2 problem. For example, strong-base ion-exchange resins, in hydroxide form, present moderate binding

strengths (< 10 kcal mol^{-1}) with gaseous CO_2, and faster kinetics than amine solutions.[401] Quinn and co-workers were the first to report that CO_2 from process gas-streams could be captured into salt hydrates containing quaternary ammonium fluoride (reaction R_3). Further, they made a curious observation that the uptake of CO_2 was inversely related to the extent of hydration in the salt hydrates.[410, 411] By flowing mixed gas-streams containing CO_2 on quaternary ammonium fluoride/acetate/chloride/hydroxide salt hydrates, they found that (i) F^- form captured CO_2 and could regenerate easily, (ii) CH_3COO^- form was sluggish at both uptake and release, (iii) heats of absorption of CO_2 by F^- and CH_3COO^- forms were moderate, ranged from 4-8 kcal mol^{-1}, (iv) Cl^- form did not uptake CO_2, and (v) hydroxide form did not regenerate, i.e. formed permanent bicarbonate.[411] Quinn and co-workers also analyzed strong-base ion-exchange resins for reversible CO_2 uptake and found results similar to salt-hydrates.[410] Recently Lackner and co-workers have spearheaded development of inexpensive, non-toxic, stable and robust materials based on hydroxide form of strong-base anion ion-exchange resins.[401, 406-408] These materials are able to reversibly uptake gaseous CO_2 from the ambient atmosphere (partial pressure ~ 38 Pa) under standard conditions simply by adjusting the relative humidity level on the resinous films. However, mechanisms underlying the reversible uptake of ambient CO_2 gas in this material are not entirely clear. We consider that the thermochemistry of hydration of OH^- ions at the gas-solid interface could explain the process.

6.4.2.2 Thermochemical Considerations

As demonstrated in Chapter 5, the chemical activity of ionic species at aqueous interfaces is extremely sensitive to the extent of hydration.[312, 412]. We consider that under dry conditions, hydroxide functionalized quaternary ammonium salts may behave as strong bases. Tetralkylammonium anion-exchange resins have been reported to be minimally solvated under dry conditions, thus, rendering hydroxide groups stronger bases than in bulk water.[413] Gas-phase thermochemistry literature reveals that hydroxide, OH^-, in gas-phase is a significantly stronger base than in bulk water (proton affinity, PA_{OH^-} = 390 kcal mol^{-1} compared to PA_{H2O} = 165 kcal mol^{-1}). Thus, extremely basic OH^- residing on the surface of a resin can neutralize an acidic gas like CO_2 subject to the hydration gradients therein. This explains the Langmuir-type surface saturation behavior as observed by researchers.[408, 411] Under dry conditions, this acid-base reaction at the gas-resin interface is exergonic and leads to formation of interfacial HCO_3^- (reaction R_3).

$$CO_{2\,(g)} + OH^-_{(s)} \text{ (Dry resin)} \longrightarrow HCO_3^-{}_{(s)} \qquad (R_3)$$

Reaction scheme III: for gaseous CO_2 capture with OH^- bound to solid resin or salt-hydrate leading to formation of bicarbonate

In the gas-phase reaction R_4 is exothermic with a $\Delta G° = -38$ kcal mol^{-1}. Thus, the equilibrium constant is described in the gaseous standard state as, $K_p = \frac{1}{[p_{CO_2}]} = e^{\frac{-\Delta G^\circ_{(g)}}{RT}}$

If pressure in gas phase is 1 bar and α describes the fraction of CO_2 left after HCO_3^-(if) formation, it can be easily shown that $\alpha \sim 0$. It means that in dry state, interfacial OH^- should bind ambient CO_2. Similar analysis explains the observations of F^-, Cl^-, CH_3COO^- and CO_3^{2-} containing salt hydrates or resin leading to the formation of interfacial bicarbonate with or without co-participation of a water molecule. Next, as the resin is gradually hydrated the standard state at the interface starts shifting from the gas-phase towards that aqueous phase shown in reaction R_4.

$$CO_{2\,(if)} + OH^-_{(aq)} \text{ (Wet resin)} \rightleftharpoons HCO_3^-{}_{(aq)} \qquad (R_4)$$

Reaction scheme IV: for binding interaction of CO_2 with OH^- (aq) in wet resin or salt-hydrate

In the aqueous phase, R5 is thermodynamically favored by a $\Delta G° = -9$ kcal mol^{-1} along with a kinetic barrier of $\Delta G^{\ddagger} = 13$ kcal mol^{-1}. Thus, the equilibrium constant is described in the condensed phase as,

$$K_p = \frac{1}{[(1-\alpha)C_{CO_2}]} = e^{\frac{-\Delta G^\circ_{(aq)}}{RT}} \qquad (R_5)$$

If the concentration of CO_2 in the condensed phase is $C_{CO2} = 1$M, and α describes the fraction of undissociated CO_2, it can be easily shown that $\alpha \sim 0.2$. Thus, in aqueous phase a significant amount of CO_2 is thermodynamically disfavored to be converted in to HCO_3^- form. Thus, a physicochemical analysis of the reaction between OH^- and CO_2 leading to HCO_3^- in appropriate standard states shows that the dry state OH^- leads to extremely low partial pressures of CO_2(g), and

the trend might reverse as the standard shifts to the aqueous phase. Similar analysis explains the observation of F^-, Cl^-, CH_3COO^- and CO_3^{2-} containing salt hydrates or resin leading to formation of interfacial bicarbonate with or without co-participation of a water molecule. Reversible conversion of gaseous CO_2 into HCO_3^- is achieved by harnessing the gas-phase thermochemistry of ion solvation at gas-solid interface. Why is CO_2 uptake in ion-exchange resins so sensitively dependent on hydration gradients? In a recent study of anion-exchange resins via x-ray absorption spectroscopy, Yuchi and co-workers found that (i) all the water molecules adsorbed at the resin-air interface were assigned to anion hydration, following which and (ii) the adsorbed water molecules were ascribed to multilayer adsorption or condensation in resin pores.[414]

6.4.2.3 Conclusions

The analysis based on standard states in gas- and condensed-phases qualitatively captures the CO_2 uptake phenomenon at gas-solid interface. In reality, neither the dry resin bound OH^- is exactly gas-phase, nor is the bound HCO_3^- in wet resin completely aqueous. We envision that with increasing hydration the interfacial anions have several intermediate hydration states to traverse through before acquiring full hydration. Figure 6.3 shows that during this gradual transition of hydration states from gas-phase to condensed phase, the interconversion of HCO_3^-(if) to OH^-(if) + CO_2(if) takes place which is constrained by a sizeable kinetic barrier in aqueous state. In the future, we hope to investigate the role of hydration in this process by theory. Based on this approach, inexpensive materials could be engineered for CO_2 absorption from the ambient atmosphere.

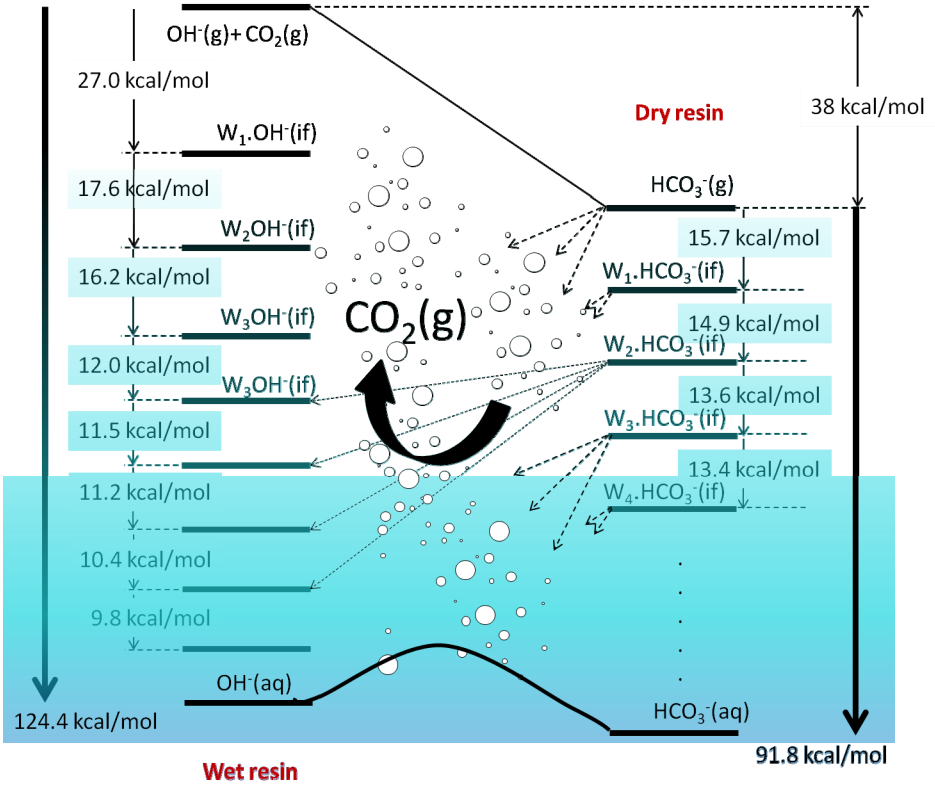

Figure 6.3: Hydration gradients at the solid-gas interface control the reversible binding of CO_2 in the resin. (The numbers represent qualitative energy landscape since interfacial OH^- has only a partial gas-phase character)

6.4.3 Faster Autodissociation of Water at the Air-Water Interface

The ionic product of bulk water, K_w, has a fundamental bearing on both chemical and physical processes in aquatic systems and ubiquitous aqueous interfaces. Eigen and DeMayer have provided an elegant review of autodissociation and proton transport in water. [292] At the time of this dissertation, it is well established regarding water that (1) the forward dissociative event is impeded by an enthalpic barrier of ΔH = 13.5 kcal mol^{-1}, $k_f \approx 2.5 \times 10^{-5}$ s^{-1}, as well as an entropic cost $\approx \Delta S$ = -30 cal.mol^{-1}K^{-1} due to tightly bound solvation shells around resulting ions, and (2) the backward-half reaction is controlled by molecular diffusion with a recombination rate, $k_b \approx 10^{11}$ LM^{-1}s^{-1}. Thus, the equilibrium autodissociation constant for bulk water is $K_{Eq} = k_f/k_b = 10^{-15.7} M$, which leads to the ionic product of water, $K_w = K_{Eq}[H_2O(aq)] = 10^{-14}$ M^2, where $[H_2O(aq)] = 55.5$ mol/L. (Figure 6.4).These results readily yield the fact that bulk water is electroneutral at pH = 7, i.e., [H_3O^+] = [OH^-] under ambient conditions (T = 298 K, and P = 1 atm). However, whether or not the value of K_w holds at aqueous interfaces with air, i.e., $K_w = K_{w,Int}$ or $K_w \neq K_{w,Int}$, remains an important question with implications across natural and applied sciences. Indeed, there are various independent reports on anomalous (1) enhancements in the proton conduction at the phospholipid-water interface,[206] (2) correlation between the contact electrification and relative humidity,[7, 354] and (3) lateral conductivity in scanning tunneling microscopy[415, 416] and spectroscopy experiments[17, 18, 30, 201, 417] of wet phospholipid membranes. These phenomena are fundamental to various natural processes, as listed in the introductory section in Chapter 1.

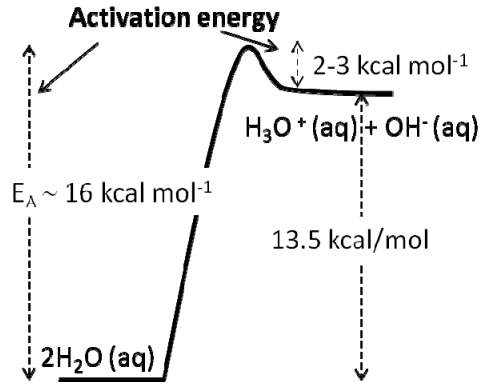

Figure 6.4: Enthalpy landscape drawn based on experimental dissociation barrier for autodissociation of water in the bulk solution.

6.4.3.1 Experimental Results

Our experimental results, validating plethora of macroscopic electrokinetic measurements of the air-water, and oil-water interfaces, unambiguously showed the isoelectric point of the air-water interface to be at pH ≈ 3. It implies that the concentration of OH^- ions at the air-water interface, i.e. top $\delta \approx 1$ nm slice, has $p[OH^-] \approx 3$, i.e. $[OH^-] = 10^{-3}$ mol/L. Imagining a slab of water with thickness $\delta \sim 1$ nm, this concentration pertains to a surface density of : $N_{OH^-} \approx 10^{-4}$ #OH^-/nm^2 that is commensurate with our calculation of the surface density of OH^- at the air-water interface as presented in section 6.2 above. This surface density is equivalent to a surface charge density of 1.6 nC/cm^2. This is a very interesting result because, owing to the charge neutrality of the aqueous slab, the concentration of the counterion, $H_3O^+ = 10^{-3}$ M in the layers below the air-water interface. Thus, we propose that the autoionization constant for the water at the air-water interface to be, $K_{W,Int} \approx 10^{-6}$ (mol/L)^2 under ambient conditions.

This finding suggests that water is not just a solvent with a large dielectric constant, high dipole moment, decent polarizability, and curiously sculpted hydrogen bond for physical interactions. Due to the faster autoionization of water at the air-water interface, the scope of roles and functions for water grows exponentially. Independence of ion concentration at the interface from the bulk pH adds a new frontier to be explored regarding surface charging, ion solvation, and transmission of electrical signals across interfaces. In fact, recent articles by Stuve and co-workers,[38, 418] and Bonn and co-workers,[39] have considered the possibility of enhanced autodissociation of water at interfaces with electrodes and phospholipids arising from excessive electrical fields of ions therein. Unfortunately, however, this explanation rapidly leads to the 'cause-effect quagmire', i.e., how did ions manifest in first place.

Herein we base our arguments primarily on entropic effects. Indeed, the natural surface charge/potential at the air-water interfaces would have a supporting influence on fast autoionization.

6.4.3.2 Thermochemical Considerations

We consider a possibility of a larger rate of unimolecular dissociation of water molecules at the air-water interface compared to bulk. Let's assume that a water molecule at the air-water interface

autoionizes unimolecularly with an activation energy equal to the experimentally measured, ΔH = 13.5 kcal/mol, of ionization in the bulk. This is the minimum energy cost of dissociating water. The resulting ions are assumed to be fully stabilized by hydration at the interface, i.e., they are at the interface but connected to the rest of water.

$$H_2O\ (aq) \longrightarrow H^+\ (aq) + OH^-\ (aq) \qquad \text{(R1)}$$

In bulk water, for a typical O-H vibrational stretch frequency at $\nu \sim 3600\ cm^{-1}$ ($\sim 1 \times 10^{14}\ s^{-1}$), we estimate a rate constant for the autodissociation reaction using the transition-state theory:

$$k_f = \frac{k_B T}{h} \times e^{\left(\Delta S_{Act}/R\right)} \times e^{\left(-\Delta H_{Act}/RT\right)} \qquad \text{(R2)}$$

Since, the experimental value for $k_f = 2 \times 10^{-5}\ s^{-1}$, and ΔH_{Act} = 13.5 kcal/mol, we expect the entropy of activation to be ΔS_{Act} = -30 cal/mol-K. Next we ask could water dissociate with a zero entropic penalty? Is so, where? Because, curiously, as the entropic penalty at the air-water interface, $\Delta S_{Act,Int}$, limits to zero, the upper limit of the forward rate of autodissociation reaction, $K_{f,Int} \sim 0.45 \times 10^2\ s^{-1}$. We expect the rate of ion recombination to remain the same, thus, leading to the equilibrium constant $K_{Eq,Int}$ and the ionic product, $K_{w,Int}$ at the air-water interface to be larger than K_w by a factor of $e^{\left(-\Delta H_{Act}/RT\right)} = 5.5 \times 10^7\ (mol/L)^2$, i.e. $K_{w,Int} \sim 10^{-6}\ (mol/L)^2$. Curiously, the predicted value matches with our experimental report on the ionic product at the air-water interface.

6.4.3.3 Vibrational Entropy at the Air-Water Interface

Assuming water to be an ideal gas of I-D harmonic oscillators, we note that the partition function for the vibrational energy for a mole to be $Q^{vib} = \left(1 - e^{-\frac{h\nu}{kT}}\right)^{N_o}$, where N_o is the Avogadro's number. For vibration frequencies of the O-H bond > 2000 cm^{-1}, $h\nu >> kT$, thus, Q^{vib} approaches unity. [419] As a result, all thermodynamic functions for vibration, such as entropy, approach zero. Interestingly, it appears that at the air-water interface, soft (collective) modes of water will play

dominant role in sampling the configuration space. Since the air-water interface is prone to reorganization, it is conceivable that autodissociation would accrue minimal entropic cost. Besides these simplistic arguments, we are conducting molecular dynamics simulations on slabs of water with vacuum on either sides, to be followed by a two-phase thermodynamics analysis to estimate entropy and enthalpy of H_3O^+ and OH^- ions at the air-water interface. [420]

6.4.3.4 Compensation Effect in Chemical Thermodynamics

The compensation effect is considered the *sine qua non* in chemical thermodynamics, i.e., with a reduction in entropy, there should be a concomitant increase in the enthalpy of the O-H bond dissociation.[421] We consider that at the air-water interface it might be possible to have the entropic penalty for proton transfer to go to zero, without affecting the enthalpic penalty by assuming that the resulting species are reasonably hydrated. Currently, we are thinking and exploring this area to come up with a reasonable theoretical explanation for our experimental results. An interesting reference in this regard is listed in [422].

6.4.3.5 Implications in Biology

We would like to consider the impact of faster autoionization of water at water-hydrophobe interfaces in biological processes dealing with proton gradients. Recently Maret and co-workers presented a curious case regarding the volume of cellular compartments and pH values ascribed to them commonly.[423] Their key observation was that several cellular compartments with volumes ranging within femto- (10^{-15}) to atto- (10^{-18}) to zeptoliters (10^{-21}) with prescribed pH ranging within ~ 5-7, at 37 ºC, are too small to contain even a single proton. They asked how do H^+ and OH^- dependent biochemical reactions take place. Our proposal for the enhanced autodissociation at water-hydrophobe interface might help resolve this issue.

6.4.3.6 Implications in Atmospheric Chemistry

Towards understanding activation of aerosol particles and growth of clouds, Davidovits and co-workers designed a beautiful set of experiments wherein they investigated the mass accommodation coefficient (MAC), and surface accommodation coefficient (SAC) of gas-phase H_2O and D_2O on the surface of water.[424] While the MAC is the probability that a gas-phase molecule alighting on the gas-liquid interface would enter the bulk phase, SAC is the probability that a gas-phase molecule alighting on the gas-liquid interface becomes a part of the surface (likely via chemisorption). Similar to our experiments described in Chapter 3, the gas-phase D_2O molecules (~ 10^{14} cm^{-3}) strike the surface of water and get adsorbed. In the absence of surface reactions, the surface-bound species would desorb, or stay attached to the surface, or enter the bulk. They found SAC to be ~ 1 and the MAC to be ~ 0.2 and insensitive to ambient thermal fluctuations. However, it has remained unclear why the SAC was so high. Our report on the presence of interfacial OH^-, and faster dissociation of the interfacial water would imply fast exchange of H-D at the surface of water.[425]

6.5 Cation-π Interactions at the Water-Hydrophobe Interface

In recent years, it has been shown that the magnitude of interactions between cations and π-systems could be comparable to hydrogen bonds, ion-pair, and hydrophobicity in aqueous phases.[426] In particular, these interactions have been shown to play key roles in neurotransmission, nicotine addiction[427], ion channels,[428] molecular recognition and catalysis,[429] and nerve signaling[430]. In an exhaustive analysis of the protein data bank, Dougherty and co-workers concluded that about a quarter of all tryptophan residues in proteins experience energetically significant cation-π interactions.[431] Cation-π interactions might also have noteworthy impact in the environment due to ubiquity of Na^+ and K^+ in surfaces. Currently, only gas-phase and liquid-phase trends in the binding energy of cation-π interactions are known and values at the interface are obtained by extrapolation. Employing the surface-specific platform at Caltech, we have recently started experiments investigating the cation-π interactions of Li^+ with pyridine and pyrrole. We found pure pyrrole to be inactive during the collision times in our experiments (results not shown). However, we found an interesting trend in the interaction of pyridine (Pyr) with Li^+ ions. As shown in Figure 6.5, the trend in cation-π interactions changed as pyridine molecules approached the air-water interface from the aerial versus the aqueous side. We found the formation of a complex of Li^+ ion with two Pyr molecules to be strongly favored when Pyr approached the air-water interface from the gas-phase.

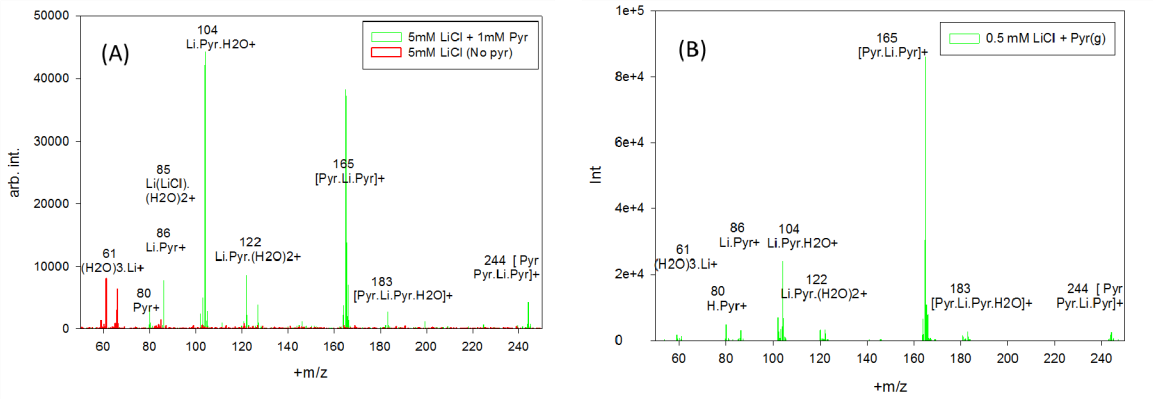

Figure 6.5: (A) Mass spectra of the cation- π species formed in the aqueous phase, (B) Mass spectra of the cation-π species at the air-water interface

In the future, more work on this problem, especially investigating the competitive cation-π interactions among, for example, H^+, Li^+, Na^+, K^+ ions and Pyr at the air-water interface could provide chemical insight about the efficacy of Li^+ ions in specific medical applications.[432]

Bibliography

[1] Szent-Gyorgyi A. Cell-Associated Water. New York: Academic Press; 1979.
[2] Jacobi J. Paracelsus: Selected Writings: Princeton University Press; 1979.
[3] Chaplin M. Opinion - Do we underestimate the importance of water in cell biology? Nature Reviews Molecular Cell Biology 2006;7:861-6.
[4] Ball P. Water as an active constituent in cell biology. Chem Rev 2008;108:74-108.
[5] Ball P. Water as a Biomolecule. Chemphyschem 2008;9:2677-85.
[6] Ball P. Life's matrix: Water in the cell. Cellular and Molecular Biology 2001;47:717-20.
[7] McCarty LS, Whitesides GM. Electrostatic charging due to separation of ions at interfaces: Contact electrification of ionic electrets. Angew Chem-Int Edit 2008;47:2188-207.
[8] Wheeler TD, Stroock AD. The transpiration of water at negative pressures in a synthetic tree. Nature 2008;455:208-12.
[9] Seinfeld JH, Pandis, S. N. Atmospheric Chemistry and Physics: From Air Pollution to Climate Change: Wiley-Interscience; 2 edition; 2006.
[10] Ramanathan V, Crutzen PJ, Kiehl JT, Rosenfeld D. Atmosphere - Aerosols, climate, and the hydrological cycle. Science 2001;294:2119-24.
[11] Gascoyne PRC, Pethig R, Szent-Gyorgyi A. Water structure-dependent charge transport in proteins. Proceedings of the National Academy of Sciences of the United States of America-Biological Sciences 1981;78:261-5.
[12] Chameides WL. Acid Dew and the Role of Chemistry in the Dry Deposition of Reactive Gases to Wetted Surfaces. J Geophys Res-Atmos 1987;92:11895-908.
[13] Griffith EC, Tuck AF, Vaida V. Ocean-Atmosphere Interactions in the Emergence of Complexity in Simple Chemical Systems. Accounts Chem Res 2012;45:2106-13.
[14] Griffith EC, Vaida V. In situ observation of peptide bond formation at the water-air interface. P Natl Acad Sci USA 2012;109:15697-701.
[15] Lo Nostro P, Ninham BW. Hofmeister Phenomena: An Update on Ion Specificity in Biology. Chem Rev 2012;112:2286-322.
[16] Alberts B, Johnson, A., Lewis, J., Raff M., Roberts, K., Walter, P. Molecular Biology of the Cell: Garland Science; 5 edition 2007.
[17] Mulkidjanian AY, Heberle J, Cherepanov DA. Protons @ interfaces: Implications for biological energy conversion. Bba-Bioenergetics 2006;1757:913-30.
[18] Mulkidjanian AY, Cherepanov DA. Probing biological interfaces by tracing proton passage across them. Photoch Photobio Sci 2006;5:577-87.
[19] Drachev LA, Kaulen AD, Skulachev VP. Correlation of Photochemical Cycle, H+ Release and Uptake, and Electric Events in Bacteriorhodopsin. Febs Lett 1984;178:331-5.
[20] Dorsam RT, Gutkind JS. G-protein-coupled receptors and cancer. Nat Rev Cancer 2007;7:79-94.
[21] Zhong C, Deng YX, Roudsari AF, Kapetanovic A, Anantram MP, Rolandi M. A polysaccharide bioprotonic field-effect transistor. Nat Commun 2011;2.
[22] Nagle JF, Mille M, Morowitz HJ. Theory of hydrogen-bonded chains in bioenergetics. J Chem Phys 1980;72:3959-71.
[23] Capasso M, DeCoursey TE, Dyer MJS. pH regulation and beyond: unanticipated functions for the voltage-gated proton channel, HVCN1. Trends Cell Biol 2011;21:20-8.

[24] Patel AJ, Varilly P, Jamadagni SN, Hagan MF, Chandler D, Garde S. Sitting at the Edge: How Biomolecules use Hydrophobicity to Tune Their Interactions and Function. J Phys Chem B 2012;116:2498-503.
[25] Nandi N, Bagchi B. Dielectric relaxation of biological water. J Phys Chem B 1997;101:10954-61.
[26] Pal SK, Peon J, Zewail AH. Biological water at the protein surface: Dynamical solvation probed directly with femtosecond resolution. P Natl Acad Sci USA 2002;99:1763-8.
[27] Nissen P, Hansen J, Ban N, Moore PB, Steitz TA. The structural basis of ribosome activity in peptide bond synthesis. Science 2000;289:920-30.
[28] Kamerlin SCL, Warshel A. At the dawn of the 21st century: Is dynamics the missing link for understanding enzyme catalysis? Proteins 2010;78:1339-75.
[29] Benkovic SJ, Hammes-Schiffer S. A perspective on enzyme catalysis. Science 2003;301:1196-202.
[30] Mulkidjanian AY. Conformationally controlled pK-switching in membrane proteins: One more mechanism specific to the enzyme catalysis? Febs Lett 1999;463:199-204.
[31] Enami S, Hoffmann MR, Colussi AJ. Dry Deposition of Biogenic Terpenes via Cationic Oligomerization on Environmental Aqueous Surfaces. J Phys Chem Lett 2012;3:3102-8.
[32] Hayase S, Yabushita A, Kawasaki M, Enami S, Hoffmann MR, Colussi AJ. Weak Acids Enhance Halogen Activation on Atmospheric Water's Surfaces. J Phys Chem A 2011;115:4935-40.
[33] Hayase S, Yabushita A, Kawasaki M, Enami S, Hoffmann MR, Colussi AJ. Heterogeneous Reaction of Gaseous Ozone with Aqueous Iodide in the Presence of Aqueous Organic Species. J Phys Chem A 2010;114:6016-21.
[34] Enami S, Hoffmann MR, Colussi AJ. Molecular Control of Reactive Gas Uptake "on Water". J Phys Chem A 2010;114:5817-22.
[35] Enami S, Hoffmann MR, Colussi AJ. Prompt Formation of Organic Acids in Pulse Ozonation of Terpenes on Aqueous Surfaces. J Phys Chem Lett 2010;1:2374-9.
[36] Enami S, Vecitis CD, Cheng J, Hoffmann MR, Colussi AJ. Global inorganic source of atmospheric bromine. J Phys Chem A 2007;111:8749-52.
[37] Enami S, Hoffmann MR, Colussi AJ. Superacid Chemistry on Mildly Acidic Water. J Phys Chem Lett 2010;1:3488-93.
[38] Stuve EM. Ionization of water in interfacial electric fields: An electrochemical view. Chem Phys Lett 2012;519-20:1-17.
[39] Mashaghi A, Partovi-Azar P, Jadidi T, Anvari M, Jand SP, Nafari N, et al. Enhanced Autoionization of Water at Phospholipid Interfaces. J Phys Chem C 2013;117:510-4.
[40] Mishra H, Enami S, Nielsen RJ, Hoffmann MR, Goddard WA, Colussi AJ. Anions dramatically enhance proton transfer through aqueous interfaces. P Natl Acad Sci USA 2012;109:10228-32.
[41] Mishra H, Nielsen RJ, Enami S, Hoffmann MR, Colussi AJ, Goddard WA. Quantum chemical insights into the dissociation of nitric acid on the surface of aqueous electrolytes. International Journal of Quantum Chemistry 2012;113:5.
[42] Enami S, Mishra H, Hoffmann MR, Colussi AJ. Protonation and Oligomerization of Gaseous Isoprene on Mildly Acidic Surfaces: Implications for Atmospheric Chemistry. J Phys Chem A 2012;116:6027-32.

[43] Colussi AJ, Yabushita, A., Enami, S., Liu, W. G., Mishra, H., Hoffmann, M. R., Goddard, W. A. Tropospheric Aerosol as Reactive Intermediate. Faraday Discussions (accepted) 2013.
[44] Kinugawa T, Enami S, Yabushita A, Kawasaki M, Hoffmann MR, Colussi AJ. Conversion of gaseous nitrogen dioxide to nitrate and nitrite on aqueous surfactants. Phys Chem Chem Phys 2011;13:5144-9.
[45] Wang L, Khalizov AF, Zheng J, Xu W, Ma Y, Lal V, et al. Atmospheric nanoparticles formed from heterogeneous reactions of organics. Nat Geosci 2010;3:238-42.
[46] Donaldson DJ, Valsaraj KT. Adsorption and Reaction of Trace Gas-Phase Organic Compounds on Atmospheric Water Film Surfaces: A Critical Review. Environ Sci Technol 2010;44:865-73.
[47] Yabushita A, Enami S, Sakamoto Y, Kawasaki M, Hoffmann MR, Colussi AJ. Anion-Catalyzed Dissolution of NO_2 on Aqueous Microdroplets. J Phys Chem A 2009;113:4844-8.
[48] Wang SZ, Bianco R, Hynes JT. Nitric Acid Dissociation at an Aqueous Surface: Occurrence and Mechanism. Israel J Chem 2009;49:251-9.
[49] Gross S, Knopf DA, Mak J, Iannone R, Bertram AK. Heterogeneous reactions of NO3 and N2O5 with a range of organic substrates. Geochimica Et Cosmochimica Acta 2009;73:A470-A.
[50] Finlayson-Pitts BJ. Reactions at Surfaces in the Atmosphere: Integration of Experiments and Theory as Necessary (but not Necessarily Sufficient) for Predicting the Physical Chemistry of Aerosols. Phys Chem Chem Phys 2009;11:7760-79.
[51] Enami S, Hoffmann MR, Colussi AJ. How phenol and alpha-tocopherol react with ambient ozone at gas/liquid interfaces. J Phys Chem A 2009;113:7002-10.
[52] Enami S, Hoffmann MR, Colussi AJ. Ozonolysis of uric acid at the air/water interface. J Phys Chem B 2008;112:4153-6.
[53] Clifford D, Donaldson DJ, Brigante M, D'Anna B, George C. Reactive uptake of ozone by chlorophyll at aqueous surfaces. Environ Sci Tech 2008;42:1138-43.
[54] Enami S, Vecitis CD, Cheng J, Hoffmann MR, Colussi AJ. Electrospray mass spectrometric detection of products and short-lived intermediates in aqueous aerosol microdroplets exposed to a reactive gas. J Phys Chem A 2007;111:13032-7.
[55] Ewing GE. Ambient thin film water on insulator surfaces. Chem Rev 2006;106:1511-26.
[56] Bianco R, Hynes JT. Heterogeneous Reactions Important in Atmospheric Ozone Depletion: A Theoretical Perspective. Acc Chem Res 2006;39:159-65.
[57] Ravishankara AR. Heterogeneous and multiphase chemistry in the troposphere. Science 1997;276:1058-65.
[58] Breslow R, Rizzo CJ. Chaotropic Salt Effects in a Hydrophobically Accelerated Diels-Alder Reaction. J Am Chem Soc 1991;113:4340-1.
[59] Breslow R. Hydrophobic Effects on Simple Organic-Reactions in Water. Accounts Chem Res 1991;24:159-64.
[60] Breslow R, Maitra U, Rideout D. Selective Diels-Alder Reactions in Aqueous-Solutions and Suspensions. Tetrahedron Lett 1983;24:1901-4.
[61] Rideout DC, Breslow R. Hydrophobic Acceleration of Diels-Alder Reactions. J Am Chem Soc 1980;102:7816-7.
[62] Narayan S, Muldoon J, Finn MG, Fokin VV, Kolb HC, Sharpless KB. "On water": Unique reactivity of organic compounds in aqueous suspension. Angew Chem Int Ed 2005;44:3275-9.

[63] Chanda A, Fokin VV. Organic Synthesis "On Water". Chem Rev 2009;109:725-48.
[64] Li CJ, Trost BM. Green chemistry for chemical synthesis. P Natl Acad Sci USA 2008;105:13197-202.
[65] Li CJ, Chen L. Organic chemistry in water. Chem Soc Rev 2006;35:68-82.
[66] Jung YS, Marcus RA. Protruding interfacial OH groups and 'on-water' heterogeneous catalysis. J Phys-Condens Mat 2010;22.
[67] Jung YS, Marcus RA. On the Theory of Organic Catalysis on Water. J Am Chem Soc 2007;129:5492-502.
[68] Thomas LL, Tirado-Rives J, Jorgensen WL. Quantum Mechanical/Molecular Mechanical Modeling Finds Diels-Alder Reactions Are Accelerated Less on the Surface of Water Than in Water. J Am Chem Soc 2010;132:3097-104.
[69] Beattie JK, McErlean CSP, Phippen CBW. The Mechanism of On-Water Catalysis. Chem-Eur J 2010;16:8972-4.
[70] Quincke G. Ueber die Fortführung materieller Theilchen durch strömende Elektricität. Ann Phys 1861;113:86.
[71] McTaggart HA. The electrification at liquid-gas surfaces. Philos Mag 1914;27:297-314.
[72] McTaggart HA. Electrification at liquid gas-surfaces. Philos Mag 1914;28:367-78.
[73] Marinova KG, Alargova RG, Denkov ND, Velev OD, Petsev DN, Ivanov IB, et al. Charging of oil-water interfaces due to spontaneous adsorption of hydroxyl ions. Langmuir 1996;12:2045-51.
[74] Takahashi M. Zeta-potential of microbubbles in aqueous solutions: Electrical properties of the gas-water interface. J Phys Chem B 2005;109:21858-64.
[75] Creux P, Lachaise J, Graciaa A, Beattie JK, Djerdjev AM. Strong Specific Hydroxide Ion Binding at the Pristine Oil/Water and Air/Water Interfaces. J Phys Chem B 2009;113:14146-50.
[76] Byrnes SJ, Geissler PL, Shen YR. Ambiguities in surface nonlinear spectroscopy calculations. Chem Phys Lett 2011;516:115-24.
[77] Tian CS, Shen YR. Structure and charging of hydrophobic material/water interfaces studied by phase-sensitive sum-frequency vibrational spectroscopy. Proc Natl Acad Sci U S A 2009;106:15148-53.
[78] Tian CS, Shen YR. Isotopic Dilution Study of the Water/Vapor Interface by Phase-Sensitive Sum-Frequency Vibrational Spectroscopy. J Am Chem Soc 2009;131:2790-+.
[79] Tian CS, Shen YR. Sum-frequency vibrational spectroscopic studies of water/vapor interfaces. Chem Phys Lett 2009;470:1-6.
[80] Tian CS, Ji N, Waychunas GA, Shen YR. Interfacial structures of acidic and basic aqueous solutions. J Am Chem Soc 2008;130:13033-9.
[81] Ji N, Ostroverkhov V, Tian CS, Shen YR. Characterization of vibrational resonances of water-vapor interfaces by phase-sensitive sum-frequency spectroscopy. Phys Rev Lett 2008;100.
[82] Du Q, Superfine R, Freysz E, Shen YR. Vibrational spectroscopy of water at the vapor water interface. Physical Review Letters 1993;70:2313-6.
[83] Otten DE, Shaffer PR, Geissler PL, Saykally RJ. Elucidating the mechanism of selective ion adsorption to the liquid water surface P Natl Acad Sci USA 2012;109:3190-.
[84] Otten DE, Onorato R, Michaels R, Goodknight J, Saykally RJ. Strong surface adsorption of aqueous sodium nitrite as an ion pair. Chem Phys Lett 2012;519-20:45-8.

[85] Petersen PB, Saykally RJ. Is the liquid water surface basic or acidic? Macroscopic vs. molecular-scale investigations. Chem Phys Lett 2008;458:255-61.
[86] Smith JD, Saykally RJ, Geissler PL. The effects of dissolved halide anions on hydrogen bonding in liquid water. J Am Chem Soc 2007;129:13847-56.
[87] Petersen PB, Saykally RJ. On the nature of ions at the liquid water surface. Annu Rev Phys Chem 2006;57:333-64.
[88] Petersen PB, Saykally RJ. Adsorption of ions to the surface of dilute electroyte solutions: The Jones-Ray effect revisited. J Am Chem Soc 2005;127:15446-52.
[89] Petersen PB, Saykally RJ. Evidence for an enhanced hydronium concentration at the liquid water surface. J Phys Chem B 2005;109:7976-80.
[90] Petersen PB, Johnson JC, Knutsen KP, Saykally RJ. Direct experimental validation of the Jones-Ray effect. Chem Phys Lett 2004;397:46-50.
[91] Lynden-Bell RM, Giovambattista N, Debenedetti PG, Head-Gordon T, Rossky PJ. Hydrogen bond strength and network structure effects on hydration of non-polar molecules. Phys Chem Chem Phys 2011;13:2748-57.
[92] Stirnemann G, Rossky PJ, Hynes JT, Laage D. Water reorientation, hydrogen-bond dynamics and 2D-IR spectroscopy next to an extended hydrophobic surface. Faraday Discuss 2010;146:263-81.
[93] Bakker HJ, Skinner JL. Vibrational Spectroscopy as a Probe of Structure and Dynamics in Liquid Water. Chem Rev 2010;110:1498-517.
[94] Ruan CY, Lobastov VA, Vigliotti F, Chen SY, Zewail AH. Ultrafast electron crystallography of interfacial water. Science 2004;304:80-4.
[95] Pal SK, Zewail AH. Dynamics of water in biological recognition. Chem Rev 2004;104:2099-123.
[96] Bhattacharyya SM, Wang ZG, Zewail AH. Dynamics of water near a protein surface. J Phys Chem B 2003;107:13218-28.
[97] Stiopkin IV, Weeraman C, Pieniazek PA, Shalhout FY, Skinner JL, Benderskii AV. Hydrogen bonding at the water surface revealed by isotopic dilution spectroscopy. Nature 2011;474:192-5.
[98] Marcus Y. Effect of Ions on the Structure of Water: Structure Making and Breaking. Chem Rev 2009;109:1346-70.
[99] Prell JS, O'Brien JT, Williams ER. Structural and Electric Field Effects of Ions in Aqueous Nanodrops. J Am Chem Soc 2011;133:4810-8.
[100] Saykally RJ. Air/water interface: Two sides of the acid–base story. Nature Chemistry 2013;5:2.
[101] Gray-Weale A, Beattie JK. An explanation for the charge on water's surface. Phys Chem Chem Phys 2009;11:10994-1005.
[102] Remsing RC, Rodgers JM, Weeks JD. Deconstructing Classical Water Models at Interfaces and in Bulk. Journal of Statistical Physics 2011;145:313-34.
[103] Zhao Y, Truhlar DG. The M06 suite of density functionals for main group thermochemistry, thermochemical kinetics, noncovalent interactions, excited states, and transition elements: two new functionals and systematic testing of four M06-class functionals and 12 other functionals. Theor Chem Acc 2008;120:215-41.
[104] Zhao Y, Truhlar DG. Density functionals for noncovalent interaction energies of biological importance. J Chem Theory Comput 2007;3:289-300.

[105] Grimme S. Semiempirical GGA-type density functional constructed with a long-range dispersion correction. J Comput Chem 2006;27:1787-99.
[106] Antony J, Grimme S. Density functional theory including dispersion corrections for intermolecular interactions in a large benchmark set of biologically relevant molecules. Phys Chem Chem Phys 2006;8:5287-93.
[107] Stern AC, Baer, M. D., Mundy, C. J., Tobias, D. J. Thermodynamics of iodide adsorption at the instantaneous air-water interface. The Journal of Chemical Physics 2013;138:8.
[108] Cheng J, Hoffmann MR, Colussi AJ. Anion fractionation and reactivity at air/water: Methanol interfaces. Implications for the origin of Hofmeister effects. J Phys Chem B 2008;112:7157-61.
[109] Salvador P, Curtis JE, Tobias DJ, Jungwirth P. Polarizability of the nitrate anion and its solvation at the air/water interface. Phys Chem Chem Phys 2003;5:3752-7.
[110] Jungwirth P, Tobias DJ. Molecular structure of salt solutions: A new view of the interface with implications for heterogeneous atmospheric chemistry. J Phys Chem B 2001;105:10468-72.
[111] Knipping EM, Lakin MJ, Foster KL, Jungwirth P, Tobias DJ, Gerber RB, et al. Experiments and simulations of ion-enhanced interfacial chemistry on aqueous NaCl aerosols. Science 2000;288:301-6.
[112] Marcus RA. Interaction between Experiments, Analytical Theories, and Computation. J Phys Chem C 2009;113:14598-608.
[113] Fenn JB. Electrospray wings for molecular elephants (Nobel lecture). Angew Chem-Int Edit 2003;42:3871-94.
[114] Cole RB. Some tenets pertaining to electrospray ionization mass spectrometry. J Mass Spectrom 2000;35:763-72.
[115] Kebarle P, Verkerk UH. Electrospray: From Ions in Solution to Ions in the Gas Phase, What We Know Now. Mass Spectrom Rev 2009;28:898-917.
[116] Schroder D. Applications of Electrospray Ionization Mass Spectrometry in Mechanistic Studies and Catalysis Research. Accounts Chem Res 2012;45:1521-32.
[117] Loo JA. Electrospray ionization mass spectrometry: a technology for studying noncovalent macromolecular complexes. Int J Mass Spectrom 2000;200:175-86.
[118] Hewavitharana AK, Herath HMDR, Shaw PN, Cabot PJ, Kebarle P. Effect of solvent and electrospray mass spectrometer parameters on the charge state distribution of peptides - a case study using liquid chromatography/mass spectrometry method development for beta-endorphin assay. Rapid Commun Mass Sp 2010;24:3510-4.
[119] Kim HI, Kim H, Shin YS, Beegle LW, Goddard WA, Heath JR, et al. Time Resolved Studies of Interfacial Reactions of Ozone with Pulmonary Phospholipid Surfactants Using Field Induced Droplet Ionization Mass Spectrometry. J Phys Chem B 2010;114:9496-503.
[120] Yamashita M, Fenn JB. Electrospray Ion-Source - Another Variation on the Free-Jet Theme. J Phys Chem-Us 1984;88:4451-9.
[121] Cheng J, Vecitis CD, Hoffmann MR, Colussi AJ. Experimental Anion Affinities for the Air/water Interface. J Phys Chem B 2006;110:25598-602.
[122] Cheng J, Hoffmann MR, Colussi AJ. Anion fractionation and reactivity at air/water:methanol interfaces. Implications for the origin of Hofmeister effects. J Phys Chem B 2008;112.

[123] Enami S, Hoffmann MR, Colussi AJ. Proton Availability at the Air/Water Interface. J Phys Chem Lett 2010;1:1599-604.
[124] Enami S, Stewart LA, Hoffmann MR, Colussi AJ. Superacid Chemistry on Mildly Acidic Water. J Phys Chem Lett 2010;1:3488-93.
[125] Kebarle P. A brief overview of the present status of the mechanisms involved in electrospray mass spectrometry. J Mass Spectrom 2000;35:804-17.
[126] Nguyen S, Fenn JB. Gas-phase ions of solute species from charged droplets of solutions. Proc Natl Acad Sci U S A 2007;104:1111-7.
[127] J. V. Iribarne BAT. On the evaporation of small ions from charged droplets. The Journal of Chemical Physics 1976;64:8.
[128] Dole M, Mack LL, Hines RL. Molecular Beams of Macroions. J Chem Phys 1968;49:2240-&.
[129] Debye P, Huckel E. The theory of electrolytes I. The lowering of the freezing point and related occurrences. Phys Z 1923;24:185-206.
[130] Debye P, Huckel E. The theory of the electrolyte II - The border law for electrical conductivity. Phys Z 1923;24:305-25.
[131] Wagner C. The surface tension of diluted electrolyte solutions. Phys Z 1924;25:474-7.
[132] Onsager L, Samaras NNT. The Surface Tension of Debye-Huckel Electrolytes. J Chem Phys 1934;2.
[133] Jones G, Ray WA. The surface tension of solutions of electrolytes as a function of the concentration I A differential method for measuring relative surface tension. J Am Chem Soc 1937;59:187-98.
[134] Jones G, Ray WA. The surface tension of deuterium oxide and of its mixtures with water. J Chem Phys 1937;5:505-8.
[135] Dole M. A theory of surface tension of aqueous solutions. J Am Chem Soc 1938;60:904-11.
[136] Enami S, Mishra H, Hoffmann MR, Colussi AJ. Hofmeister effects in micromolar electrolyte solutions. J Chem Phys 2012;136.
[137] Enami S, Colussi, A. J. Long-range ion-specific interactions in free-standing liquid nanofilms Jounal of Chemical Physics (under review) 2013.
[138] Caleman C, Hub JS, van Maaren PJ, van der Spoel D. Atomistic simulation of ion solvation in water explains surface preference of halides. P Natl Acad Sci USA 2011;108:6838-42.
[139] Ou S, Patel, S. Temperature dependence and energetics of single ions at the aqueous liquid-vapor interface. J Phys Chem B 2013;(Just accepted).
[140] Tian CS, Byrnes SJ, Han HL, Shen YR. Surface Propensities of Atmospherically Relevant Ions in Salt Solutions Revealed by Phase-Sensitive Sum Frequency Vibrational Spectroscopy. J Phys Chem Lett 2011;2:1946-9.
[141] Tian CS, Ji N, Waychunas GA, Shen YR. Interfacial structures of acidic and basic aqueous solutions. J Am Chem Soc 2008;130:13033-9.
[142] Pieniazek PA, Tainter CJ, Skinner JL. Interpretation of the water surface vibrational sum-frequency spectrum. J Chem Phys 2011;135.
[143] D'Auria R, Tobias DJ. Relation between Surface Tension and Ion Adsorption at the Air-Water Interface: A Molecular Dynamics Simulation Study. J Phys Chem A 2009;113:7286-93.

[144] Jungwirth P, Tobias DJ. Specific ion effects at the air/water interface. Chemical Reviews 2006;106:1259-81.
[145] Dang LX, Chang TM. Molecular mechanism of ion binding to the liquid/vapor interface of water. J Phys Chem B 2002;106:235-8.
[146] Ahadi E, Konermann L. Surface Charge of Electrosprayed Water Nanodroplets: A Molecular Dynamics Study. J Am Chem Soc 2010;132:11270-7.
[147] Saykally RJ. Liquid/vapor interface of aqueous salt solutions. Abstr Pap Am Chem S 2004;228:U243-U.
[148] Otten DE, Petersen PB, Saykally RJ. Observation of nitrate ions at the air/water interface by UV-second harmonic generation. Chem Phys Lett 2007;449:261-5.
[149] Gurau MC, Lim SM, Castellana ET, Albertorio F, Kataoka S, Cremer PS. On the mechanism of the Hofmeister effect. J Am Chem Soc 2004;126:10522-3.
[150] Jungwirth P. Spiers Memorial Lecture Ions at aqueous interfaces. Faraday Discuss 2009;141:9-30.
[151] Jungwirth P, Finlayson-Pitts BJ, Tobias DJ. Introduction: Structure and chemistry at aqueous interfaces. Chem Rev 2006;106:1137-9.
[152] Brown EC, Mucha M, Jungwirth P, Tobias DJ. Structure and vibrational spectroscopy of salt water/air interfaces: Predictions from classical molecular dynamics simulations. J Phys Chem B 2005;109:7934-40.
[153] Marcus Y. Ion Properties. New York: CRC Press; Har/Dskt edition; 1997.
[154] Mishra H, Enami S, Nielsen RJ, Stewart LA, Hoffmann MR, Goddard WA, et al. Bronsted basicity of the air-water interface. P Natl Acad Sci USA 2012;109:18679-83.
[155] Enami S, Hoffmann MR, Colussi AJ. Ozone Oxidizes Glutathione to a Sulfonic Acid. Chem Res Toxicol 2009;22:35-40.
[156] Enami S, Hoffmann MR, Colussi AJ. Simultaneous detection of cysteine sulfenate, sulfinate, and sulfonate during cysteine interfacial ozonolysis. J Phys Chem B 2009;113:9356-8.
[157] Enami S, Vecitis CD, Cheng J, Hoffmann MR, Colussi AJ. Mass spectrometry of interfacial layers during fast aqueous aerosol/ozone gas reactions of atmospheric interest. Chem Phys Lett 2008;455:316-20.
[158] Enami S, Hoffmann MR, Colussi AJ. Acidity enhances the formation of a persistent ozonide at aqueous ascorbate/ozone gas interfaces. Proc Acad Natl Sci USA 2008;105:7365-9.
[159] Enami S, Hoffmann AR, Colussi AJ. Ozonolysis of uric acid at the air/water interface. J Phys Chem B 2008;112:4153-6.
[160] Clegg SL, Brimblecombe P. Equilibrium partial pressures and mean activity and osmotic coefficients of 0-100 percent nitric acid as a function of temerature. J Phys Chem-Us 1990;94:5369-80.
[161] Enami S, Hoffmann MR, Colussi AJ. Proton Availability at the Air/Water Interface. J Phys Chem Lett 2010;1:1599-604.
[162] Davidovits P, Kolb CE, Williams LR, Jayne JT, Worsnop DR. Mass accommodation and chemical reactions at gas-liquid interfaces. Chem Rev 2006;106:1323-54.
[163] Siwick BJ, Cox MJ, Bakker HJ. Long-range proton transfer in aqueous acid-base reactions. J Phys Chem B 2008;112:378-89.
[164] Duffin AM, Saykally RJ. Electrokinetic hydrogen generation from liquid water microjets. J Phys Chem C 2007;111:12031-7.

[165] Buch V, Milet A, Vacha R, Jungwirth P, Devlin JP. Water surface is acidic. Proc Natl Acad Sci U S A 2007;104:7342-7.
[166] Beattie JK, Djerdjev AN, Warr GG. The surface of neat water is basic. Faraday Discuss 2009;141:31-9.
[167] Takahashi H, Maruyama K, Karino Y, Morita A, Nakano M, Jungwirth P, et al. Energetic Origin of Proton Affinity to the Air/Water Interface. J Phys Chem B 2011;115:4745-51.
[168] Shinichi Enami HM, Michael R. Hoffmann, Agustín J. Colussi Protonation and oligomerization of gaseous isoprene on mildly acidic surfaces: Implications for atmospheric chemistry. J Phys Chem A 2012;(in press).
[169] Wick CD. Hydronium Behavior at the Air-Water Interface with a Polarizable Multistate Empirical Valence Bond Model. J Phys Chem C 2012;116:4026-38.
[170] Platt JR. Strong Inference - Certain Systematic Methods of Scientific Thinking May Produce Much More Rapid Progress Than Others. Science 1964;146:347-&.
[171] Marcus RA. Spiers Memorial Lecture Interplay of theory and computation in chemistry-examples from on-water organic catalysis, enzyme catalysis, and single-molecule fluctuations. Faraday Discuss 2010;145:9-14.
[172] Laskin J, Laskin A, Nizkorodov SA. New mass spectrometry techniques for studying physical chemistry of atmospheric heterogeneous processes. International Reviews in Physical Chemistry 2013;32:128-70.
[173] Enami S, Mishra H, Hoffmann MR, Colussi AJ. Protonation and Oligomerization of Gaseous Isoprene on Mildly Acidic Surfaces. J Phys Chem A 2012;116:10.1021/jp 2110133.
[174] Mitchell P. Coupling of phosphorylation to electron and hydrogen transfer by a chemi-osmotic type of mechanism. Nature 1961;191:144-50.
[175] Hoegh-Guldberg O, Mumby PJ, Hooten AJ, Steneck RS, Greenfield P, Gomez E, et al. Coral reefs under rapid climate change and ocean acidification. Science 2007;318:1737-42.
[176] Sanden T, Salomonsson L, Brzezinski P, Widengren J. Surface-Coupled Proton Exchange of a Membrane-Bound Proton Acceptor. Proc Natl Acad Sci U S A 2010;107:4129-34.
[177] Lane N, Allen JF, Martin W. How did LUCA make a living? Chemiosmosis in the origin of life. Bioessays 2010;32:271-80.
[178] Villa J, Warshel A. Energetics and dynamics of enzymatic reactions. J Phys Chem B 2001;105:7887-907.
[179] Ball P. Water as an active constituent in cell biology. Chem Rev 2008;108:74-108.
[180] Eigen M. Proton transfer acid-base catalysis & enzymatic hydrolysis. I. elementary processes. Angew Chem-Int Edit 1964;3:1-15.
[181] Arnett EM. Gas-Phase Proton Transfer - a Breakthrough for Solution Chemistry. Accounts Chem Res 1973;6:404-9.
[182] Hunter EPL, Lias SG. Evaluated Gas Phase Basicities and Proton Affinities of Molecules: An Update. J Phys Chem Ref Data 1998;27:413-656.
[183] Caleman C, Hub JS, van Maaren PJ, van der Spoel D. Atomistic simulation of ion solvation in water explains surface preference of halides. P Natl Acad Sci USA 2011;108:6838-42.
[184] Wang SZ, Bianco R, Hynes JT. Depth-Dependent Dissociation of Nitric Acid at an Aqueous Surface: Car-Parrinello Molecular Dynamics. J Phys Chem A 2009;113:1295-307.

[185] Shamay ES, Buch V, Parrinello M, Richmond GL. At the Water's Edge: Nitric Acid as a Weak Acid. J Am Chem Soc 2007;129:12910-3.
[186] Cheng J, Hoffmann MR, Colussi AJ. Anion fractionation and reactivity at air/water: Methanol interfaces. Implications for the origin of Hofmeister effects. J Phys Chem B 2008;112:7157-61.
[187] Cheng J, Vecitis CD, Hoffmann MR, Colussi AJ. Experimental anion affinities for the air/water interface. J Phys Chem B 2006;110:25598-602.
[188] Enami S, Hoffmann MR, Colussi AJ. Acidity enhances the formation of a persistent ozonide at aqueous ascorbate/ozone gas interfaces. P Natl Acad Sci USA 2008;105:7365-9.
[189] Vandoren JM, Watson LR, Davidovits P, Worsnop DR, Zahniser MS, Kolb CE. Temperature dependence of the uptake coefficients of HNO_3, HCl and N_2O_5 by water droplets. J Phys Chem 1990;94:3265-9.
[190] Ardura D, Donaldson DJ. Where does acid hydrolysis take place? Phys Chem Chem Phys 2009;11:857-63.
[191] Dempsey LP, Brastad SM, Nathanson GM. Interfacial Acid Dissociation and Proton Exchange Following Collisions of DCl with Salty Glycerol and Salty Water. J Phys Chem Lett 2011;2:622-7.
[192] Cox MJ, Siwick BJ, Bakker HJ. Influence of Ions on Aqueous Acid-Base Reactions. Chemphyschem 2009;10:236-44.
[193] Otten DE, Shaffer PR, Geissler PL, Saykally RJ. Elucidating the mechanism of selective ion adsorption to the liquid water surface. Proc Natl Acad Sci USA 2012;109:701-5.
[194] Bianco R, Wang SZ, Hynes JT. Theoretical Study of the Dissociation of Nitric Acid at a Model Aqueous Surface. J Phys Chem A 2007;111:11033-42.
[195] Jarvis NL, Scheiman MA. Surface potentials of aqueous electrolyte solutions. J Phys Chem 1968;72:74-8.
[196] Petersen PB, Saykally RJ. Adsorption of ions to the surface of dilute electroyte solutions: The Jones-Ray effect revisited. J Am Chem Soc 2005;127:15446-52.
[197] Lu SY, Jiang YJ, Zhou P, Zou JW, Wu TX. Geometric characteristics and energy landscapes of halogen-water-hydrogen bridges at protein-ligand interfaces. Chem Phys Lett;485:348-53.
[198] Tian CS, Byrnes SJ, Han HL, Shen YR. Surface Propensities of Atmospherically Relevant Ions in Salt Solutions Revealed by Phase-Sensitive Sum Frequency Vibrational Spectroscopy. J Phys Chem Lett 2011;2:1946-9.
[199] Petersen PB, Saykally RJ. Probing the interfacial structure of aqueous electrolytes with femtosecond second harmonic generation spectroscopy. J Phys Chem B 2006;110:14060-73.
[200] Dole M. A theory of surface tension of aqueous solutions. J Am Chem Soc 1938;60:904-11.
[201] Springer A, Hagen V, Cherepanov DA, Antonenko YN, Pohl P. Protons migrate along interfacial water without significant contributions from jumps between ionizable groups on the membrane surface P Natl Acad Sci USA 2011;108:18185-.
[202] Mitchell P. Chemiosmotic coupling in oxidative and photosynthetic phosphorylation. Bba-Bioenergetics 2011;1807:1507-38.
[203] Mitchell P. Chemiosmotic Coupling in Oxidative and Photosynthetic Phosphorylation. Biochem J 1961;79:P23-&.
[204] Mitchell P. Conduction of Protons through Membranes of Mitochondria and Bacteria by Uncouplers of Oxidative Phosphorylation. Biochem J 1961;81:P24-&.

[205] Mitchell P. Coupling of Phosphorylation to Electron and Hydrogen Transfer by a Chemi-Osmotic Type of Mechanism. Nature 1961;191:5.
[206] Prats M, Teissie J, Tocanne JF. Lateral proton conduction at lipid water interfaces and its implications for the chemiosmotic-coupling hypothesis. Nature 1986;322:756-8.
[207] Meot-Ner M. The ionic hydrogen bond. Chem Rev 2005;105:213-84.
[208] Leopold KR. Hydrated Acid Clusters. Annu Rev Phys Chem 2011;62:327-49.
[209] Zhao XL, Subrahmanyan S, Eisenthal KB. Determination of pK_a at the air/water interface by second harmonic generation. Chem Phys Lett 1990;171:558-62.
[210] Lewis T, Winter B, Stern AC, Baer MD, Mundy CJ, Tobias DJ, et al. Does Nitric Acid Dissociate at the Aqueous Solution Surface? J Phys Chem C 2011;115:21183-90.
[211] Xu X, Goddard WA. The X3LYP extended density functional for accurate descriptions of nonbond interactions, spin states, and thermochemical properties. P Natl Acad Sci USA 2004;101:2673-7.
[212] Xu X, Goddard WA. Bonding properties of the water dimer: A comparative study of density functional theories. J Phys Chem A 2004;108:2305-13.
[213] Su JT, Xu X, Goddard WA. Accurate energies and structures for large water clusters using the X3LYP hybrid density functional. J Phys Chem A 2004;108:10518-26.
[214] Becke AD. Density functional thermochemistry .3. The role of exact exchange. J Chem Phys 1993;98:5648-52.
[215] Lee CT, Yang WT, Parr RG. Development of the Colle-Salvetti correlation energy fromula into a functional of the electron density. Phys Rev B 1988;37:785-9.
[216] Clark T, Chandrasekhar J, Spitznagel GW, Schleyer PV. Efficient diffuse function-augmented basis sets for anion calculations. 3.The 3-21+G basis set for 1^{ST}-row elements, LI-F. J Comput Chem 1983;4:294-301.
[217] Francl MM, Pietro WJ, Hehre WJ, Binkley JS, Gordon MS, Defrees DJ, et al. Self-consistent molecular orbital methods. 23. A polarization type basis set for 2^{ND}-row elements. J Chem Phys 1982;77:3654-65.
[218] Wang SZ, Bianco R, Hynes JT. Dissociation of nitric acid at an aqueous surface: Large amplitude motions in the contact ion pair to solvent-separated ion pair conversion. Phys Chem Chem Phys 2010;12:8241-9.
[219] Wang SZ, Bianco R, Hynes JT. Depth-Dependent Dissociation of Nitric Acid at an Aqueous Surface: Car-Parrinello Molecular Dynamics. J Phys Chem A 2009;113:1295-307.
[220] Wang SZ, Bianco R, Hynes JT. Dissociation of nitric acid at an aqueous surface: large amplitude motions in the contact ion pair to solvent-separated ion pair conversion. Phys Chem Chem Phys 2009;12:8241-9.
[221] Bianco R, Wang S, Hynes JT. Theoretical studies of the dissociation of sulfuric acid and nitric acid at model aqueous surfaces. Adv Quantum Chem 2008;55:387-405.
[222] Bianco R, Wang SZ, Hynes JT. Theoretical study of the dissociation of nitric acid at a model aqueous surface. J Phys Chem A 2007;111:11033-42.
[223] Brown SS, Burkholder JB, Talukdar RK, Ravishankara AR, Bianco R, Hynes JT. Mechanistic study of the reaction of hydroxyl radicals with nitric acid: Isotopically substituted reactions, product yields, and comparison to theory. Abstr Pap Am Chem S 2000;219:U276-U7.
[224] Wales DJ, Hodges MP. Global minima of water clusters (H2O)(n), n <= 21, described by an empirical potential. Chem Phys Lett 1998;286:65-72.

[225] Hartke B. Morphing Lennard-Jones clusters to TIP4P water clusters: Why do water clusters look like they do? Chem Phys 2008;346:286-94.
[226] Jarvis NL, Scheiman MA. Surface Potentials of Aqueous Electrolyte Solutions. J Phys Chem 1968;72:74-&.
[227] Otten DE, Shaffer PR, Geissler PL, Saykally RJ. Elucidating the mechanism of selective ion adsorption to the liquid water surface. P Natl Acad Sci USA 2012;109:701-5.
[228] Baer MD, Mundy CJ, McGrath MJ, Kuo IFW, Siepmann JI, Tobias DJ. Re-examining the properties of the aqueous vapor-liquid interface using dispersion corrected density functional theory. J Chem Phys 2011;135.
[229] Wang SZ, Bianco R, Hynes JT. Dissociation of nitric acid at an aqueous surface: Large amplitude motions in the contact ion pair to solvent-separated ion pair conversion. Phys Chem Chem Phys 2010;12:8241-9.
[230] Miller Y, Thomas JL, Kemp DD, Finlayson-Pitts BJ, Gordon MS, Tobias DJ, et al. Structure of Large Nitrate-Water Clusters at Ambient Temperatures: Simulations with Effective Fragment Potentials and Force Fields with Implications for Atmospheric Chemistry. J Phys Chem A 2009;113:12805-14.
[231] Brown MA, Winter B, Faubel M, Hemminger JC. Spatial Distribution of Nitrate and Nitrite Anions at the Liquid/Vapor Interface of Aqueous Solutions. J Am Chem Soc 2009;131:8354-+.
[232] Wren SN, Donaldson DJ. Glancing-angle Raman study of nitrate and nitric acid at the air-aqueous interface. Chem Phys Lett 2012;522:1-10.
[233] Marx D. Proton Transfer 200 Years after von Grotthuss: Insights from Ab Initio Simulations. Chemphyschem 2006;7:1848-70.
[234] Mmereki BT, Hicks JM, Donaldson DJ. Adsorption of atmospheric gases at the air-water interface. 3: Methylamines. J Phys Chem A 2000;104:10789-93.
[235] Harper K, Minofar B, Sierra-Hernandez MR, Casillas-Ituarte NN, Roeselova M, Allen HC. Surface Residence and Uptake of Methyl Chloride and Methyl Alcohol at the Air/Water Interface Studied by Vibrational Sum Frequency Spectroscopy and Molecular Dynamics. J Phys Chem A 2009;113:2015-24.
[236] Warshel A, Sharma PK, Kato M, Xiang Y, Liu HB, Olsson MHM. Electrostatic basis for enzyme catalysis. Chem Rev 2006;106:3210-35.
[237] Mulkidjanian AY, Heberle J, Cherepanov DA. Protons @ interfaces: Implications for biological energy conversion. Biochim Biophys Acta-Bioenerg 2006;1757:913-30.
[238] Sanden T, Salomonsson L, Brzezinski P, Widengren J. Surface-coupled proton exchange of a membrane-bound proton acceptor. P Natl Acad Sci USA 2010;107:4129-34.
[239] Bell RC, Wu K, Iedema MJ, Schenter GK, Cowin JP. The Oil-Water Interface: Mapping the Solvation Potential. J Am Chem Soc 2009;131:1037-42.
[240] Ariga K, Nakanishi T, Hill JP. A paradigm shift in the field of molecular recognition at the air-water interface: from static to dynamic. Soft Matter 2006;2:465-77.
[241] McGorty R, Fung J, Kaz D, Manoharan VN. Colloidal self-assembly at an interface. Mater Today 2010;13:34-42.
[242] Buch V, Milet A, Vacha R, Jungwirth P, Devlin JP. Water surface is acidic. P Natl Acad Sci USA 2007;104:7342-7.
[243] Petersen PB, Saykally RJ. Is the liquid water surface basic or acidic? Macroscopic vs. molecular-scale investigations. Chem Phys Lett 2008;458:255-61.

[244] Enami S, Hoffmann MR, Colussi AJ. Proton Availability at the Air/Water Interface. J Phys Chem Lett 2010;1:1599-604.
[245] Mulkidjanian AY. Proton in the well and through the desolvation barrier. Biochim Biophys Acta 2006;1757:415-27.
[246] Mishra H, Enami S, Nielsen RJ, Hoffmann MR, Goddard WA, Colussi AJ. Anions dramatically enhance proton transfer through water interfaces. P Natl Acad Sci USA 2012:10.1073/pnas.1200949109.
[247] Fawcett WR. The ionic work function and its role in estimating absolute electrode potentials. Langmuir 2008;24:9868-75.
[248] Petersen PB, Saykally RJ. Adsorption of ions to the surface of dilute electrolyte solutions: the Jones-Ray effect revisited. J Am Chem Soc 2006;127:15446-52.
[249] Pegram LM, Record MT. Quantifying accumulation or exclusion of H^+, HO^-, and Hofmeister salt ions near interfaces. Chem Phys Lett 2008;467:1-8.
[250] Byrnes SJ, Geissler PL, Shen YR. Ambiguities in surface nonlinear spectroscopy calculations. Chem Phys Lett 2011;516:115-24.
[251] Gray-Weale A, Beattie JK. An explanation for the charge on water's surface. Phys Chem Chem Phys 2009;11:10994-1005.
[252] Kudin KN, Car R. Why are water-hydrophobic interfaces charged? J Am Chem Soc 2008;130:3915-9.
[253] Iuchi S, Chen HN, Paesani F, Voth GA. Hydrated Excess Proton at Water-Hydrophobic Interfaces. J Phys Chem B 2009;113:4017-30.
[254] Vacha R, Buch V, Milet A, Devlin P, Jungwirth P. Autoionization at the surface of neat water: is the top layer pH neutral, basic, or acidic? Phys Chem Chem Phys 2007;9:4736-47.
[255] Zangi R, Engberts JBFN. Physisorption of hydroxide ions from aqueous solution to a hydrophobic surface. J Am Chem Soc 2005;127:2272-6.
[256] Nic M, Jirat J, Kosata B, Jenkins A. IUPAC. Compendium of Chemical Terminology http://goldbook.iupac.org/B00611.html. 2nd ed ed. Oxford: Blackwell Scientific; 2006.
[257] Zhao XL, Ong SW, Wang HF, Eisenthal KB. New method for determination of surface pK_A using 2^{nd} harmonic generation. Chem Phys Lett 1993;214:203-7.
[258] Rowlinson JS, Widom B, Abraham DB, Evans R, Sullivan DE, Schofield P, et al. Structure of the Interfacial Region - General Discussion. Faraday Symp Chem S 1981:205-56.
[259] Luo GM, Malkova S, Yoon J, Schultz DG, Lin BH, Meron M, et al. Ion distributions near a liquid-liquid interface. Science 2006;311:216-8.
[260] Netz RR, Orland H. Beyond Poisson-Boltzmann: Fluctuation effects and correlation functions. Eur Phys J E 2000;1:203-14.
[261] Cherepanov DA. Force oscillations and dielectric overscreening of interfacial water. Phys Rev Lett 2004;93.
[262] Enami S, Stewart LA, Hoffmann MR, Colussi AJ. Superacid Chemistry on Mildly Acidic Water. J Phys Chem Lett 2010;1:3488-93.
[263] Handbook of Chemistry & Physics (2012) http://www.hbcpnetbase.com/: Taylor and Francis)
[264] Hunter EPL, Lias SG. Evaluated gas phase basicities and proton affinities of molecules: An update. J Phys Chem Ref Data 1998;27:413-656.
[265] Meot-Ner M. The ionic hydrogen bond. Chem Rev 2005;105:213-84.

[266] Park JM, Laio A, Iannuzzi M, Parrinello M. Dissociation mechanism of acetic acid in water. J Am Chem Soc 2006;128:11318-9.
[267] Jacquemin D, Perpete EA, Ciofini I, Adamo C, Valero R, Zhao Y, et al. On the Performances of the M06 Family of Density Functionals for Electronic Excitation Energies. J Chem Theory Comput 2010;6:2071-85.
[268] Bryantsev VS, Diallo MS, van Duin ACT, Goddard WA. Evaluation of B3LYP, X3LYP, and M06-Class Density Functionals for Predicting the Binding Energies of Neutral, Protonated, and Deprotonated Water Clusters. J Chem Theory Comput 2009;5:1016-26.
[269] Mishra H, Nielsen RJ, Enami S, Hoffmann MR, Goddard WA, Colussi AJ. Quantum chemical insights into the dissociation of nitric acid on the surface of aqueous electrolytes. Int J Quantum Chem 2012;doi: 10.1002/qua.24151.
[270] Zhao Y, Truhlar DG. The M06 suite of density functionals for main group thermochemistry, thermochemical kinetics, noncovalent interactions, excited states, and transition elements: two new functionals and systematic testing of four M06-class functionals and 12 other functionals. Theor Chem Acc 2008;120:215-41.
[271] Francl MM, Pietro WJ, Hehre WJ, Binkley JS, Gordon MS, Defrees DJ, et al. Self-consistent molecular-orbital methods. 23. A polarization-type basis set for 2nd row elements. J Chem Phys 1982;77:3654-65.
[272] Clark T, Chandrasekhar J, Spitznagel GW, Schleyer PV. Efficient diffuse function-augmented basis sets for anion calculations. 3. The 3-21+G basis set for 1st row elements, Li-F. J Comput Chem 1983;4:294-301.
[273] Maheshwary S, Patel N, Sathyamurthy N, Kulkarni AD, Gadre SR. Structure and stability of water clusters $(H_2O)_n$, n = 8-20: An ab initio investigation. J Phys Chem A 2001;105:10525-37.
[274] Grimme S. Semiempirical GGA-type density functional constructed with a long-range dispersion correction. J Comput Chem 2006;27:1787-99.
[275] Dahlke EE, Truhlar DG. Improved density functionals for water. J Phys Chem B 2005;109:15677-83.
[276] Mundy CJ, Kuo IFW, Tuckerman ME, Lee HS, Tobias DJ. Hydroxide anion at the air-water interface. Chem Phys Lett 2009;481:2-8.
[277] Xu XF, Alecu IM, Truhlar DG. How Well Can Modern Density Functionals Predict Internuclear Distances at Transition States? J Chem Theory Comput 2011;7:1667-76.
[278] Kathmann SM, Kuo IFW, Mundy CJ, Schenter GK. Understanding the Surface Potential of Water. J Phys Chem B 2011;115:4369-77.
[279] Kudin KN, Car R. Why are water-hydrophobic interfaces charged? J Am Chem Soc 2008;130:3915-9.
[280] Takahashi M. ξ potential of microbubbles in aqueous solutions: Electrical properties of the gas-water interface. J Phys Chem B 2005;109:21858-64.
[281] Liu M, Beattie JK, Gray-Weale AA. The surface relaxation of water. J Phys Chem B 2012;10.1021/jp21810v.
[282] Vacha R, Rick SW, Jungwirth P, de Beer AGF, de Aguiar HB, Samson JS, et al. The Orientation and Charge of Water at the Hydrophobic Oil Droplet-Water Interface. J Am Chem Soc 2011;133:10204-10.
[283] Ben-Amotz D. Unveiling Electron Promiscuity. J Phys Chem Lett 2011;2:1216-22.

[284] Kuhne TD, Pascal TA, Kaxiras E, Jung Y. New Insights into the Structure of the Vapor/Water Interface from Large-Scale First-Principles Simulations. J Phys Chem Lett 2011;2:105-13.
[285] Vacha R, Marsalek O, Willard AP, Bonthuis DJ, Netz RR, Jungwirth P. Charge Transfer between Water Molecules As the Possible Origin of the Observed Charging at the Surface of Pure Water. J Phys Chem Lett 2012;3:107-11.
[286] Zhan CG, Dixon DA. The nature and absolute hydration free energy of the solvated electron in water. J Phys Chem B 2003;107:4403-17.
[287] Buchner F, Schultz T, Lubcke A. Solvated electrons at the water-air interface: surface versus bulk signal in low kinetic energy photoelectron spectroscopy. Phys Chem Chem Phys 2012;14:5837-42.
[288] Mundy CJ, Kuo IFW, Tuckerman ME, Lee HS, Tobias DJ. Hydroxide anion at the air-water interface. Chem Phys Lett 2009;481:2-8.
[289] Takahashi H, Maruyama K, Karino Y, Morita A, Nakano M, Jungwirth P, et al. Energetic Origin of Proton Affinity to the Air/Water Interface. J Phys Chem B 2011;115:4745-51.
[290] Enami S, Mishra H, Hoffmann MR, Colussi AJ. Hofmeister Effects in Micromolar Electrolyte Solutions. J Chem Phys 2012.
[291] Eigen M. Immeasurably fast reactions. Nobel Lecture 1967.
[292] Eigen M, Demaeyer L. Self-dissociation and protonic charge transport in water and ice Proceedings of the Royal Society of London Series a-Mathematical and Physical Sciences 1958;247:505-33.
[293] Donten ML, VandeVondele J, Hamm P. Speed Limits for Acid Base Chemistry in Aqueous Solutions. Chimia 2012;66:182-6.
[294] Morokuma K. Potential-Energy Surface of the Sn2 Reaction in Hydrated Clusters. J Am Chem Soc 1982;104:3732-3.
[295] Keisuke Doi ET, Sotiris S. Xantheas, Ryuzo Nakanishi, Takashi Nagata,, Takayuki Ebata aYI. Microhydration Effects on the Intermediates of the SN2 Reaction of Iodide Anion with Methyl Iodide. Angewandte Chemie 2013;52:5.
[296] Arnett EM. Gas-phase proton-transfer - breakthrough for solution chemistry. Accounts Chem Res 1973;6:404-9.
[297] Cherepanov DA. Force oscillations and dielectric overscreening of interfacial water. Physical Review Letters 2004;93.
[298] Teschke O, de Souza EF. Water molecular arrangement at air/water interfaces probed by atomic force microscopy. Chem Phys Lett 2005;403:95-101.
[299] Li CJ, Trost BM. Green chemistry for chemical synthesis. P Natl Acad Sci USA 2008;105:13197-202.
[300] Engberts JBFN, Feringa BL, Keller E, Otto S. Lewis-acid catalysis of carbon carbon bond forming reactions in water. Recl Trav Chim Pay B 1996;115:457-&.
[301] Li CJ. Organic-Reactions in Aqueous-Media - with a Focus on Carbon-Carbon Bond Formation. Chem Rev 1993;93:2023-35.
[302] Sangwan NK, Schneider HJ. The Kinetic Effects of Water and of Cyclodextrins on Diels-Alder Reactions - Host-Guest Chemistry .18. J Chem Soc Perk T 2 1989:1223-7.
[303] Breslow R. Determining the geometries of transition states by use of antihydrophohic additives in water. Accounts Chem Res 2004;37:471-8.

[304] Jorgensen WL, Blake JF, Lim DC, Severance DL. Investigation of Solvent Effects on Pericyclic-Reactions by Computer-Simulations. J Chem Soc Faraday T 1994;90:1727-32.
[305] Otto S, Blokzijl W, Engberts JBFN. Diels-Alder Reactions in Water - Effects of Hydrophobicity and Hydrogen-Bonding. J Org Chem 1994;59:5372-6.
[306] Creux P, Lachaise J, Graciaa A, Beattie JK, Djerdjev AM. Strong Specific Hydroxide Ion Binding at the Pristine Oil/Water and Air/Water Interfaces. J Phys Chem B 2009;113:14146-50.
[307] Olah GA. Superacid Chemistry. New York: Wiley; 2009.
[308] Liggio J, Li SM, Brook JR, Mihele C. Direct polymerization of isoprene and alpha-pinene on acidic aerosols. Geophys Res Lett 2007;34.
[309] Connelly BM, Tolbert MA. Reaction of Isoprene on Thin Sulfuric Acid Films: Kinetics, Uptake, and Product Analysis. Environ Sci Technol 2010;44:4603-8.
[310] Maleknia SD, Bell TL, Adams MA. PTR-MS analysis of reference and plant-emitted volatile organic compounds. Int J Mass Spectrom 2007;262:203-10.
[311] Rowlinson JS. Thermodynamics of Inhomogeneous Systems. Pure Appl Chem 1993;65:873-82.
[312] Kazansky VB. Solvation as a main factor that determines the strength of liquid superacids and the selectivity of the acid-catalyzed reactions of olefins. Catalysis Today 2002;73:127-37.
[313] Bryantsev VS, Diallo MS, Goddard WA. Computational Study of Copper(II) Complexation and Hydrolysis in Aqueous Solutions Using Mixed Cluster/Continuum Models. J Phys Chem A 2009;113:9559-67.
[314] Sarotti AM, Suarez AG, Spanevello RA. DFT calculations induced a regiochemical outcome revision of the Diels-Alder reaction between levoglucosenone and isoprene. Tetrahedron Lett 2011;52:3116-9.
[315] Kelly CP, Cramer CJ, Truhlar DG. Predicting Adsorption Coefficients at Air-Water Interfaces Using Universal Solvation and Surface Area Models. J Phys Chem B 2004;108:12882-97.
[316] Simon L, Goodman JM. How reliable are DFT transition structures? Comparison of GGA, hybrid-meta-GGA and meta-GGA functionals. Org Biomol Chem 2011;9:689-700.
[317] Francl MM, Pietro WJ, Hehre WJ, Binkley JS, Gordon MS, Defrees DJ, et al. Self-consistent molecular orbital methods. 23. A polarization type basis set for 2nd -row elements. J Chem Phys 1982;77:3654-65.
[318] Clark T, Chandrasekhar J, Spitznagel GW, Schleyer PV. Efficient Diffuse Function-Augmented Basis Sets for Anion Calculations. Iii. The 3-21+G Basis Set for First-Row Elements, Li-F. J Comput Chem 1983;4:294-301.
[319] Kazansky VB. Solvation effects in catalytic transformations of olefins in sulfuric acid. Catal Rev 2001;43:199-232.
[320] Kazansky VB. Solvation of protons and the strength of superacids. Top Catal 2000;11:55-60.
[321] Jacob DJ, Wofsy SC. Photochemistry of Biogenic Emissions over the Amazon Forest. J Geophys Res-Atmos 1988;93:1477-86.
[322] Makar PA, Fuentes JD, Wang D, Staebler RM, Wiebe HA. Chemical processing of biogenic hydrocarbons within and above a temperate deciduous forest. J Geophys Res-Atmos 1999;104:3581-603.

[323] Hurst JM, Barket DJ, Herrera-Gomez O, Couch TL, Shepson PB, Faloona I, et al. Investigation of the nighttime decay of isoprene. J Geophys Res-Atmos 2001;106:24335-46.
[324] Guenther A, Karl T, Harley P, Wiedinmyer C, Palmer PI, Geron C. Estimates of global terrestrial isoprene emissions using MEGAN (Model of Emissions of Gases and Aerosols from Nature). Atmos Chem Phys 2006;6:3181-210.
[325] Zimmerman PR, Greenberg JP, Westberg CE. Measurements of Atmospheric Hydrocarbons and Biogenic Emission Fluxes in the Amazon Boundary-Layer. J Geophys Res-Atmos 1988;93:1407-16.
[326] Goldstein AH, Galbally IE. Known and unexplored organic constituents in the earth's atmosphere. Environ Sci Technol 2007;41:1514-21.
[327] McCurdy PR, Hess WP, Xantheas SS. Nitric acid-water complexes: Theoretical calculations and comparison to experiment. J Phys Chem A 2002;106:7628-35.
[328] Finlayson-Pitts BJ. Reactions at surfaces in the atmosphere: integration of experiments and theory as necessary (but not necessarily sufficient) for predicting the physical chemistry of aerosols. Phys Chem Chem Phys 2009;11:7760-79.
[329] Mochida M, Finlayson-Pitts BJ. FTIR Studies of the Reaction of Gaseous NO with HNO_3 on Porous Glass: Implications for Conversion of HNO_3 to Photochemically Active NO_x in the Atmosphere. J Phys Chem A 2000;104:9705-11.
[330] Molina MJ, Zhang R, Wooldridge PJ, Mcmahon JR, Kim JE, Chang HY, et al. Physical-Chemistry of the $H_2SO_4/HNO_3/H_2O$ System - Implications for Polar Stratospheric Clouds. Science 1993;261:1418-23.
[331] Chandler D. Interfaces and the driving force of hydrophobic assembly. Nature 2005;437:640-7.
[332] De Vivo M, Ensing B, Dal Peraro M, Gomez GA, Christianson DW, Klein ML. Proton shuttles and phosphatase activity in soluble epoxide hydrolase. J Am Chem Soc 2007;129:387-94.
[333] Marcus RA. Spiers Memorial Lecture Interplay of Theory and Computation in Chemistry- Examples from On-Water Organic Catalysis, Enzyme Catalysis, and Single-Molecule Fluctuations. Faraday Discuss 2010;145:9-14.
[334] Kamerlin SCL, Warshel A. At the dawn of the 21st century: Is dynamics the missing link for understanding enzyme catalysis? Proteins 2010;78:1339-75.
[335] Springer A, Hagen V, Cherepanov DA, Antonenko YN, Pohl P. Protons migrate along interfacial water without significant contributions from jumps between ionizable groups on the membrane surface. P Natl Acad Sci USA 2011;108:14461-6.
[336] Yamashita T, Voth GA. Properties of Hydrated Excess Protons near Phospholipid Bilayers. J Phys Chem B 2010;114:592-603.
[337] Knight C, Voth GA. The Curious Case of the Hydrated Proton. Accounts Chem Res 2012;45:101-9.
[338] Iuchi S, Chen HN, Paesani F, Voth GA. Hydrated Excess Proton at Water-Hydrophobic Interfaces. J Phys Chem B 2009;113:4017-30.
[339] Alty T. The cataphoresis of gas bubbles in water. P R Soc Lond a-Conta 1924;106:315-40.
[340] Rayleigh L. The influence of electricity on colloiding water drops. Proceedings of the Royal Society of London 1879;28:15.
[341] Franklin B. Farther experiments and observations in electricity. Science 1956;123:47-50.

[342] Blanchard DC. From Raindrops to Volcanoes: Adventures with Sea Surface Meteorology: Dover Publications; 2004.
[343] Pahtz T, Herrmann HJ, Shinbrot T. Why do particle clouds generate electric charges? Nat Phys 2010;6:364-8.
[344] Ristenpart WD, Bird JC, Belmonte A, Dollar F, Stone HA. Non-coalescence of oppositely charged drops. Nature 2009;461:377-80.
[345] Williams ER. Large-Scale Charge Separation in Thunderclouds. J Geophys Res-Atmos 1985;90:6013-25.
[346] Ochs HT, Czys RR. Charge Effects on the Coalescence of Water Drops in Free-Fall. Nature 1987;327:606-8.
[347] Anderson R, Bjornsso.S, Blanchar.Dc, Gathman S, Hughes J, Jonasson S, et al. Electricity in Volcanic Clouds - Investigations Show That Lightning Can Result from Charge-Separation Processes in a Volcanic Crater. Science 1965;148:1179-&.
[348] Harrison RG, Aplin KL, Leblanc F, Yair Y. Planetary atmospheric electricity. Space Sci Rev 2008;137:5-10.
[349] Zilch LW, Maze JT, Smith JW, Ewing GE, Jarrold MF. Charge Separation in the Aerodynamic Breakup of Micrometer-Sized Water Droplets. J Phys Chem A 2008;112:13352-63.
[350] Zilch LW, Maze JT, Smith JW, Jarrold MF. Freezing, fragmentation, and charge separation in sonic sprayed water droplets. Int J Mass Spectrom 2009;283:191-9.
[351] Bhattacharyya I, Maze JT, Ewing GE, Jarrold MF. Charge Separation from the Bursting of Bubbles on Water. J Phys Chem A 2011;115:5723-8.
[352] Levin Z, Hobbs PV. Splashing of Water Drops on Solid and Wetted Surfaces - Hydrodynamics and Charge Separation. Philos Tr R Soc S-A 1971;269:555-&.
[353] Blanchard DC. Electrically Charged Drops from Bubbles in Sea Water and Their Meteorological Significance. J Meteorol 1958;15:383-96.
[354] Pence S, Novotny VJ, Diaz AF. Effect of Surface Moisture on Contact Charge of Polymers Containing Ions. Langmuir 1994;10:592-6.
[355] Djerdjev AM, Beattie JK, O'Brien RW. The electrokinetic sonic amplitude effect in filtration membranes: Part I. Experimental. J Membrane Sci 2012;401:13-24.
[356] Finney, Jungwirth, Bako, Beattie, Debenedetti, Bain, et al. General discussion. Faraday Discuss 2009;141:81-98.
[357] Beattie JK, Djerdjev AN, Warr GG. The surface of neat water is basic. Faraday Discuss 2009;141:31-9.
[358] Djerdjev AM, Beattie JK. Electroacoustic and ultrasonic attenuation measurements of droplet size and zeta-potential of alkane-in-water emulsions: effects of oil solubility and composition. Phys Chem Chem Phys 2008;10:4843-52.
[359] Beattie JK, Djerdjev AM. The pristine oil/water interface: Surfactant-free hydroxide-charged emulsions. Angew Chem-Int Edit 2004;43:3568-71.
[360] Kong L, Beattie JK, Hunter RJ. Electroacoustic study of adsorption of PEO on sunflower oil-in-water emulsion drops. Langmuir 2003;19:540-7.
[361] Winter B, Faubel M, Vacha R, Jungwirth P. Behavior of hydroxide at the water/vapor interface. Chem Phys Lett 2009;474:241-7.
[362] Winter B, Faubel M, Vacha R, Jungwirth P. Reply to comments on Frontiers Article 'Behavior of hydroxide at the water/vapor interface'. Chem Phys Lett 2009;481:19-21.

[363] Vacha R, Buch V, Milet A, Devlin P, Jungwirth P. Autoionization at the surface of neat water: is the top layer pH neutral, basic, or acidic? Phys Chem Chem Phys 2007;9:4736-47.
[364] Mucha M, Frigato T, Levering LM, Allen HC, Tobias DJ, Dang LX, et al. Unified molecular picture of the surfaces of aqueous acid, base, and salt solutions. J Phys Chem B 2005;109:7617-23.
[365] Marx D, Chandra A, Tuckerman ME. Aqueous Basic Solutions: Hydroxide Solvation, Structural Diffusion, and Comparison to the Hydrated Proton. Chem Rev 2010;110:2174-216.
[366] Petersen MK, Iyengar SS, Day TJF, Voth GA. The hydrated proton at the water liquid/vapor interface. J Phys Chem B 2004;108:14804-6.
[367] Ben-Amotz D. Unveiling Electron Promiscuity. J Phys Chem Lett 2011;2:1216-22.
[368] Baer MD, Stern AC, Levin Y, Tobias DJ, Mundy CJ. Electrochemical Surface Potential Due to Classical Point Charge Models Drives Anion Adsorption to the Air-Water Interface. J Phys Chem Lett 2012;3:1565-70.
[369] Kathmann SM, Kuo IFW, Mundy CJ. Electronic effects on the surface potential at the vapor-liquid interface of water. J Am Chem Soc 2008;130:16556-61.
[370] Schmitt UW, Voth GA. The computer simulation of proton transport in water. J Chem Phys 1999;111:9361-81.
[371] Schmitt UW, Voth GA. Multistate empirical valence bond model for proton transport in water. J Phys Chem B 1998;102:5547-51.
[372] Pan YD, Birdsey RA, Fang JY, Houghton R, Kauppi PE, Kurz WA, et al. A Large and Persistent Carbon Sink in the World's Forests. Science 2011;333:988-93.
[373] Carlton AG, Wiedinmyer C, Kroll JH. A review of Secondary Organic Aerosol (SOA) formation from isoprene. Atmos Chem Phys 2009;9:4987-5005.
[374] Verdaguer A, Sacha GM, Bluhm H, Salmeron M. Molecular structure of water at interfaces: Wetting at the nanometer scale. Chem Rev 2006;106:1478-510.
[375] Israelachvili J. Intermolecular and surface forces. 1992.
[376] VanHove LWA, Adema EH. The effective thickness of water films on leaves. Atmos Environ 1996;30:2933-6.
[377] Burkhardt J, Eiden R. Thin Water Films on Coniferous Needles. Atmos Environ 1994;28:2001-11.
[378] Dreyer SA, Seymour V, Cleland RE. Low Proton Conductance of Plant Cuticles and Its Relevance to the Acid-Growth Theory. Plant Physiol 1981;68:664-7.
[379] Schonherr J, Huber R. Plant Cuticles Are Polyelectrolytes with Isoelectric Points around 3. Plant Physiol 1977;59:145-50.
[380] Vanhove LWA, Adema EH, Vredenberg WJ, Pieters GA. A Study of the Adsorption of NH_3 and SO_2 on Leaf Surfaces. Atmos Environ 1989;23:1479-86.
[381] Sorgel M, Trebs I, Serafimovich A, Moravek A, Held A, Zetzsch C. Simultaneous HONO measurements in and above a forest canopy: influence of turbulent exchange on mixing ratio differences. Atmos Chem Phys 2011;11:841-55.
[382] Su H, Cheng YF, Oswald R, Behrendt T, Trebs I, Meixner FX, et al. Soil Nitrite as a Source of Atmospheric HONO and OH Radicals. Science 2011;333:1616-8.
[383] Fierer N, Jackson RB. The diversity and biogeography of soil bacterial communities. P Natl Acad Sci USA 2006;103:626-31.

[384] Lauber CL, Hamady M, Knight R, Fierer N. Pyrosequencing-Based Assessment of Soil pH as a Predictor of Soil Bacterial Community Structure at the Continental Scale. Appl Environ Microb 2009;75:5111-20.
[385] Cleveland CC, Yavitt JB. Consumption of atmospheric isoprene in soil. Geophys Res Lett 1997;24:2379-82.
[386] Unsworth MH. Evaporation from Forests in Cloud Enhances the Effects of Acid Deposition. Nature 1984;312:262-4.
[387] Grantz DA, Garner JHB, Johnson DW. Ecological effects of particulate matter. Environment International 2003;29:213-39.
[388] Waldman JM, Munger JW, Jacob DJ, Flagan RC, Morgan JJ, Hoffmann MR. Chemical-Composition of Acid Fog. Science 1982;218:677-80.
[389] Clegg SL, Brimblecombe P, Wexler AS. Extended AIM Aerosol Thermodynamic Model. 2011.
[390] van Duin ACT, Dasgupta S, Lorant F, Goddard WA. ReaxFF: A reactive force field for hydrocarbons. J Phys Chem A 2001;105:9396-409.
[391] Mayo SL, Olafson BD, Goddard WA. Dreiding- a generic force-field for molecular simulations. J Phys Chem-Us 1990;94:8897-909.
[392] Shinoda W, Shiga M, Mikami M. Rapid estimation of elastic constants by molecular dynamics simulation under constant stress. Phys Rev B 2004;69.
[393] Martyna GJ, Tobias DJ, Klein ML. Constant-pressure molecular dynamics algorithms. J Chem Phys 1994;101:4177-89.
[394] Parrinello M, Rahman A. Polymorphic transitions in single-crystals: a new molecular dynamics method. J Appl Phys 1981;52:7182-90.
[395] Tuckerman ME, Alejandre J, Lopez-Rendon R, Jochim AL, Martyna GJ. A Liouville-operator derived. measure-preserving integrator for molecular dynamics simulations in the isothermal-isobaric ensemble. Journal of Physics a-Mathematical and General 2006;39:5629-51.
[396] Bako I, Megyes T, Balint S, Grosz T, Chihaia V. Water-methanol mixtures: topology of hydrogen bonded network. Phys Chem Chem Phys 2008;10:5004-11.
[397] Batista da Silva JA, Brady Moreira FG, Leite dos Santos VM, Longo RL. On the hydrogen bond networks in the water-methanol mixtures: topology, percolation and small-world. Phys Chem Chem Phys 2011;13:6452-61.
[398] Lackner KS. Can fossil carbon fuel the 21st century? Int Geol Rev 2002;44:1122-33.
[399] Olah GA, Prakash GKS, Goeppert A. Anthropogenic Chemical Carbon Cycle for a Sustainable Future. J Am Chem Soc 2011;133:12881-98.
[400] Prepared by working group III of the Intergovernmental Panel on Climate Change CUP, Cambridge, United Kingdom and NewYork,USA,. IPCC special report on Carbon Dioxide Capture and Storage. http://wwwipcc-wg3de/publications/special-reports/special-report-on-carbon-dioxide-capture-and-storage 2005.
[401] Lackner KS. Capture of carbon dioxide from ambient air. European Physical Journal-Special Topics 2009;176:93-106.
[402] Chang PH, Chang YP, Chen SY, Yu CT, Chyou YP. Ca-Rich Ca-Al-Oxide, High-Temperature-Stable Sorbents Prepared from Hydrotalcite Precursors: Synthesis, Characterization, and CO2 Capture Capacity. Chemsuschem 2011;4:1844-51.
[403] Strazisar BR, Anderson RR, White CM. Degradation pathways for monoethanolamine in a CO2 capture facility. Energ Fuel 2003;17:1034-9.

[404] Vaidya PD, Kenig EY. CO2-alkanolamine reaction kinetics: A review of recent studies. Chem Eng Technol 2007;30:1467-74.
[405] Lackner KS. Washing carbon out of the air. Sci Am 2010;302:66-71.
[406] Wang T, Lackner KS, Wright AB. Moisture-swing sorption for carbon dioxide capture from ambient air: a thermodynamic analysis. Phys Chem Chem Phys 2013;15:504-14.
[407] Lackner KS, Brennan S, Matter JM, Park AHA, Wright A, van der Zwaan B. The urgency of the development of CO2 capture from ambient air. P Natl Acad Sci USA 2012;109:13156-62.
[408] Wang T, Lackner KS, Wright A. Moisture Swing Sorbent for Carbon Dioxide Capture from Ambient Air. Environmental Science & Technology 2011;45:6670-5.
[409] Cole R, Shulman HL. Adsorbing Sulfur Dioxide on Dry Ion Exchange Resins ... For Reducing Air Pollution. Ind Eng Chem 1960;52:859-60.
[410] Quinn R. Ion exchange resins as reversible acid gas absorbents. Separ Sci Technol 2003;38:3385-407.
[411] Quinn R, Appleby JB, Pez GP. Salt Hydrates - New Reversible Absorbents for Carbon-Dioxide. J Am Chem Soc 1995;117:329-35.
[412] Enami S, Stewart LA, Hoffmann MR, Colussi AJ. Superacid Chemistry on Mildly Acidic Water. J Phys Chem Lett 2010;1:3488-93.
[413] Okada T, Harada M, Ohki T. Hydration of Ions in Confined Spaces and Ion Recognition Selectivity. Anal Sci 2009;25:167-75.
[414] Yuchi A, Kuroda S, Takagi M, Watanabe Y, Nakao S. Effects of the Exchange Capacity and Cross-Linking Degree on the Hydration States of Anions in Quantitative Loading onto Strongly Basic Anion-Exchange Resins. Anal Chem 2010;82:8611-7.
[415] Heim M, Cevc G, Guckenberger R, Knapp HF, Wiegrabe W. Lateral electrical conductivity of mica-supported lipid bilayer membranes measured by scanning tunneling microscopy. Biophys J 1995;69:489-97.
[416] Guckenberger R, Heim M, Cevc G, Knapp HF, Wiegrabe W, Hillebrand A. Scanning-tunneling microscopy of insulators and biological specimens on lateral conductivity of ultrathin water films. Science 1994;266:1538-40.
[417] Agmon N, Gutman M. Bioenergetics: Proton fronts on membranes. Nature Chemistry 2011;3:840-2.
[418] Manghani R, Stuve EM. Enhanced field ionization of water adsorbed on a carbon monoxide-covered, platinum field emitter tip. Surf Sci 2009;603:165-72.
[419] Benson SW. Thermochemical Kinetics (Table A.17): John Wiley & Sons; 1976.
[420] Lin ST, Blanco M, Goddard WA. The two-phase model for calculating thermodynamic properties of liquids from molecular dynamics: Validation for the phase diagram of Lennard-Jones fluids. J Chem Phys 2003;119:11792-805.
[421] Benson SW. Thermochemical Kinetics: John Wiley & Sons; 1976.
[422] Sharp K. Entropy-enthalpy compensation: Fact or artifact? Protein Sci 2001;10:661-7.
[423] Bal W, Kurowska E, Maret W. The Final Frontier of pH and the Undiscovered Country Beyond. Plos One 2012;7.
[424] Davidovits P, Worsnop DR, Jayne JT, Kolb CE, Winkler P, Vrtala A, et al. Mass accommodation coefficient of water vapor on liquid water. Geophys Res Lett 2004;31.
[425] Nathanson G. H-D exchange at the air-water interface. 2012.
[426] Ma JC, Dougherty DA. The cation-pi interaction. Chem Rev 1997;97:1303-24.

[427] Xiu XA, Puskar NL, Shanata JAP, Lester HA, Dougherty DA. Nicotine binding to brain receptors requires a strong cation-pi interaction. Nature 2009;458:534-U10.
[428] Kumpf RA, Dougherty DA. A Mechanism for Ion Selectivity in Potassium Channels - Computational Studies of Cation-Pi Interactions. Science 1993;261:1708-10.
[429] Zacharias N, Dougherty DA. Cation-pi interactions in ligand recognition and catalysis. Trends Pharmacol Sci 2002;23:281-7.
[430] Lester HA, Dibas MI, Dahan DS, Leite JF, Dougherty DA. Cys-loop receptors: new twists and turns. Trends Neurosci 2004;27:329-36.
[431] Dougherty DA. The cation-π interaction. Accounts Chem Res 2013;DOI: 10.1021/ar300265y.
[432] Catalan JF, Quezada MP. Lithium: Molecular Interactions, Clinical Actions. Transl Neurosci 2012;3:61-6.

APPENDIX I

Hofmeister Effects in Micromolar Electrolyte Solutions

ABSTRACT: Ions both induce specific (Hofmeister) and non-specific (Coulomb) effects at aqueous interfaces. After more than a century, the origin of specific ion effects (SIE) eludes explanation, mainly because the causal electrostatic and non-electrostatic interactions are neither local nor separable. Since Coulomb effects essentially vanish below ~ 10 μM (i.e., at > 50 nm average ion separations), we decided to investigate whether SIE still operate at, hitherto unexplored, lower concentrations. Herein we report the direct detection of SIE above ~ 0.1 μM in experiments in which relative iodide/bromide populations, $\chi = I^-/Br^-$, on the surface of aqueous (NaI + NaBr) jets were determined by online electrospray mass spectrometry in the presence of XCl (X = H, Na, K, Cs, NH_4 and $N(C_4H_9)_4$) and NaY (Y = OH, Cl, NO_3 and ClO_4). We found that (1) all tested electrolytes begin to affect χ below ~ 1 μM, (2) I^- and Br^- are preferentially suppressed by co-ions that match their individual interfacial affinities. We infer that these phenomena, by falling outside the reach of even the longest-ranged electrostatic forces, are dynamical in nature.

.

I. INTRODUCTION

The specific partitioning of ions of the same valence to water-hydrophobe interfaces underlies important chemical, physical and biological phenomena.[1-4] Specific ion adsorption at the surface of the ocean is reflected by the distinct composition of marine aerosols,[5-8] and its significant impact on the chemistry of the atmospheric boundary layer.[5,9-14] Enzyme activities,[15] protein binding[16] and self-assembly processes in general[17-22] also show pronounced specific ion effects (SIE). Controlling the self-aggregation of nanoparticles and biopolymers via SIE is a tantalizing goal that requires a full understanding of the role and relative contributions of structural, Coulombic and non-electrostatic effects at low, intermediate and high concentrations.[21] It has become apparent that the specificity and range of SIE cannot be explained by merely appending many-body electrodynamic (dipolar and dispersive) forces to electrostatics, as assumed by the classical DLVO theory of surface interactions.[4,23-27] The full consequences of quantum fluctuations within extended dielectric media in the presence of charges are being investigated using molecular dynamics (MD) simulations,[28] and continuum non-local electrostatics models based on a dielectric function $\varepsilon(\boldsymbol{r, r'})$ of both the local electric field and the long-range polarization of the surrounding medium.[29-31]

A key parameter in models dealing with cooperative effects is the length of correlations, λ, in this case those induced by hydrated ions on the structure of interfacial water. Hitherto an adjustable model parameter, λ should be independently determined by experiments. A recent experimental study has provided evidence of SIE in < 50 μM electrolytes (one ion in > 10^6 water molecules) at a solid/water interface,[4,32] suggesting that the dilution threshold or, equivalently, the limiting value of λ had not been reached. The operation of unidentified long-range interactions on the surface of electrolyte solutions had been surmised from the surface tension minima observed in electrolyte solutions at ~ 1 mM.[33-35] Seventy five years ago, Dole realized that a model that invoked electrostatic interactions among ions that saturate the surface of water at ~ 1 mM could formally account for such minima, but was physically implausible. He conjectured that 'some other (unknown) factor such as an electric effect (by ions on the solvent)' was involved.[33] The fact that Dole's 'unknown' factor remains to be characterized points to a phenomenon whose interpretation might require new perspectives.

We recently exploited the high sensitivity, surface selectivity and unambiguous identification capabilities of online electrospray mass spectrometry (ESMS) (see below)[36,37] to investigate SIE on the surface of electrolyte solutions at low concentrations (See EXPERIMENTAL SECTION).[38] ESMS is conventionally used to investigate the composition of bulk liquids.[39] However, we have demonstrated that by changing the instrumental configuration and operating parameters it is possible to selectively sample the interfacial

layers of liquid jets under ambient temperature and pressure conditions.[5,36,37,40-42] An inherent challenge in studying liquid surfaces is that, because of the relatively small surface-to-volume ratios prevalent in most experiments, they are easily contaminated by the accumulation of ubiquitous surfactant species. Present experiments should be minimally influenced by contamination both because they are performed on fast-flowing, continually refreshed water jets, and monitor simultaneously the ions whose ratio, $\chi = I^-/Br^-$, is the observable reported herein (see below). We had validated the claim that the mass spectra obtained in our instrumental configuration reflect the ion composition of the outermost layers of the jet by showing that: (1) relative anion abundances, i.e., relative mass spectral signal intensities, measured in jets consisting of *equimolar* multi-electrolyte solutions follow a normal Hofmeister series,[6,7,43] and are specifically affected by added cationic or anionic surfactants,[6,42] (2) our mass spectra detect products necessarily formed in the air-water layers of jets exposed to reactive gases.[36,37,40,41,44] Herein, we report relative iodide/bromide ion abundances, $\chi = I^-/Br^-$, in air-water interfacial layers of mixed electrolyte solutions in the sub-μM to ~ 1 mM range.

II. EXPERIMENTAL SECTION

Our experiments involve the injection of aqueous electrolyte solutions as jets into the spraying chamber of an electrospray mass spectrometer (ESMS, Agilent 6130 Quadrupole LC/MS Electrospray System, Kyoto University) held at 1 atm and 298 K. The ion composition of the outermost layers of the jet is monitored *in situ* via online mass spectrometry, after the electroneutral jets are nebulized by an annular coaxial nebulizer gas into droplets possessing net charge of either sign. The excess anions (i.e., the fraction lacking balancing counterions) carried by the negatively charged droplets are ultimately ejected to the gas-phase and become amenable to mass spectrometric detection.[45] The present experimental setup is essentially the same as that reported in previous reports from our group.[36,37,41,42] Iodide and bromide ions already present on the surface of the injected liquid are monitored and quantified by online ESMS in less than a few milliseconds. Solutions are pumped (100 μL min^{-1}) into the spraying chamber through a grounded stainless steel needle (100 μm bore) coaxial with a sheath issuing nebulizer N_2(g) at high flow rates. The fast nebulizer gas strips the interfacial layers of the much slower liquid jet into microdroplets that carry excess anions or cations. Note that the production of charged microdroplets from a neutral liquid is the normal outcome of the charge fluctuations expected in a statistical breakup process.[39,46-48] Thus, droplet charging via nebulization does not require the application of an external electric bias to the needle, as in classic ('Taylor cone') electrospray mass spectrometry.[49] Charged microdroplets subsequently evaporate solvent while being drawn to the electrically polarized inlet of the mass spectrometer with increasing acceleration. Since sampled microdroplets are the progeny of the nascent droplets stripped from the surface of the jet, they are naturally enriched with interfacial species. We had

previously verified that this setup operates as a quasi-linear transfer device, that is ESMS signals are directly proportional to ion concentrations (up to ~ 0.1 mM) prior to their breakup, in experiments in which we monitored the acid-base equilibrium of dissolved tri-methyl-ammonium as a function of bulk pH.[36,42] We have presented detailed data analysis, based on mass balances and the application of the kinetic theory of gases to fast gas-liquid reactions, which strongly suggest (but do not conclusively prove) that the thickness of the interfacial layers sampled in these experiments is likely less than one nm, and certainly within a few nm.[36] Further experimental details and validation tests could be found in previous publications.[36,37,41,42]

III. RESULTS AND DISCUSSION

Anions generally approach the air-water interface closer than cations. This is borne out by the negative surface potential of most electrolyte solutions,[50,51] by surface-specific spectroscopic studies,[34,52-54] and by model calculations.[2,55-58] A recent phase-sensitive sum-frequency vibrational spectroscopy (PS-SFVS) study reported interfacial ion affinities in the order $I^- > NO_3^- > NH_4^+ > Cl^- > K^+ > Na^+$ between 1 M and 2 M.[54]

Figure 1 shows the negative ion ES mass spectra obtained from 1 μM equimolar (NaI + NaBr) aqueous solutions in the absence and presence of 10, 100 and 1000 □M NaCl. It is apparent that: (1) the population of I^- in the interfacial layers, P_{127}, as reported by m/z = 127 signal intensities, is about three times larger (more precisely 3.04 ± 0.24 times, the average of fifteen independent measurements) than that of Br^-, P_{79+81}, i.e., the sum of m/z = 79 and 81 signal intensities, confirming previous reports by Cheng et al.,[6,7] (2) both P_{127} and P_{79+81} decrease with increasing NaCl concentrations. The larger interfacial affinity of iodide relative to bromide is consistent with a number of previous independent experimental results and theoretical predictions.[34,52,57,59,60]

Figure 2 shows how both P_{127} and P_{79+81} decrease in the presence of increasing concentrations of XCl, where X is H, Na, K, Cs, NH_4 or $N(C_4H_9)_4$. Note that the surfactant $N(C_4H_9)_4^+$ has the largest depressing effect on both P_{127} and P_{79+81}, which decrease by 50%, respectively, upon addition of ~11 μM and ~ 20 μM $N(C_4H_9)_4Cl$. Similar effects require the addition of ~ 110 μM and ~70 μM NaCl, respectively. Interestingly, the depressing efficiencies of the large Cs^+ and of the small, non-polarizable H^+ (or H_3O^+) on P_{127} are found to be similar.

Figure 3 shows the specificity of co-ion effects upon addition of NaY, where Y = OH, Cl, NO_3 and ClO_4. It is immediately apparent that anions both induce larger and more specific effects than cations, in accord with the Hofmeister effects observed in most phenomena.[4,16,61,62] Note that among the anions studied,

ClO_4^- and OH^- have the strongest and weakest effects respectively: P_{127} is halved by ~ 1 μM $NaClO_4$ and ~ 230 μM NaOH. The weak effect of OH^- on interfacial ions is intriguing because the negative potential of the air-water interface has been ascribed to strong OH^- adsorption to water-hydrophobe interfaces in general.[51,63,64]

Figure 4A, which displays the ratio $\chi = P_{127}/P_{79+81} = I^-/Br^-$ as a function of NaY concentrations, reveals that ClO_4^- and NO_3^- have the largest depressing effects on P_{127} and P_{79+81}, respectively. From the relative affinities of Br^- ($f \equiv 1.0$), NO_3^- ($f = 1.4$), I^- ($f = 3.1$) and ClO_4^- ($f = 19$) for the air-water interface previously measured in a similar setup,[6] we infer that stronger effects occur among anions having closer interfacial affinities. Present results are in qualitative agreement with the PS-SFVS results showing that $f(Cl^-) < f(NO_3^-) < f(I^-)$.[54] χ is also a function of (NaI + NaBr) concentration, displaying a broad minimum at ~ 50 μM, in the absence of added electrolytes (Figure S2). Counter-ions have significant specific effects on χ (Figure 4B). The significant depressing effect of tetra-butyl-ammonium chloride on χ (Figure 4B) is consistent with previous findings by Cheng et al., that the cetyl-trimethyl ammonium chloride (CTAC) cationic surfactant strongly enhances the interfacial populations of Br^- and NO_3^- without affecting that of I^-.[6] Notably, the depressing efficiency of the small H^+ (or H_3O^+) is similar to that of the large surfactant $N(C_4H_9)_4^+$. Neither P_{127}, P_{79+81} nor χ are affected by the addition of up to 1.3 mM 2-propanol.

We had previously proposed, on the basis of the strict exponential dependence of relative anion affinities on ion radius rather than ion polarizability observed in our experiments,[6,7] that anions, by having a dielectric permittivity lower than the solvent but higher than air: $\varepsilon_W > \varepsilon_{ion} > 1$, are necessarily rejected to the air-water interface by many-body electrodynamic interactions.[26,27,51,65] However, since $\varepsilon_W(z)$ is not a monotonic but oscillating function of depth z, which displays both positive and negative values separated by sharp discontinuities within 0.5 nm of the interface,[29,66-68] interfacial ion distributions would not be expected to be monotonic or even continuous functions of depth.[66] From this standpoint, relative ion affinities would reflect the dissimilar depths, z_i, at which ions balance the electrodynamic forces driving them to the interface with the entropic losses partially associated with the creation of interfacial ion concentration gradients. Thus, different ions are envisioned to populate interfacial layers of different depths rather than a common interfacial region with different probabilities, as confirmed by the charge-specific effects induced by cationic versus anionic surfactants.[6,14,44]

The similar effects of H^+ and $N(C_4H_9)_4^+$ on χ therefore suggest that H^+, *once it emerges to the surface* at pH < 4,[36,37,42] reaches interfacial layers of depths intermediate between those occupied by I^- and Br^-. We have previously shown that gaseous trimethylamine is protonated in collisions with aqueous jets only at

pH < 4.[36,42] Thus, present results confirm that H^+ becomes available in the outermost layers below pH ~ 4.[36,37,42] Our results, by showing that OH^- barely affects I^- or Br^-, in contradistinction with NO_3^- or ClO_4^-, indicate that OH^- *from NaOH* does not reach the outermost interfacial layers sampled herein. This conclusion will be consistent with a recent analysis of surface tension data showing that the surface-to-bulk partitioning ratios are in the order $H^+ > Li^+ \sim K^+ \sim Na^+$ in XCl and $I^- > NO_3^- > Br^- > OH^-$ in NaY.[69] However, OH^-, as an intrinsic ion at aqueous interfaces, may not conform to the general pattern established by other anions. Whether and under what conditions OH^- becomes available to gaseous acids at the air-water is the subject of an upcoming report from our group.[70] Summing up, the results of Figure 4 represent compelling evidence of specific interactions among ions at the air-water interface down to the hitherto unexplored sub-micromolar range.

It should be emphasized the observed SIE in micromolar electrolyte solutions cannot be solely accounted for by electrostatic interactions across interfacial water layers characterized by a dielectric constant ε_W.[71] In the < 1 μM solutions studied herein, the average ion-ion separations $\langle R_{\text{ion-ion}} \rangle > 120$ nm exceeds the Bjerrum length (i.e., the separation at which the electrostatic energy of an ion pair becomes commensurate with thermal energy): $\lambda_B = e^2/(4\pi\varepsilon_0\varepsilon k_B T) = 56$ nm in vacuum ($\varepsilon = 1$).[27] Furthermore, the requisite interactions carry specific chemical information over long ranges. A definitive explanation may not be provided at this time, but it is conceivable that thermal capillary waves, which are powered by the thermal surroundings and span broad frequency ω_{CW} and wavelength λ_{CW} domains,[76] could be the carriers that propagate such perturbations. Recent simulations have shown that anions significantly bias surface height fluctuations several molecular diameters away by pinning thermal capillary waves.[77] The fact that the preceding dipole moments of water molecules bound to interfacial anions, in contrast with those bound to cations, can generate oscillating fields parallel to the surface might be part of the propagation mechanism.[78,79]

IV. CONCLUSIONS

We found that the populations of I^- and Br^- on the surface of equimolar 1 μM (NaI + NaBr) solutions are significantly and specifically affected by the presence of various NaY and XCl electrolytes in the 0.1 μM to 10^3 μM range. Our results represent clear evidence that Hofmeister effects operate even in sub-micromolar electrolyte solutions. The specificity of the observed effects indicates that I^- and Br^- are suppressed more strongly by those ions having similar interfacial affinities, e.g.: I^- by ClO_4^- and Br^- by NO_3^-. Remarkably, H^+ and the cationic surfactant $N(C_4H_9)_4^+$ have similar effects on $\chi = I^-/Br^-$, whereas OH^- has none. We infer that these phenomena, because they fall outside the reach of even the longest-ranged electrostatic forces, are dynamical in essence. Given the importance and universality of

Hofmeister effects across many fields, present findings may have deep implications for understanding specificity in biology and chemistry at aqueous interfaces.

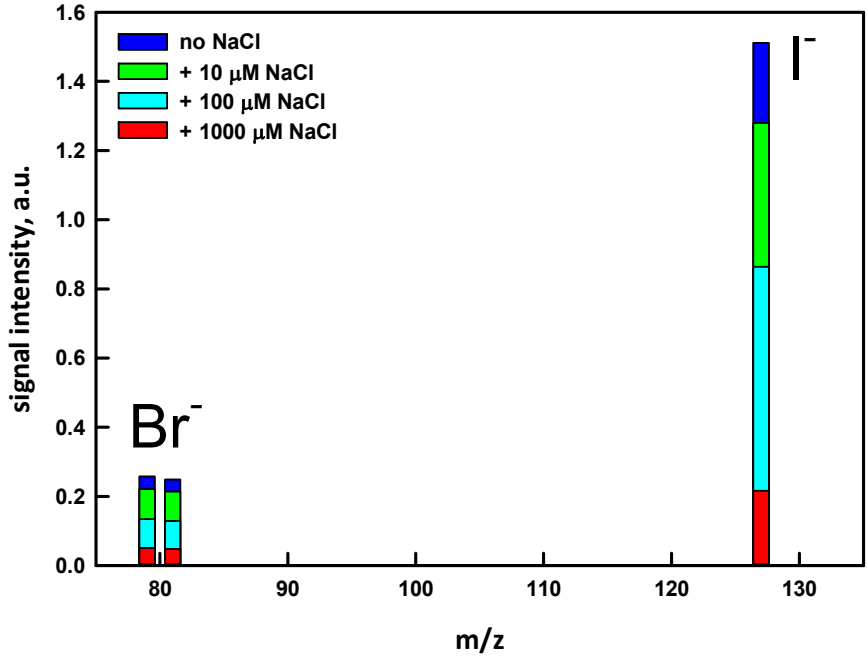

FIGURE 1 Negative ion ES mass spectra from aqueous (1 μM NaI + 1 μM NaBr) jets before and after adding 10, 100, 1000 μM NaCl.

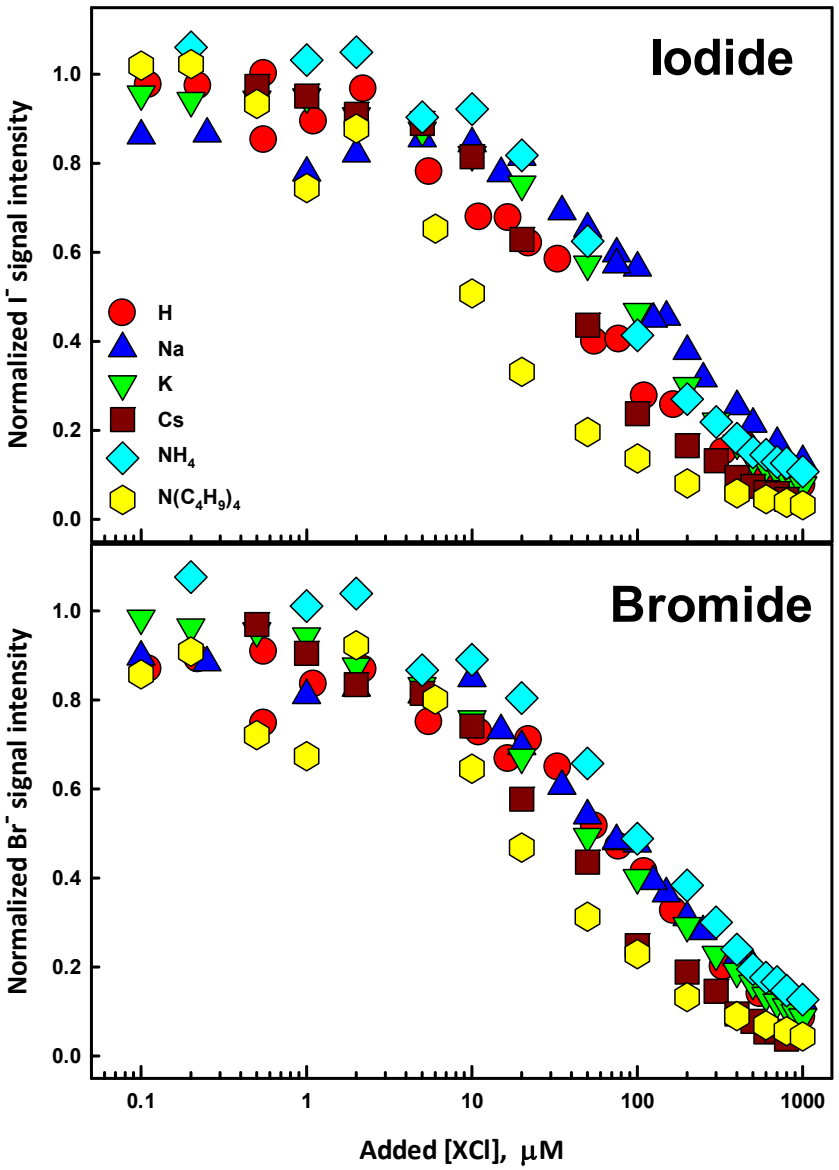

FIGURE 2 Semi-logarithmic plots of normalized I^- (upper panel) and Br^- (lower panel) ES mass spectral signal intensities from aqueous (1 μM NaI + 1 μM NaBr) jets as a function of added XCl concentrations. X ≡ H, Na, K, Cs, NH_4 or $N(C_4H_9)_4$.

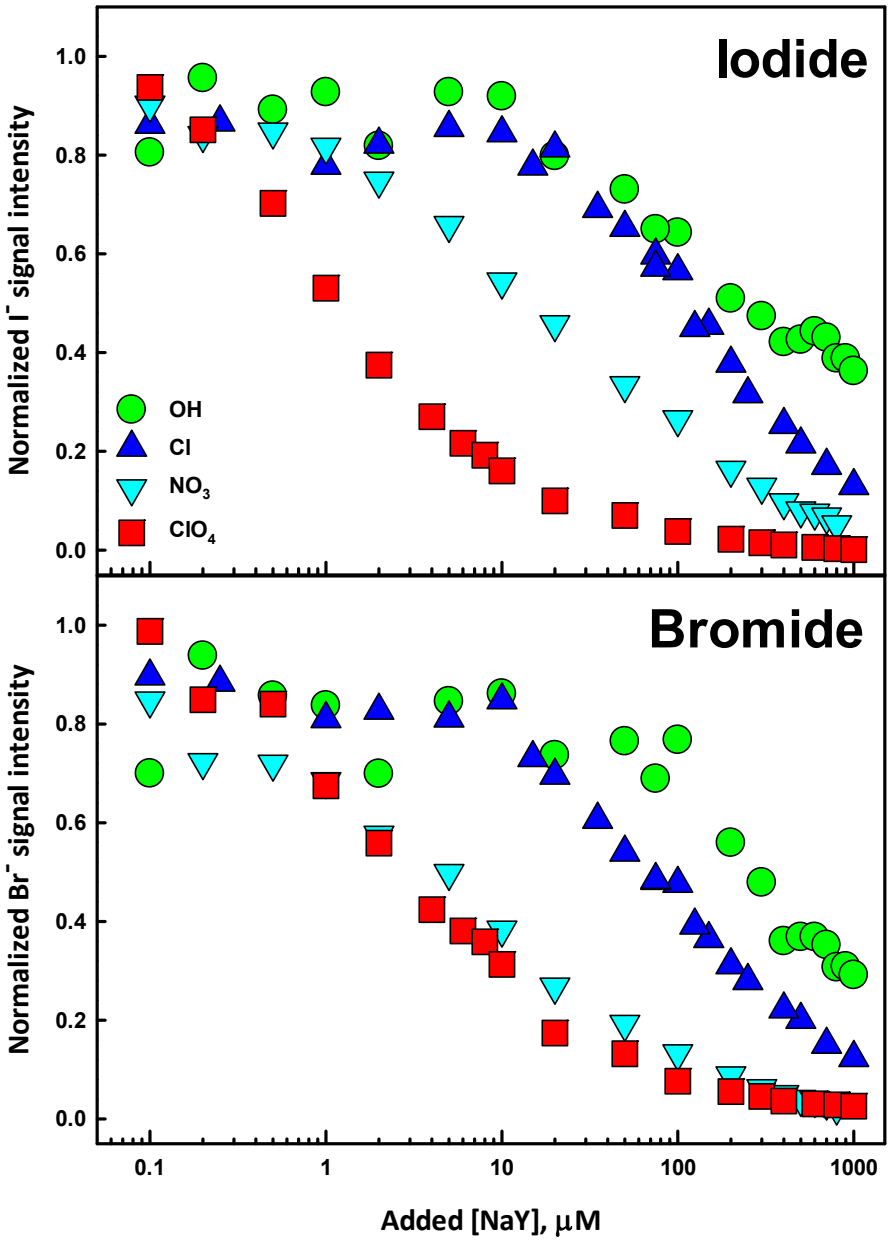

FIGURE 3 Semi-logarithmic plots of normalized I^- (upper panel) and Br^- (lower panel) ES mass spectral signal intensities from aqueous equimolar (1 μM NaI + 1 μM NaBr) jets as a function of added NaY concentrations. Y ≡ OH, Cl, NO_3 or ClO_4.

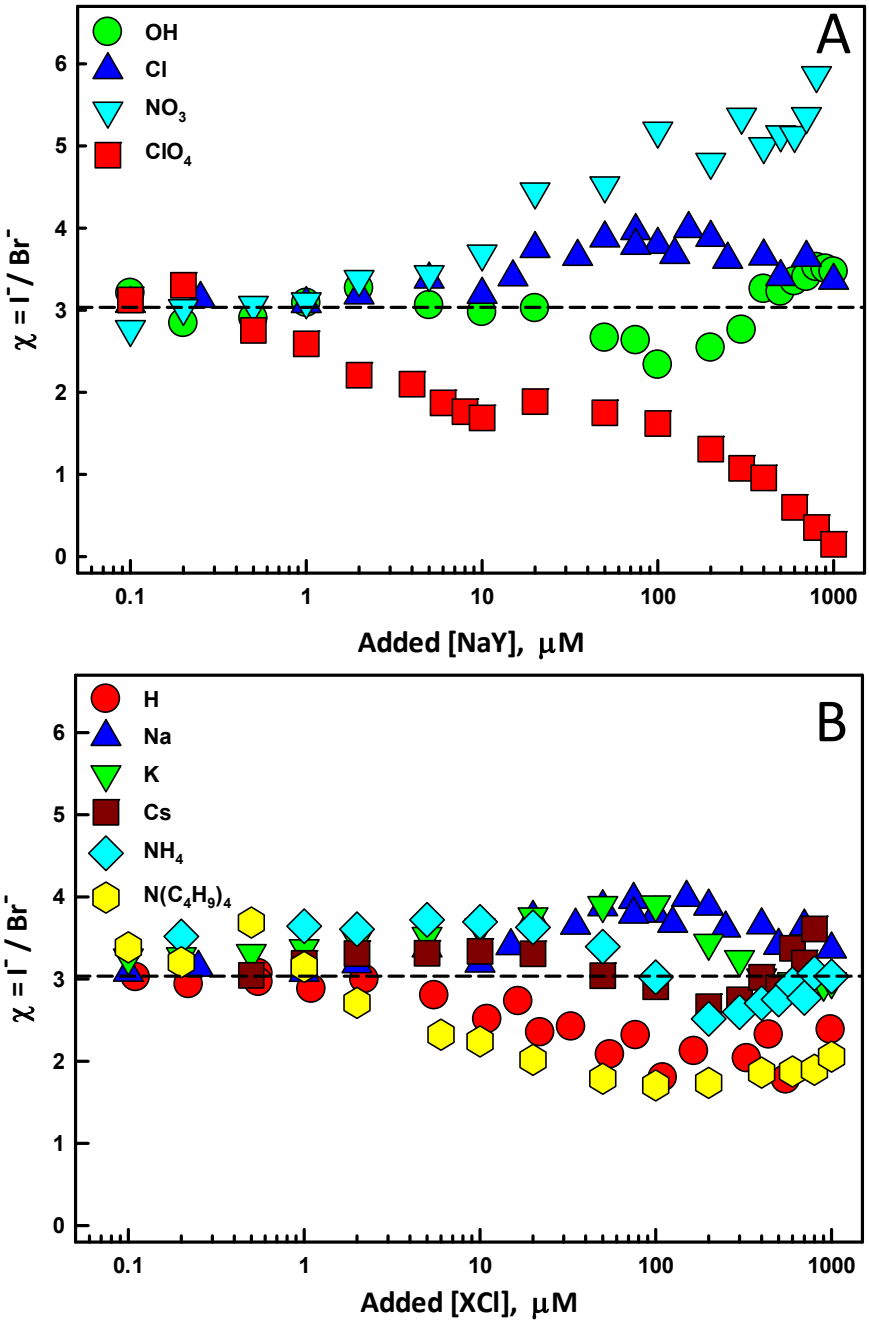

FIGURE 4 Semi-logarithmic plots of the ratio of ES mass spectral signal intensities $\chi = I^-/Br^-$ from aqueous (1 μM NaI + 1 μM NaBr) jets as a function of added NaY (Y ≡ OH, Cl, NO_3 or ClO_4) (A) and XCl (X ≡ H, Na, K, Cs, NH_4 or $N(C_4H_9)_4$) (B) concentrations. Dashed horizontal lines correspond to $\chi(0) = 3.04 \pm 0.24$.

References

1 P. B. Petersen and R. J. Saykally, Annu. Rev. Phys. Chem. **57**, 333 (2006).

2 P. Jungwirth and D. J. Tobias, Chem. Rev. **106**, 1259 (2006).

3 L. S. McCarty and G. M. Whitesides, Angew. Chem.-Int. Edit. **47** (12), 2188 (2008).

4 D. F. Parsons, M. Bostrom, P. Lo Nostro, and B. W. Ninham, Phys. Chem. Chem. Phys. **13** (27), 12352 (2011).

5 S. Enami, C. D. Vecitis, J. Cheng, M. R. Hoffmann, and A. J. Colussi, J. Phys. Chem. A **111**, 8749 (2007).

6 J. Cheng, C. Vecitis, M. R. Hoffmann, and A. J. Colussi, J. Phys. Chem. B **110**, 25598 (2006).

7 J. Cheng, M. R. Hoffmann, and A. J. Colussi, J. Phys. Chem. B **112**, 7157 (2008).

8 P. S. Liss and R. A. Duce, *The sea surface and global change*. (Cambridge University Press, Cambridge, UK, 1997).

9 P. Davidovits, C. E. Kolb, L. R. Williams, J. T. Jayne, and D. R. Worsnop, Chem. Rev. **106**, 1323 (2006).

10 B. J. Finlayson-Pitts, Phys. Chem. Chem. Phys. **11** (36), 7760 (2009).

11 E. M. Knipping, M. J. Lakin, K. L. Foster, P. Jungwirth, D. J. Tobias, R. B. Gerber, D. Dabdub, and B. J. Finlayson-Pitts, Science **288** (5464), 301 (2000).

12 D. J. Donaldson and K. T. Valsaraj, Environ. Sci. Technol. **44** (3), 865 (2010).

13 S. Hayase, A. Yabushita, M. Kawasaki, S. Enami, M. R. Hoffmann, and A. J. Colussi, J. Phys. Chem. A **115** (19), 4935 (2011).

14 T. Kinugawa, S. Enami, A. Yabushita, M. Kawasaki, M. R. Hoffmann, and A. J. Colussi, Phys. Chem. Chem. Phys. **13** (11), 5144 (2011).

15 M. C. Pinna, P. Bauduin, D. Touraud, M. Monduzzi, B. W. Ninham, and W. Kunz, J Phys Chem B **109** (34), 16511 (2005).

16 L. M. Pegram, T. Wendorff, R. Erdmann, I. Shkel, D. Bellissimo, D. J. Felitsky, and M. T. Record, Proc. Natl. Acad. Sci. U.S.A. **107** (17), 7716 (2010).

17 E. Leontidis, Curr. Opin. Colloid Interface Sci. **7** (1-2), 81 (2002).

18 L. J. Han, S. J. Hyung, J. J. S. Mayers, and B. T. Ruotolo, J Am Chem Soc **133** (29), 11358 (2011).

19 X. F. Li, S. Lettieri, N. Wentzel, and J. D. Gunton, J Chem Phys **129** (16), Doi 10.1063/1.2999608 (2008).

20 B. C. Gibb, Isr J Chem **51** (7), 798 (2011).

21 B. W. Ninham and P. Lo Nostro, *Molecular Forces and Self Assembly*. (Cambridge University Press, Cambridge, U.K., 2010).

22 N. Schelero and R. von Klitzing, Soft Matter **7** (6), 2936 (2011).

23 W. Kunz, P. Lo Nostro, and B. W. Ninham, Curr. Opin. Colloid Interface Sci. **9**, 1 (2004).

24 V. V. Yaminsky and B. W. Ninham, Adv. Colloid Interface Sci. **83** (1-3), 227 (1999).

25 J. K. Beattie, Chem. Phys. Lett. **481** (1-3), 17 (2009).

26 Dzyaloshinskii, I.E., E. M. Lifshitz, and L. P. Pitaevskii, Adv. Phys. **10**, 165 (1961).

27 J. Israelachvilii, *Intermolecular & Surface Forces*, 3rd ed. (Academic Press, London, 2011).

28 R. C. Remsing, J. M. Rodgers, and J. D. Weeks, J Stat Phys **145** (2), 313 (2011).

29 D. J. Bonthuis, S. Gekle, and R. R. Netz, Phys Rev Lett **107** (16), Doi 10.1103/Physrevlett.107.166102 (2011).

30 D. Ben-Yaakov, D. Andelman, and R. Podgornik, J Chem Phys **134** (7), Doi 10.1063/1.3549915 (2011).

31 A. Hildebrandt, R. Blossey, S. Rjasanow, O. Kohlbacher, and H. P. Lenhof, Phys. Rev. Lett. **93**, 108104 (2004).

32 J. M. Borah, S. Mahiuddin, N. Sarma, D. F. Parsons, and B. W. Ninham, Langmuir **27** (14), 8710 (2011).

33 M. Dole, J. Am. Chem. Soc. **60**, 904 (1938).

34 P. B. Petersen and R. J. Saykally, J. Am. Chem Soc. **127**, 15446 (2006).

35 G. Jones and W. A. Ray, J Am Chem Soc **59**, 187 (1937).

36 S. Enami, M. R. Hoffmann, and A. J. Colussi, J. Phys. Chem. Lett. **1** (10), 1599 (2010).

37 S. Enami, L. A. Stewart, M. R. Hoffmann, and A. J. Colussi, J. Phys. Chem. Lett. **1** (24), 3488 (2010).

38 See supplementary material of Enami et al., ***Journal of Chemical Physics*** (2012) 136(15), 154707 (pg 1-7).

39 I. Manisali, D. D. Y. Chen, and B. B. Schneider, Trends. Anal. Chem. **25**, 243 (2006).

40 S. Enami, M. R. Hoffmann, and A. J. Colussi, Proc. Natl. Acad. Sci. U. S. A. **105** (21), 7365 (2008).

41 S. Enami, M. R. Hoffmann, and A. J. Colussi, J. Phys. Chem. Lett. **1** (15), 2374 (2010).

42 S. Enami, M. R. Hoffmann, and A. J. Colussi, J. Phys. Chem. A **114** (18), 5817 (2010).

43 E. Psillakis, J. Cheng, M. R. Hoffmann, and A. J. Colussi, J. Phys. Chem. A **113** (31), 8826 (2009).

44 S. Enami, M. R. Hoffmann, and A. J. Colussi, J. Phys. Chem. B **113** (23), 7977 (2009).

45 J. V. Iribarne and B. A. Thomson, J. Chem. Phys. **64**, 2287 (1976).

46 A. Hirabayashi, M. Sakairi, and H. Koizumi, Anal. Chem. **66** (24), 4557 (1994).

47 A. Hirabayashi, M. Sakairi, and H. Koizumi, Anal. Chem. **67** (17), 2878 (1995).

48 L. W. Zilch, J. T. Maze, J. W. Smith, G. E. Ewing, and M. F. Jarrold, J. Phys. Chem. A **112** (51), 13352 (2008).

49 S. Nguyen and J. B. Fenn, Proc. Natl. Acad. Sci. U. S. A. **104** (4), 1111 (2007).

50 N. L. Jarvis and M. A. Scheiman, J. Phys. Chem. **72** (1), 74 (1968).

51 A. Gray-Weale and J. K. Beattie, Phys. Chem. Chem. Phys. **11** (46), 10994 (2009).

52 P. B. Petersen and R. J. Saykally, Chem. Phys. Lett. **397** (1-3), 51 (2004).

53 C. S. Tian and Y. R. Shen, Proc. Natl. Acad. Sci. U. S. A. **106** (36), 15148 (2009).

54 C. S. Tian, S. J. Byrnes, H. L. Han, and Y. R. Shen, J. Phys. Chem. Lett. **2** (15), 1946 (2011).

55 K. N. Kudin and R. Car, J. Am. Chem. Soc. **130** (12), 3915 (2008).

56 C. D. Wick and L. X. Dang, J. Chem. Phys. **133** (2), 10.1063/1.3455332 (2010).

57 M. D. Baer and C. J. Mundy, J. Phys. Chem. Lett. **2** (9), 1088 (2011).

58 D. Ben-Amotz, J. Phys. Chem. Lett. **2** (10), 1216 (2011).

59 S. Ghosal, J. C. Hemminger, H. Bluhm, B. S. Mun, E. L. D. Hebenstreit, G. Ketteler, D. F. Ogletree, F. G. Requejo, and M. Salmeron, Science **307**, 563 (2005).

60 P. Jungwirth and D. J. Tobias, J. Phys. Chem. B **106** (25), 6361 (2002).

61 F. Hofmeister, Arch. Exp. Pathol. Pharmakol. (Leipzig) **24**, 247 (1888).

62 K. D. Collins and M. W. Washabaugh, Quart. Rev. Biophys. **18**, 323 (1985).

63 J. K. Beattie, A. N. Djerdjev, and G. G. Warr, Faraday Discuss. **141**, 31 (2009).

64 P. Creux, J. Lachaise, A. Graciaa, J. K. Beattie, and A. M. Djerdjev, J. Phys. Chem. B **113** (43), 14146 (2009).

65 V. A. Parsegian, *Van der Waals Forces*. (Cambridge University Press, New York, 2006).

66 R. Podgornik and V. A. Parsegian, J Chem Phys **121** (15), 7467 (2004).

67 M. V. Fedorov and A. A. Kornyshev, Mol Phys **105** (1), 1 (2007).

68 T. G. Philbin, C. Xiong, and U. Leonhardt, Ann Phys-New York **325** (3), 579 (2010).

69 L. M. Pegram and M. T. Record, Proc. Natl. Acad. Sci. U.S.A. **103**, 14278 (2006).

70 S. Enami, H. Mishra, M. R. Hoffmann, and A. J. Colussi, Submitted (2011).

71 J. B. Klauda, X. W. Wu, R. W. Pastor, and B. R. Brooks, J Phys Chem B **111** (17), 4393 (2007).

72 F. Behroozi and N. Podolefsky, Eur. J. Phys. **22** (3), 225 (2001).

73 C. Fradin, A. Braslau, D. Luzet, D. Smilgies, M. Alba, N. Boudet, K. Mecke, and J. Daillant, Nature **403** (6772), 871 (2000).

74 A. P. Willard and D. Chandler, J Phys Chem B **114** (5), 1954 (2010).

75 J. S. Rowlinson and B. Widom, *Molecular Theory of Capillarity*. (Oxford University Press, New York, 1989).

76 D. Aarts, M. Schmidt, and H. N. W. Lekkerkerker, Science **304** (5672), 847 (2004).

77 D. E. Otten, P. R. Shaffer, P. L. Geissler, and R. J. Saykally, Proc Natl Acad Sci USA **109** (3), 701 (2012).

78 K. J. Tielrooij, S. T. van der Post, J. Hunger, M. Bonn, and H. J. Bakker, J Phys Chem B **115** (43), 12638 (2011).

79 D. L. Cheung, J Chem Phys **135** (5), 054704 (2011).

APPENDIX-II

Boron-Selective Resins from Hyperbranched Polyethyleneimine

Abstract

Extraction of boron from aqueous solutions using selective resins is important in a variety of applications including desalination, ultrapure water production, and nuclear power generation. Today's commercial boron-selective resins are exclusively prepared by functionalization of styrene-divinylbenzene (STY-DVB) beads with N-methylglucamine to produce resins with boron-chelating groups. However, such boron-selective resins have a limited binding capacity with a maximum free base content of 0.7 eq/L, which corresponds to a boron sorption capacity of 1.16 ± 0.03 mMol/g in aqueous solutions with equilibrium boron concentration of ~70 mM. In this article, we describe the synthesis and characterization of a new resin that can selectively extract boron from aqueous solutions. We show that branched polyethylenimine (PEI) beads obtained from an inverse suspension process can be reacted with glucono-1,5-D-lactone to afford a resin consisting of spherical beads with high density of boron-chelating groups. This new resin has a boron sorption capacity of 1.93 ± 0.04 mMol/g in aqueous solution with equilibrium boron concentration of ~70 mM, which is 66% percent larger than that of standard commercial STY-DVB resins. Our new boron-selective resin also shows excellent regeneration efficiency using the standard acid/base wash required for regeneration.

Introduction

Extraction of boron from aqueous solutions is important in a variety of applications including (i) desalination, (ii) ultrapure water treatment, (iii) the production of high purity magnesium oxide from brines and (iv) nuclear power generation.[1-4] Boron is an essential nutrient for plants.[5] However, it adversely affects plant growth and damages crops (e.g. citrus and corn) when desalinated water containing more than 0.3 mg/L of boron is used in irrigation.[2] In semiconductor manufacturing, boron is used as a p-type dopant to silicon.[6] To control the level of boron in a silicon chip, ultrapure water with boron concentrations less than 1 ppb (μg/L) is required. In the production of high purity magnesium oxides by pyrohydrolysis of magnesium chloride ($MgCl_2$.) brine, excess boron (> 10 mg/L) in the brine causes embrittlment of the final metal oxide products.[3] In nuclear power generation, ^{10}B-enriched mixtures of boric acid with lithium hydroxide provide inexpensive yet efficient neutron-absorbing media in the primary coolant water of pressurized water reactors. The availability of an efficient and highly selective boric acid recovery system is the key bottleneck for the wide scale implementation of these neutron absorbing media.[4, 7]

Sorption with selective and regenerable resins has emerged as an efficient and cost-effective process for extracting boron from aqueous solutions. [2] The predominant boron species in aqueous solutions, H_3BO_3 versus $B(OH)_4^-$, is determined by the pH of the solution [H_3BO_3(aq), pK_a = 9.24]. It is well known that boron/borate can selectively complex with organic moeities containing two or more vicinal hydroxyl groups (e.g. diols).[8] For example, host functionalization with diol-bearing compounds has been carried out on a variety of polymeric matrices and hybrid organic-inorganic meosoporous materials to synthesize boron-selective ligands and sorbents.[7, 9-11] Today's commercial boron-chelating resins are exclusively prepared by functionalization of crosslinked styrene-divinylbenzene (STY-DVB) beads with diol-bearing compounds such as N-methylglucamine. However, commercial STY-DVB resins with N-methylglucamine groups (e.g. the Amberlite IRA-743 resin) have a limited capacity with a maximum free base of 0.7 eq/L, which corresponds to a nominal boron binding capacity of 1.09 mMol/g in aqueous solutions with equilibrium boron concentration of ~100 mM.[12] In this article, we describe the synthesis and characterization of a new family of resins that can selectively extract boron from aqueous solutions. We show that crosslinked branched

polyethylenimine (PEI) beads obtained from an inverse suspension process can be reacted with glucono-1,5-D-lactone to afford a resin consisting of spherical beads with high density of boron-chelating groups. This regenerable resin has a boron sorption capacity of 1.93 ± 0.04 mMol/g in aqueous solution with equilibrium boron concentration of ~70 mM, which is 66% percent larger than that of standard commercial STY-DVB resins. The overall results of our studies suggest that crosslinked branched PEI beads provide versatile and promising building blocks for the preparation of reusable boron-chelating resins with high binding capacity.

Experimental Methods and Procedures

Chemical and Materials

Reagent grade chemicals were used to synthesize all the base PEI beads and boron-selective PEI resins described in this study. Reagent grade (> 98 wt%) anhydrous potassium chloride (KCl), sodium chloride (NaCl), sodium sulfate (Na_2SO_4) and ACS grade (99.5%) boric acid were purchased from Alfa Aesar. Concentrated hydrochloric acid (12 M) was purchased from EMD. The precursor polyethyleneimine macromolecules (PEI) [SP-018 (molecular weight M_n = 1800) and SP-200 (M_n = 10,000)] were purchased from Nippon Shokubai Co., Ltd. Sulfonic 100 (branched dodecyl benzene sulfonic acid, 97%) was purchased from the Stepan Company. Reagent grade (≥99.0%) D-Glucono-1,5-lactone, 1-bromo-3-chloropropane (BCP), diisopropyl ethylamine (DIPEA) and epichlorohydrin (ECH) were purchased from Sigma-Aldrich. Methanol, ethanol, toluene, sodium bicarbonate ($NaHCO_3$), calcium chloride dihydrate ($CaCl_2$-$2H_2O$), magnesium chloride hexahydrate ($MgCl_2$-$6H_2O$), and sodium hydroxide (NaOH) were purchased from Mallinckrodt Chemicals. Deionized (DI) water was obtained from a Milli-Q filtration unit (minimum resistivity 18 MΩ). All chemicals were used as received. The commercial STY-DVB resin Amberlite IRA-743, which was specifically designed to remove boric acid and borate from aqueous solutions, was purchased from the Dow Chemical Company (Midland, MI, USA).

Resin Synthesis

All base PEI beads (**BPEI-1** and **BPEI-2**) were synthesized using an inverse suspension of water-in-toluene stabilized by a surfactant. (Figure 1). The base PEI beads were functionalized, respectively, with 2-oxiranylmethanol and glucono-1, 5-D-lactone to produce two new boron-selective resins (**BSR-1** and **BSR-2**) with boron-chelating groups (Figure 1).

Resin Characterization

The boron-selective PEI resins (**BSR-1** and **BSR-2**) were characterized using a broad range of analytical techniques/assays including (i) FT-IR spectroscopy, (ii) scanning electron microscopy (SEM), (iii) particle size distribution (PSD) analysis and (iv) measurements of water and amine contents. The FT-IR spectra were acquired using a Bruker VERTEX 70/70v FT-IR spectrometer with potassium bromide (KBr) pellets and OPUS software for data processing. All of the reported IR spectra represent averages of more than 100 consecutive scans. The SEM images were acquired using a Zeiss 1500VP field-emission scanning electron microscope (FESEM). Prior to imaging, each resin sample was coated with a conducting 20 nm graphite film. The average diameter of the **BSR-1** beads was determined using the ImageJ software.[13] The mean diameter of the **BSR-2** beads was measured using a Malvern Hydro 2000S particle size analyzer.

The water content of each resin was determined by drying a 2 g sample of media in a dessicator at ambient temperature under vacuum and recording its weight until it remained constant. The free base capacity (amine content) of each resin was determined by performing a Mohr titration as described in ASTM 2187 sections 100-109.[14] In a typical titration experiment, 4 g of resin was mixed with 10 mL of deionized water. The resin slurry was packed in a graduated cylinder and allowed to equilibrate for 1 h. The bed volume (BV) of the resin was then measured. Subsequently, the resin slurry was packed in a fritted glass column and filled with 1 L of 1.2 M HCl. The acid was passed through the sample at the rate of 20 to 25mL/min, keeping the samples submerged in acid at all times. Following this, the liquid was drained to the level of the samples and the effluent liquid was discarded. The column was then washed with 600-750 mL of ethanol until a 10 mL portion of the effluent mixed with 10 mL of water achieved a constant pH >3.9. The chloride ions bound to the protonated amine groups of the resins were then eluted out with a 1 L of 2.0 wt% solution of sodium nitrate ($NaNO_3$). Following this, the concentration of chloride in the effluent was measured by titrating 100 mL of the effluent solution with a solution of silver nitrate ($AgNO_3$). The total amine content [TAC] (meq/mL) was expressed as:

$$TAC = V \times N \times DR/BV \qquad \text{Eq. 1}$$

where V and N are, respectively, the volume (mL) and normality (meq/mL) of the $AgNO_3$ solution, BV (mL) is the volume of the swollen resin and DR is the dilution ratio, which is equal to 10 in this case.

Boron Sorption onto Pristine Resins

To evaluate the performance of our new boron-selective resins, we carried out batch studies to measure their sorption capacity in deionized (DI) water and model electrolyte solutions. Batch sorption studies were carried out to measure the boron sorption capacity of the pristine **BSR-1 and BSR-2** resins in DI water, 0.1 M NaCl solution and a model seawater reverse osmosis (RO) permeate. To benchmark the performance of the **BSR-1 and BSR-2** resins, we also measured the boron sorption capacity of the commercial IRA-743 resin in DI water. Boron sorption onto each resin was measured by mixing known quantities of dry resin mass, *m*, with aqueous solutions containing varying concentrations of boron at ambient pH. Following equilibration of the vials for 24 hours, the amount of boron sorbed onto the resin (q_{sorbed}) [millimoles of boron per g of resin] was determined using the equation given below:

$$q_{sorbed} = (C_{bi} - C_{bf})/(1000 \times m) \qquad \text{Eq. 2}$$

where C_{bi} and C_{bf} are, respectively, the initial and final amounts of boron (mM) in solution measured by titration against 0.05N NaOH and *m* is the dry-mass of resin per 50 ml solution. Congruence of initial boron concentrations, C_{bi°, and those experimentally measured by the titration method, C_{bi}, within 0.5-3% in the range $C_b > 2$ mM confirmed accuracy and precision of this method.[8] The errors in measurements increased in the lower concentration limit. For this purpose (excess) 10 mL of 0.5 M mannitol solution was added to the analyte, $V_{analyte}$ = 1 ml, obtained from the supernatant from each equilibrated solution. Excess mannitol ensured binding of the dissolved boron thereby releasing H_3O^+.[8] Subsequently, in presence of phenolphthalein (indicator), the solution was titrated against 0.05M NaOH solution until it became and remained pink for more than 30 seconds. Concentration of boron in the supernatant solution, C_{bf}, after equilibration was calculated using the normality equation as:

$$C_{bf} = V_{NaOH} \times N_{NaOH} / V_{analyte} \qquad \text{Eq. 3}$$

where V_{NaOH} and N_{NaOH} are, respectively, the volume (mL) and normality (mEq/L) of the NaOH solution.

Boron Sorption onto Regenerated Resins

We also carried out batch studies to measure the boron sorption capacity of the **BSR-1** and **BSR-2** resins following one regeneration cycle to assess their regeneration potential. In a typical experiment, 1 g of resin (dry-weight equivalent) was packed in a fritted glass column and eluted with a 50 mM of boric acid solution until the effluent concentration was equal to the feed concentration. The resin was regenerated by elution with a 1.0 M HCl followed by neutralization a solution with 0.1 M NaOH. Similar regeneration conditions were employed in previous studies of boron-selective resins. [9-10, 12] Each regenerated resin was subsequently washed with DI water until the pH of the rinse water achieved remained constant. The

neutralized resins were collected by filtration over a Büchner funnel. Batch sorption studies were subsequently carried out to measure the boron sorption capacity of the regenerated BSRs in DI water using the procedures described above.

Results and Discussion

Synthesis and Characterization of Boron-Selective PEI Resins

Boron-selective resins (BSRs) such as the commercial Amberlite IRA-743 resin are prepared by functionalization of crosslinked STY-DVB beads using a two-step process.[15] In the first step, chloromethyl groups are attached to the STY-DVB resins via a Friedel-Crafts reaction involving the aromatic rings of the resin and an alkyl halide such as chloromethoxymethane in the presence of a Lewis acid catalyst. In the second step, the chloromethyl groups are reacted with N-methylglucamine to produce boron-chelating resins with vicinal diol groups. While the amination of chloromethylated STY-DVB beads is a facile reaction, which takes place in high yield, extensive side-reactions including the secondary crosslinking the aromatic rings of STY-DVB beads via "methylene bridging" occur during chlomethylation.[15, 16] This reduces the number of functional sites available for amination and, as a result, STY-DVB resins with N-methylglucamine groups such as the Amberlite IRA-743 resin have a limited capacity with a maximum free base of 0.7 eq/L. In our efforts to develop boron-selective resins (BSRs) with higher binding capacity than those of commercial STY-DVB resins, we selected branched polyethyleneimine (PEI) as precursor both for its high content of reactive primary/secondary amine groups and availability from commercial sources.[7, 17, 18] The new BSRs were prepared using a two-step process as illustrated in the reaction schemes shown in Figure 1. During the first step, two branched PEI macromolecules [with molar mass (M_n) of 1800 and 10,000 Da] were, respectively, crosslinked with epichlorohydrin and a mixture of epichlorohydrin (ECH) and 1-bromo-3-chloropropane (DCP) to afford spherical beads using the inverse suspension process described by Chang et al.[19] In the second step, the PEI beads [prepared using the PEI precursors with Mn= 1800 and 10,000 Da] were functionalized, respectively, with 2-oxiranylmethanol and glucono-1,5-D-lactone to prepare two new boron-selective resins (**BSR-1** and **BSR-2**) with boron-chelating groups. These new resins were characterized using a broad range of analytical techniques/assays including (i) measurements of water and amine contents, (ii) FT-IR spectroscopy, (iii) SEM imaging and (iii) particle size distribution analysis.

Table 1 lists the total amine contents (TAC) of the **BSR-1** and **BSR-2** resins along with those of the base **BPE-1** and **BPE-2** beads that were, respectively, used to prepare these resins. Not surprisingly, the TAC of the **BPE-1** and **BPEI-2** resins are both equal to ~9.0 mMol/g. However, consistent with the reaction

schemes of Figure 1, the TAC of the **BSR-2 resin** (7.21 mMol/g) is lower than that of the BSR-1 resin (8.02 mMol/g). Figure 2 shows the FT-IR spectra of the **BSR-2** and **BPEI-2** resins. Consistent with the reaction schemes of Figure 1, the FT-IR spectrum of the **BSR-2** resin (Figure 2) exhibits some characteristic features of compounds with amide groups (e.g. C=O stretch at 1660 cm^{-1}) and hydroxyl groups (e.g. OH stretching at 3257 cm^{-1}). Using the ImageJ image analysis software[13] , we estimate the average diameter of the **BSR-1** resin beads to be equal to 60.4 μm ± 11. Note that the average diameter of the **BSR-1** resin beads is significantly lower than those of STY-DVB resin beads. The particle size distribution (PSD) of such commercial resin beads range from 300 μm to 1200 μm with a mean diameter of 700 μm.[15] In this case, the PSD of **t**he **BSR-2** beads, which was measured using a Malvern Hydro 2000S particle size analyzer, range from 352 μm to 829 μm with a volume-averaged mean diameter of 551 μm.

Boron Sorption onto Selective PEI Resins

Figure 3A shows the sorption isotherms of boron onto the **BSR-1**, **BSR-2** and Amberlite IRA 743 resins in DI water. Figure 3B highlights the reproducibility of the sorption measurements. We subsequently used the IGOR Pro 6 [20] software to fit the sorption isotherms to a Langmuir model as given below:

$$q_{sorbed} = \frac{K_b C_{max} C_{eq}}{1.0 + K_b C_{max}} \qquad \text{Eq. 4}$$

where q_{sorbed} (mMol/g) is the mass of sorbed boron, C_{max} (mMol/g) is the resin sorption capacity at saturation, K_b (mM^{-1}) is the resin sorption constant and C_{eq} (mM) is the equilibrium concentration of boron in the aqueous phase. Table 2 of lists the estimated C_{max} and K_b values for the **BSR-1**, **BSR-2** and Amberlite IRA-743 resins. Table 2 shows that the boron sorption capacity (C_{max} =1.21 ± 0.13 mMol/g) of the **BSR-1** resin in DI water is comparable to that of a commercial resin (Amberlite IRA-743), which has a sorption C_{max} =1.16 ± 0.03 mMol/g. Note that our estimated C_{max} value for the Amberlite IRA-743 resin is very close to the measured value of 1.09 mMol/g reported by Xiao et al.[12] Table 2 shows that the **BSR-2** resin has a boron sorption capacity of 1.93 ± 0.04 mMol/g in aqueous solution with equilibrium boron concentration of ~70 mM. This sorption capacity is 66% percent larger than that of the Amberlite IRA-743 resin. Note that Figure 3A suggests the Amberlite IRA-743 resin has a higher sorption capacity at lower boron concentration, i. e. ~ 2 mM. However, additional studies using more sensitive boron assays are needed to quantify the performance of the BSRs in aqueous solutions containing low concentration of boron due to the limited sensitivity of our boron detection method by titration. As a preliminary assessment of the selectivity of the **BSR-1** and **BSR-2** resins, we measured their boron sorption isotherms in (i) a 0.1 M NaCl solution and (ii) a simulated permeate of a seawater reverse osmosis (SWRO)

desalination plant. We simulated a seawater desalination RO permeateusing the software IMSDesign 2007.[21]. Figure 4 shows a slight but consistent increase of boron uptake for the BSR-1 resin in 0.1M NaCl solutions compared to that in DI Water. For the BSR-2 resin, however, this increase is negligible. In this case, the C_{max} value of the BSR-2 resin in the simulated seawater RO permeate is very close to that in DI water (Figure 4 and Table 2). We speculate that the increase in boron uptake by the BSR-1 in 0.1 M NaCl compared to that in DI is the result of two synergistic effects: (i) an increase in borate $[B(OH)_4^-]$ concentration with increasing solution ion strength and (ii) borate binding to the protonated tertiary amine groups of the BSRs via ion pairing.[22] However, additional experiments are needed to validate this hypothesis. We also evaluated the regeneration potential of the **BSR-1** and **BSR-2** resins by measuring their boron sorption capacity in DI water after eluting the boron-laden resins with a 1.0 N HCl solution followed by a rinse with DI water and a wash with 0.1 N NaOH. Similar regeneration conditions were employed in previous studies of the Amberlite IRA-743 resin. [9-10, 12] We found that the boron sorption capacities of the pristine BSR-1 and BSR-2 resins in DI water were not affected by regeneration (Figure 5 and Table 3).

The overall results of the sorption experiments show that branched PEI beads provide versatile building blocks for the preparation of boron-chelating resins. As shown in Table 1, the base PEI beads have a high content of N groups (9.0 mMol/g) including reactive primary and secondary amine groups. Thus, they can be functionalized with polyols and lactones to afford resins with high densities of boron-chelating groups.[7, 17, 18] Based on the mechanisms of boron coordination with vicinal diol groups proposed by Yoshimura et al.[23], we postulate the formation of two types of boron-diol complexes in our boron-selective PEI resins. For the **BSR-1** resin, we hypothesize that the mechanism of boron coordination involves the formation of a tetradentate and bischelate complexes with $[B(OH)_4)]^-$ involving two hydroxyl groups from two different and contiguous branches of the resin (Figure 6). For the **BSR-2** resin, we postulate a mechanism of boron coordination involving the formation of a tetradentate and monochelate complexes with boron/borate involving four hydroxyl groups from the same branch of a resin bead (Figure 6). Note that in both coordination models, the tertiary amines of the **BSR-1** and **BSR-2** resins are not coordinated to boron (Figure 6). We postulate that these tertiary amine groups provide buffering capacity inside the **BSR-1** and **BSR-2** resins for favorable boron sorption at lower pH by binding the protons released by boric acid following complexation by the resin diol groups.[23] We also speculate that the protonated tertiary amines of the **BSR-1** and **BSR-2** resins could bind additional borate $[B(OH)_4)]^-$ via ion-pairing. Additional investigations are being conducted in our laboratory to validate the postulated mechanisms of boron coordination with the resin boron-specific groups (Figure 6).

Environmental Implications

As previously stated in the introduction, extraction of boron from solutions is important in various environmental/industrial processes including (i) desalination, (ii) ultrapure water treatment and (iv) nuclear power generation.[1-4] In SWRO desalination plants, several strategies have been evaluated to extract boron from aqueous solutions water including (i) the addition of 1-2 additional RO passes with high pH (~9) adjustment [24, 25] and (ii) the utilization of enhanced membrane processes such a micellar enhanced ultrafiltration [24]. However, due to its ease of implementation, sorption with selective and regenerable resins has emerged as an efficient process extracting boron from aqueous solutions. The overall results of our experiments show that crosslinked branched polyethyleneimine (PEI) beads provide versatile building blocks for the preparation of boron-selective resins (BSRs) with high sorption capacity. Additional investigations are being conducted in our laboratory to optimize the physical properties (e.g. particle size distribution and mechanical strength) and performance (e.g. sorption capacity and regeneration efficiency) of our new and PEI-based boron-selective resins in environmentally relevant conditions, e.g. dilute electrolyte solutions containing low concentrations of boron (< 5 mM).

References

1. Elimelech, M.; Phillip, W. A., The Future of Seawater Desalination: Energy, Technology, and the Environment. *Science* **2011,** *333*, (6043), 712-717.
2. Xu, Y.; Jiang, J. Q., Technologies for boron removal. *Industrial & Engineering Chemistry Research* **2008,** *47*, (1), 16-24.
3. Grinstead, R. R., Removal of Boron and Calcium from Magnesium Chloride Brines by Solvent-Extraction. *Ind Eng Chem Prod Rd* **1972,** *11*, (4), 454-&.
4. Ocken, H., An evaluation report of enriched boric acid in European PWRs *Electric Power Research Institute* **2001**, 114.
5. Blevins, D. G.; Lukaszewski, K. M., Boron in plant structure and function. *Annu Rev Plant Phys* **1998,** *49*, 481-500.
6. Campbell, S. A., The Science and Engineering of Microelectronic Fabrication. *Oxford University Press, USA; 2 edition* **2001**.
7. Smith, B. F.; Robison, T. W.; Carlson, B. J.; Labouriau, A.; Khalsa, G. R. K.; Schroeder, N. C.; Jarvinen, G. D.; Lubeck, C. R.; Folkert, S. L.; Aguino, D. I., Boric acid recovery using polymer filtration: studies with alkyl monool, diol, and triol containing polyethylenimines. *Journal of Applied Polymer Science* **2005,** *97*, (4), 1590-1604.
8. Vogel, A. I.; Svehla, G., Quantitative Inorganic Analysis. *Longman* **1987**.
9. Simonnot, M. O.; Castel, C.; Nicolai, M.; Rosin, C.; Sardin, M.; Jauffret, H., Boron removal from drinking water with a boron selective resin: Is the treatment really selective? *Water Research* **2000,** *34*, (1), 109-116.
10. Kaftan, O.; Acikel, M.; Eroglu, A. E.; Shahwan, T.; Artok, L.; Ni, C. Y., Synthesis, characterization and application of a novel sorbent, glucamine-modified MCM-41, for the removal/preconcentration of boron from waters. *Analytica Chimica Acta* **2005,** *547*, (1), 31-41.
11. Gazi, M.; Galli, G.; Bicak, N., The rapid boron uptake by multi-hydroxyl functional hairy polymers. *Separation and Purification Technology* **2008,** *62*, (2), 484-488.
12. Xiao, Y. K.; Liao, B. Y.; Liu, W. G.; Xiao, Y.; Swihart, G. H., Ion exchange extraction of boron from aqueous fluids by Amberlite IRA 743 resin. *Chinese Journal of Chemistry* **2003,** *21*, (8), 1073-1079.
13. Rasband, W. S. *ImageJ*, 1997-2011.
14. Standard Test Methods for Physical and Chemical Properties of Particulate Ion-Exchange Resins. In ASTM: 2009.
15. Harland, C. E., Ion-exchange : theory and practice. *Royal Society of Chemistry, London* **1994,** *2nd, Ed.*
16. Sherrington, D. C., Preparation, structure and morphology of polymer supports. *Chemical Communications* **1998,** *21*, 12.
17. Frechet, J. M. J.; Boz, E.; Chi, Y.; Diallo, M. S. Extraction of Anions from Solutions and Mixtures Using Hyperbranched Macromolecules 2009.
18. Diallo, M. S.; Yu, CJ. Soluble Anion Exchangers from Hyperbranched Macromolecules. US Patent Application. 2011.
19. Chang, H. T.; Charmot, D.; Zard, S. P. , Polyamine Polymers. *US Patent 7,342,083 B2*. **2008**.
20. WaveMetrics, I. *IGOR Pro*, 2010.
21. Hydranautics *IMSDesign*, 2007.

22. Hershey, J. P.; Fernandez, M.; Milne, PJ; Millero, FJ, The ionization of boric acid in NaCl, Na-Ca-Cl and Na-Mg-Cl solutions at 25-degrees-C. *Geochim. Cosmochim. Acta* **1986,** *50*, (1), 143-148.
23. Yoshimura, K.; Miyazaki, Y.; Ota, F.; Matsuoka, S.; Sakashita, H., Complexation of boric acid with the N-methyl-D-glucamine group in solution and in crosslinked polymer. *J Chem Soc Faraday T* **1998,** *94*, (5), 683-689.
24. Busch, M., Boron Removal in Sea Water Desalination. In Dow Deutschland GmbH & Co. OHG: 2003.
25. Roh, J.; Bartels, C.; Wilf, M. *Use of Dendrimers to Enhance Selective Separation of Nanofiltration and Reverse Osmosis Membranes*; 40; 2009.

Table 1. Water and Total Amine Contents of the Boron-Selective and Base PEI Resins Evaluated in This Study.

Resin	Matrix	Functional group	Water Content (%)	Total Amine Content (mMol/g)
BSR-1	[a]Crosslinked PEI	*cis*-diol	37	8.02
BSR-2	[b]Crosslinked PEI	pentahydroxyhexanamide	43	7.21
BPEI-1	[a]Crosslinked PEI	amines[a]	68	~9.0
BPEI-2	[b]Crosslinked PEI	amines[a]	65	~9.0

[a]The base PEI resins BPEI resins contain primary, secondary and tertiary amines.

bAvailable online at http://www.amberlyst.com/literature/a4/743.pdf

Table 2: Estimated Sorption Capacities (C_{max}) and Sorption Constants (K_b) for BSR-1, BSR-2 and Amberlite IRA-743 Resins in Deionized Water and Model Electrolytes. The C_{max} and K_b values were determined by fitting the sorption isotherms to a Langmuir model (See Eq. 4).

Resin	C_{max} (mMol/g)	K_b (mM^{-1})
BSR-1 (Deionized Water)	1.21 ± 0.13	0.13 ± 0.05
BSR-1 (0.1 M NaCl)	1.17 ± 0.08	0.32 ± 0.11
BSR-2 (Deionized Water)	1.93 ± 0.04	0.26 ± 0.03
BSR-2 (RO Permeate)	2.13 ± 0.10	0.20 ± 0.03
IRA-743 (Deionized Water)	1.16 ± 0.03	6.60 ± 2.03

We subsequently used the IGOR Pro 6 software [20] to fit the sorption isotherms to a Langmuir model as given below:

Table 3: Estimated Sorption Capacities (C_{max}) and Sorption Constants (K_b) for Pristine and Regenerated BSR-1 and BSR-2 Resins in Deionized Water. The C_{max} and K_b values were determined by fitting the sorption isotherms to a Langmuir model (See Eq. 4).

Resin	C_{max} (mMol/g)	K_b (mM^{-1})
BSR-1 (Pristine)	1.21 ± 0.13	0.13 ± 0.05
BSR-1 (Regenerated)	1.23 ± 0.16	0.13 ± 0.06
BSR-2 (Pristine)	1.93 ± 0.04	0.26 ± 0.03
BSR-2 (Regenerated)	1.92 ± 0.05	0.26 ± 0.04

Figure 1: Functionalization of PEI Resins with Boron-Chelating **Groups.**

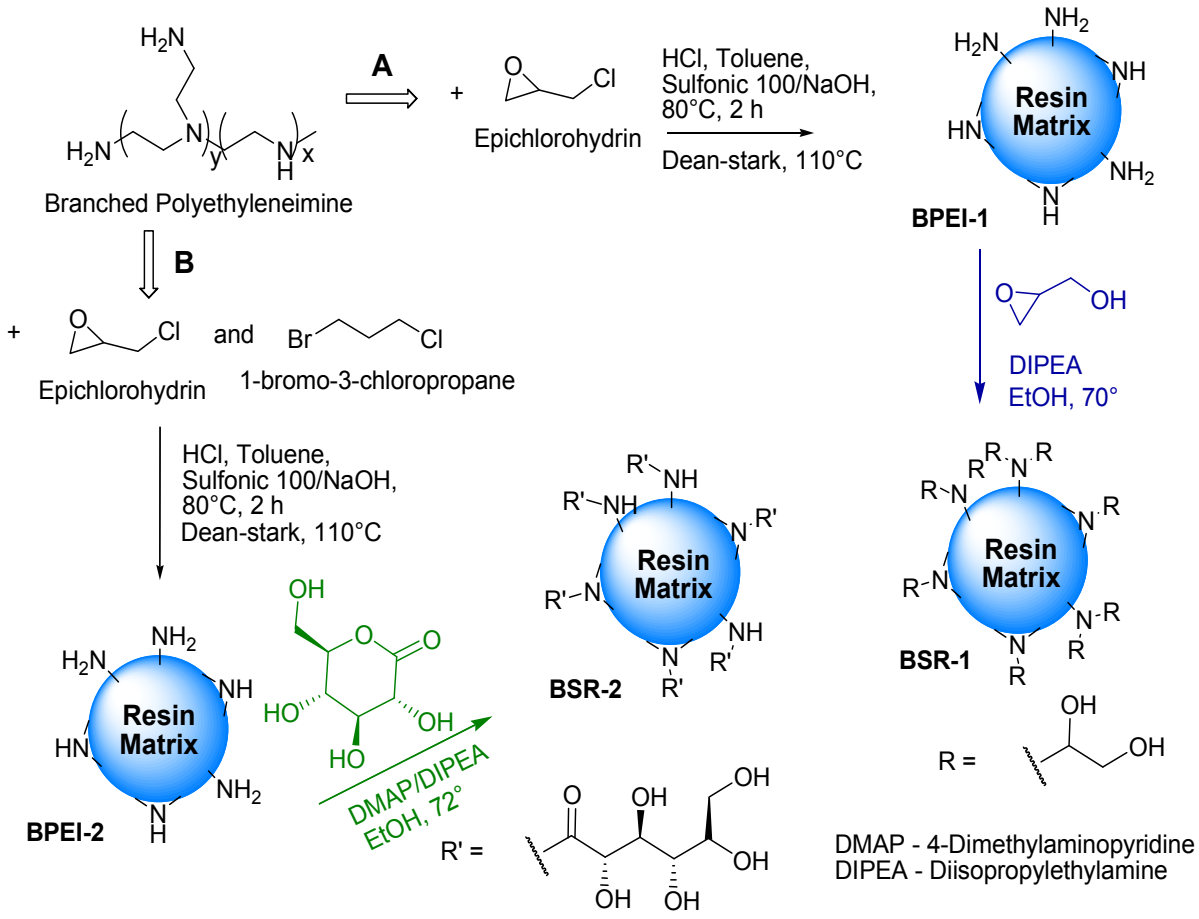

Figure 2: FT-IR Spectra of the BSR-2 Resin and the Corresponding Base BPEI-2 Resin.

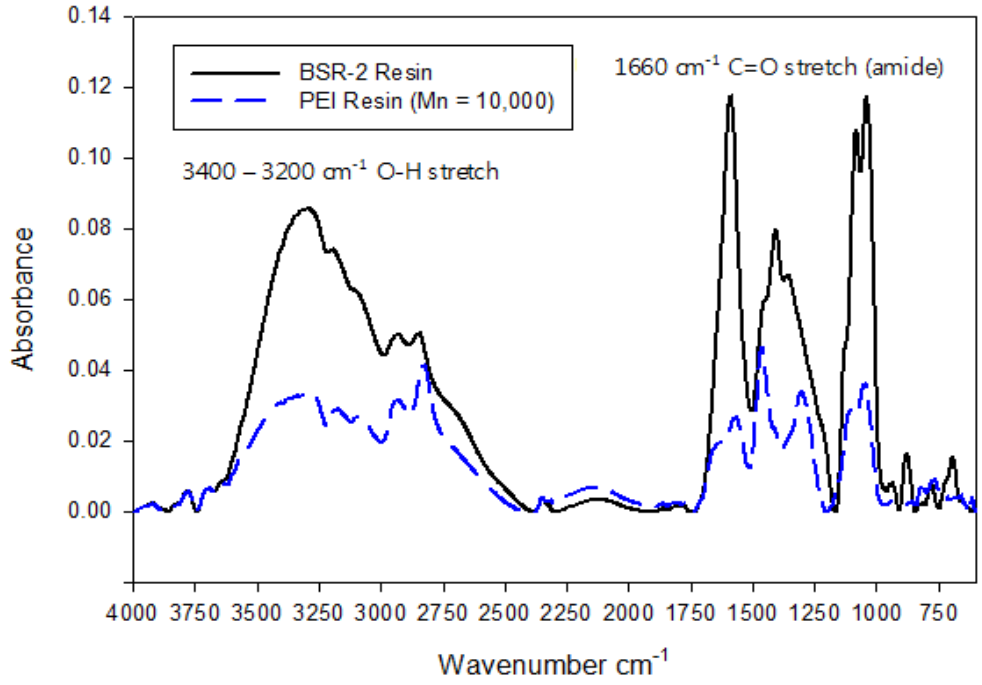

Figure 3: Boron Sorption onto the BSR-1 and BSR-2 Resins and Commercial Amberlite IRA-743 Resin in Deionized Water at Room Temperature.

A.

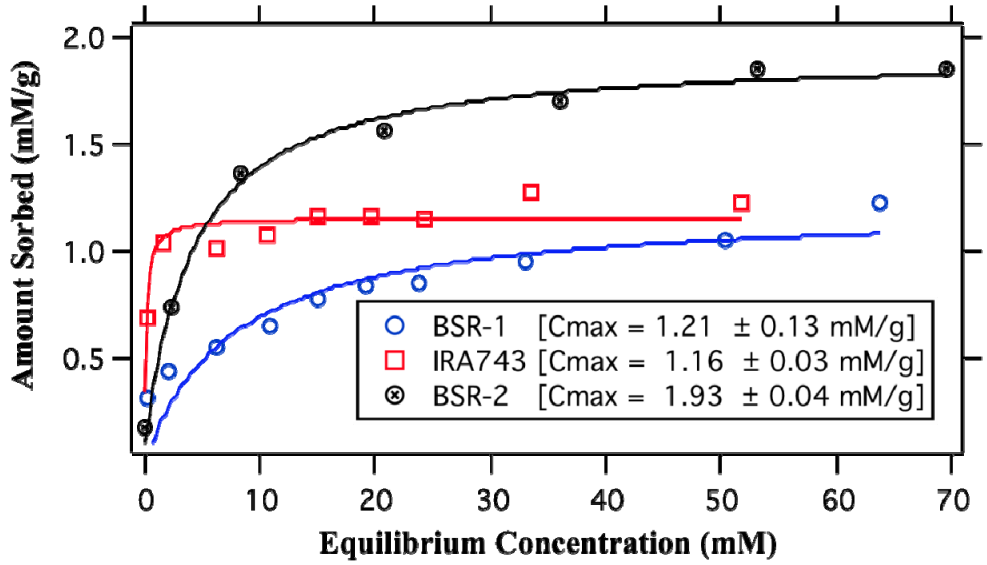

B.

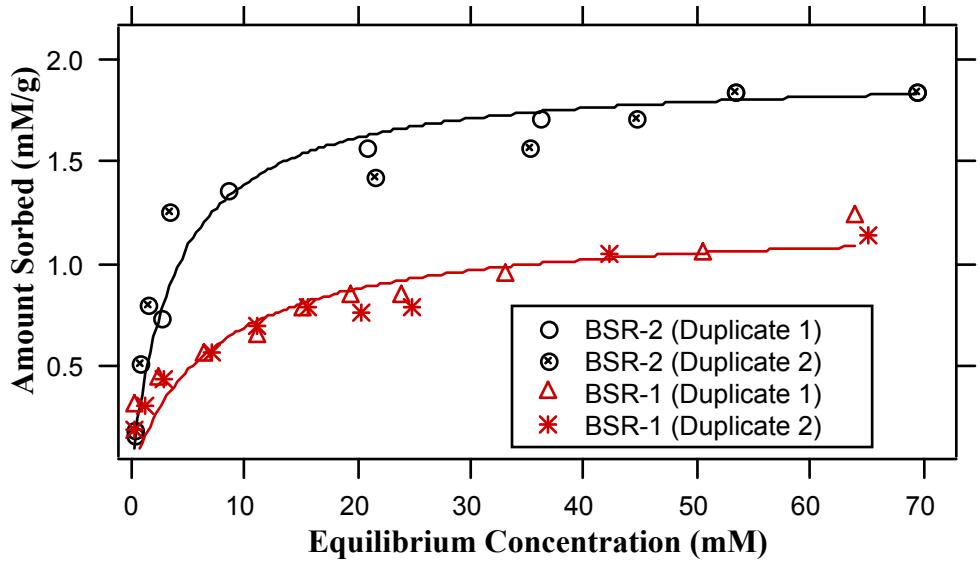

Figure 4: Boron Sorption onto the BSR-1 and BSR-2 PEI Resins in 0.1 M NaCl and Model Model RO Permeate.

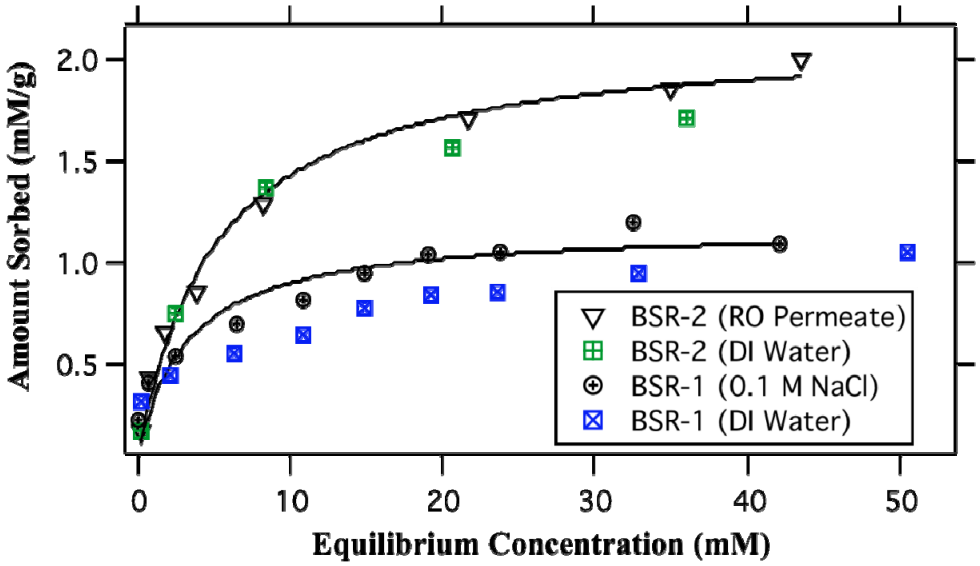

Figure 5: Boron Sorption onto the Regenerated BSR-1 and BSR-2 PEI Resins in Deionized Water at Room Temperature.

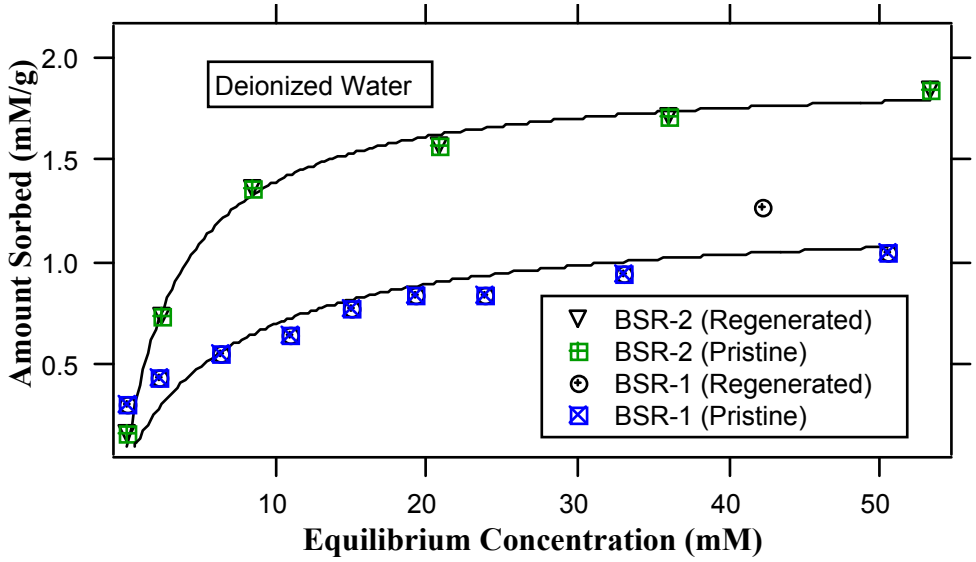

Figure 6: Postulated Mechanisms of Boron Coordination With the BSR-1 and BSR-2 PEI Resins in Aqueous Solutions. These coordination models have not been validated by independent spectroscopic and atomistic simulation studies.